

Numerical and Experimental Investigations of Pulsatile Blood Flow through  
a Dysfunctional Mechanical Heart Valve

Othman Ahmed Smadi

A Thesis  
In the Department  
of  
Mechanical and Industrial Engineering

Presented in Partial Fulfillment of the Requirements  
For the Degree of  
Doctoral of Philosophy (Mechanical Engineering) at  
Concordia University  
Montreal, Quebec, Canada

December 2011

© Othman Ahmed Smadi, 2011

**CONCORDIA UNIVERSITY**

**SCHOOL OF GRADUATE STUDIES**

This is to certify that the thesis prepared

By: **Othman Smadi**

Entitled: **Numerical and Experimental Investigations of Pulsatile Blood Flow through a Dysfunctional Mechanical Heart Valve**

and submitted in partial fulfillment of the requirements for the degree of

**DOCTOR OF PHILOSOPHY (Mechanical Engineering)**

complies with the regulations of the University and meets the accepted standards with respect to originality and quality.

Signed by the final examining committee:

\_\_\_\_\_ Chair  
Dr. M.N.S. Swamy

\_\_\_\_\_ External Examiner  
Dr. P. Oshkai

\_\_\_\_\_ External to Program  
Dr. A. Ben Hamza

\_\_\_\_\_ Examiner  
Dr. H.D. Ng.

\_\_\_\_\_ Examiner  
Dr. G.J. Gouw

\_\_\_\_\_ Thesis Co-Supervisor  
Dr. L. Kadem

\_\_\_\_\_ Thesis Co-Supervisor  
Dr. I. Hassan

Approved by \_\_\_\_\_  
Dr. W-F. Xie, Graduate Program Director

December 14, 2011

\_\_\_\_\_  
Dr. Robin A.L. Drew, Dean  
Faculty of Engineering & Computer Science

## **ABSTRACT**

### **Numerical and Experimental Investigations of Pulsatile Blood Flow through a Dysfunctional Mechanical Heart Valve**

Othman Ahmed Smadi, Ph.D.

Concordia University, 2011

Despite the marked improvement in prosthetic heart valve design and functionality, thromboembolism, structural failure, endocarditis and hemolysis are still possible complications. In such cases, native heart valve disease is replaced with “prosthetic heart valve disease”. Bileaflet Mechanical Heart Valve (BMHV) dysfunction can cause serious and potentially fatal complications.

*In vivo, in vitro, and Computational Fluid Dynamics (CFD) studies were conducted on dysfunctional BMHVs in order to: (1) investigate the relationship between blood flow patterns downstream of the dysfunctional BMHV and the levels of hemolysis and/or thrombus formation; (2) to evaluate the limitations of the hemodynamic parameters and cutoff values suggested by the American Society of Echocardiography (ASE) guidelines; and (3) to improve the accuracy of the current diagnosis methods using the same clinical modalities and settings.*

Pulsatile two-dimensional and two phase flow numerical simulations revealed that the flow upstream and downstream of a dysfunctional mechanical heart valve was highly influenced by dysfunction severity and this resulted in discrepancies between Doppler echocardiography and numerically derived transvalvular pressure gradients. Moreover,

the flow downstream of the dysfunctional valve was characterized by abnormally elevated shear stress and large-scale vortices. These flow characteristics can predispose to blood components damage.

Three-dimensional Fluid-Structure Interaction (FSI) numerical modeling showed that the flow nature is three-dimensional and time dependent, especially with the existence of valve dysfunction. A pulsatile 3-D FSI numerical model should be used when the evolution of the vortical structure downstream of the BMHV is the objective of the study. Only flow characteristics through the central orifice are measured by the current diagnosis methods. Therefore, revisiting the assumptions and the theory behind the current clinical method is critical in order to include the flow through the two lateral orifices.

A practical mathematical model was proposed for predicting the normal reference values of Doppler-derived parameters for BMHVs. The new theoretical model overcomes the shortcomings of the parameters suggested by the ASE guidelines by taking into account flow conditions (Left Ventricle Outflow Tract (LVOT) measurements), valve size and valve type. The accuracy of diagnosis significantly improved using the new theoretical parameters compared to those suggested by the ASE. Finally, the new method improved the way to evaluate of the performance of BMHVs, not only after implantation, but also early during the stage of design and manufacturing.

## **ACKNOWLEDGMENTS**

First of all, I would like to express my appreciation to my supervisors, Dr. Lyes Kadem and Dr. Ibrahim Hassan for believing in me and for their continuous support during my research.

I am also grateful to our Cardiovascular Fluid Dynamics (LCFD) group for their technical support and for the healthy and competitive environment that we work in.

I am also grateful to Dr. Peter Oshkai, Dr. Abdessamad Ben Hamza, Dr. Gerard Gouw, and Dr. Hoi Dick Ng for reviewing my work and attending my examination committee.

# Table of Contents

List of Figures .....	ix
List of Tables.....	xii
Nomenclature .....	xiii
Abbreviations .....	xv
Introduction.....	1
Motivation.....	3
Chapter 1.....	6
Literature Review .....	6
1.1 Numerical Studies.....	6
1.1.1 Laminar Blood Flow .....	7
1.1.2 Turbulent Flow.....	10
1.2 Experimental Studies .....	15
1.2.1 Laser Doppler Anemometry (LDA).....	15
1.2.2 Particle Image Velocimetry (PIV) .....	17
1.2.3 <i>In Vivo</i> Diagnostic Parameters.....	20
Chapter 2.....	24
Potential Clinical Complications Associated With Dysfunction of Bileaflet Mechanical Heart Valve: CFD and In Vitro Study.....	24
2.1 Introduction .....	24
2.2 Models and Methods.....	26
2.2.1 Numerical Method .....	26
2.2.2 Experimental Method.....	30
2.3 Results .....	33
2.3.1 Doppler-echocardiographic Measurements .....	33
2.3.2 Platelet Activation.....	34
2.4 Discussion .....	38
2.4.1 Clinical Diagnosis .....	38
2.4.2 TSS and Residential Time (platelet activation) .....	40
2.5 Conclusion.....	41
Chapter 3.....	42
Bileaflet Prosthetic Heart Valve Disease: Numerical Approach Using 3-D Fluid-Structure Interaction Model with Realistic Aortic Root.....	42
3.1 Introduction .....	42

3.2 Numerical Method .....	44
3.2.1 Turbulent-FSI Approach .....	45
3.3 Results and Discussion.....	46
3.3.1 Velocity Contours .....	46
3.3.2 Coherent Structures.....	49
3.4 Conclusion.....	53
Chapter 4.....	54
Performance of Doppler-echocardiographic Parameters for the Detection of Aortic Mechanical Prosthetic Valve Dysfunction.....	54
4.1 Introduction .....	54
4.2 Methods.....	56
4.2.1 <i>In Vitro</i> Study.....	56
4.2.2 <i>In Vivo</i> Study .....	58
4.3 Results .....	61
4.3.1 <i>In Vitro</i> Results .....	61
4.3.2 <i>In Vivo</i> Results .....	71
4.4 Discussion .....	71
4.4.1 Peak Doppler Velocity and Mean Transvalvular Pressure Gradient .....	71
4.4.2 Doppler Velocity Index .....	73
4.4.3 Effective Orifice Area .....	74
4.4.4 Low Cardiac Output State .....	76
4.5 Conclusion.....	76
Chapter 5.....	78
Theoretical Prediction of the Hemodynamic Performance of Bileaflet Mechanical Heart Valves .....	78
5.1 Introduction .....	78
5.2 Methods Used for the Validation of the Proposed Theoretical Parameters .....	80
5.2.1 Experimental Setup .....	80
5.2.2 <i>In Vivo</i> Data .....	84
5.2.3 Mathematical Model for Proposed Parameters.....	84
5.3 Results .....	88
5.3.1 Validation Against <i>In Vitro</i> Data.....	89
5.3.2 Validation Against <i>In-Vivo</i> Data.....	102
5.4 Discussion .....	102
5.4.1 Velocities and Pressure Gradients.....	103

5.4.2 Effective Orifice Area .....	108
5.4.3 Mild to Moderate Severity of Valve Dysfunction (50% Dysfunction) .....	108
5.5 Conclusion .....	110
Conclusions and Future work.....	111
Conclusions .....	111
Future Work .....	113
References.....	115

## List of Figures

Figure 1.1 Schematic of the St. Jude Medical (SJM) valve with leaflets shown in open and closed (dotted line) positions (Dasi et al., 2007). .....	7
Figure 2.1 Models for the five different cases: 1) 0% dysfunction; 2) 25% dysfunction; 3) 50% dysfunction; 4) 75% dysfunction; 5) 100% dysfunction. ....	27
Figure 2.2 (a) Velocity profile at the vicinity of the valve for different grid solutions; (b) Fine-grids solution with discretization error bars.....	31
Figure 2.3 (a) Schematic representation of the mock flow model; (b) Alteration of the lower leaflet opening position using a small stop pin. ....	32
Figure 2.4 Comparisons between numerical and Doppler-echocardiographic results; (a) maximum velocity; (b) The mean and the maximum transvalvular pressure gradients (TPG). ....	35
Figure 2.5 Comparison of platelets paths downstream of the valve during the deceleration phase a) 0-50 ms after the peak b) 100-150 ms after the peak and for different percentages of dysfunction.....	36
Figure 2.6 Platelets level of activation during the deceleration phase (100-150 ms after the peak) for different percentages of dysfunction. (a) Particles released from the upper valve orifice. (b) Particles released from the lower valve orifice. ....	39
Figure 3.1. The geometry (high right corner) and the mesh quality (lower part) of 25 mm St. Jude Hemodynamic Plus (SJHP) with the instantaneous velocity (high left corner) as an inlet condition. ....	45
Figure 3.2 Contours for velocity magnitude through the bileaflet valve for different percentage of dysfunctions at two time instants (at the peak and late during the deceleration).....	48
Figure 3.3 3-D coherent structure based on Q-criterion at peak and late during deceleration phase. ....	51
Figure 3.4 The difference between the two-component and three-component velocity magnitude ( $V(u,v,w)$ and $V(u,w)$ ) at the central plane (B-datum) and the peak systole. ....	52
Figure 4.1 Sketch for the custom-made cardiac simulator .....	57
Figure 4.2 Measured peak Doppler velocity grouped by prosthetic valves' type, dysfunction and size. ....	62

Figure 4.3 Measured mean pressure gradient grouped by prosthetic valves' type, dysfunction and size. ....	64
Figure 4.4 <i>In vitro</i> Doppler velocity index, calculated as the ratio of peak velocity in the left ventricle outflow tract to that of the transprosthetic peak velocity in 0% dysfunction, 50% dysfunction and 100% dysfunction of SJHP (left) and On-X (right) prosthetic valves and for different cardiac outputs. Bars, mean±SD of the measured values each valve size .....	66
Figure 4.5 <i>In vitro</i> effective orifice area (cm <sup>2</sup> ) in 0% dysfunction, 50% dysfunction, and 100% dysfunction of SJHP (left) and On-X (right) prosthetic valves and for different cardiac outputs. Bars, mean ± SD of the measured values each valve size. ....	67
Figure 4.6 <i>In vivo</i> measurements for different Doppler derived parameters for Normal and dysfunctional BMHVs.....	72
Figure 4.7 The effect of LVOT narrowing or dilatation on Doppler velocity index. Narrowing of LVOT diameter with the implantation of normal aortic prosthetic SJHP27 valve (→), and Dilatation of LVOT diameter with the implantation of normal aortic prosthetic SJHP21 (←) .....	75
Figure 5.1 Sketch for the custom-made cardiac simulator, and the maximum opening position for the leaflets. ....	83
Figure 5.2 Schematic representation for blood flow through bileaflet mechanical heart valve. Where $Q_{\text{peak-LVOT}}$ is peak systolic flowrate (L/min) at the left ventricle outflow tract location, $Q_C$ is the flowrate (L/min) through the central orifice, and $Q_L$ is the flowrate (L/min) through the lateral orifice. ....	86
Figure 5.3 Measured peak transvalvular velocity for different flowrates and different percentages of valve dysfunction. Theoretically predicted peak velocity of normally functioning valve (0% dysfunction) for different flowrates is also plotted. ....	91
Figure 5.4 Measured mean transvalvular velocity for different flowrates and different percentages of valve dysfunction. Theoretically predicted mean velocity of normally functioning valve (0% dysfunction) for different flowrates is also plotted. ....	92
Figure 5.5 (a) <i>In vitro</i> correlations between predicted and measured peak Doppler velocity. (b) Differences between predicted and measured peak Doppler velocity are presented on a Bland-Altman plot. ....	93
Figure 5.6 (a) <i>In vitro</i> correlations between predicted and measured mean Doppler velocity. (b) Differences between predicted and measured mean Doppler velocity are presented on a Bland-Altman plot. ....	94

Figure 5.7 Measured mean transvalvular pressure gradient for different flowrates and different percentages of dysfunction. The theoretically predicted mean transvalvular pressure gradient of normally functioning valve (0% dysfunction) for different flowrates is also plotted.....	96
Figure 5.8 (a) <i>In vitro</i> correlation between predicted and measured mean transvalvular pressure gradient; (b) Differences between predicted and measured mean transvalvular pressure gradient are presented on a Bland-Altman plot.....	97
Figure 5.9 Measured EOA for different flowrates and different percentages of dysfunction. The theoretically predicted EOA of normally functioning valves (0% dysfunction) for different flowrates is also plotted. ....	100
Figure 5.10 (a) <i>In vitro</i> correlations between predicted and measured EOA; (b) Differences between predicted and measured EOA are presented on a Bland-Altman plot. ....	101
Figure 5.11 (a) <i>In vivo</i> correlation between predicted and measured peak Doppler velocity; (b) Differences between predicted and measured peak Doppler velocity are presented on a Bland-Altman plot.....	107
Figure 5.12 Plotted charts show relationships between peak/mean flowrate and predicted Doppler-derived parameters; a) peak flowrate vs. Peak velocity; b) mean flowrate vs. mean velocity; c) mean flowrate vs. mean transvalvular pressure gradient (TPG <sub>mean</sub> ). ....	109

## List of Tables

Table 1.1 List of the most used diagnosis parameters for MHV. ....	20
Table 4.1 Sensitivity and specificity analysis for different echo Doppler parameters .....	70
Table 4.2 Sensitivity and specificity analysis for different echo Doppler parameters (excluding 50% dysfunction cases) .....	70
Table 4.3 <i>In vivo</i> Doppler-derived data for normal aortic bileaflet valves .....	72
Table 4.4 <i>In vivo</i> Doppler-derived data for dysfunctional aortic bileaflet valves .....	<b>Error!</b>
<b>Bookmark not defined.</b>	
Table 5.1 Variability of <i>in vitro</i> extracted Doppler-derived parameters for St. Jude and On-X prosthetic valves .....	82
Table 5.2 Validation of measured EOA normal reference values .....	99
Table 5.3 Doppler-derived data for normal aortic bileaflet valves .....	104
Table 5.4 Doppler-derived data for obstructed aortic bileaflet valves .....	105
Table 5.5 Doppler-derived data for obstructed aortic bileaflet valves (Aoyagi et al., 2000) .....	105

## Nomenclature

$k$	Turbulent kinetic energy, $\left(\frac{\text{m}^2}{\text{s}^2}\right)$
$p$	Pressure, (Pa)
$\Delta p$	Pressure difference, (Pa)
$Q$	Volume flowrate, $\left(\frac{\text{m}^3}{\text{s}}\right)$
$r$	Radial coordinate, (m)
$Re$	Reynolds number
$SV$	Stroke volume, $(\text{m}^3)$
$S_{ij}$	Strain rate tensor, $\left(\frac{1}{\text{s}}\right)$
$t$	Time, (s)
$\Delta t$	Time step, (s)
$u_i$	Time-averaged velocity component, $\left(\frac{\text{m}}{\text{s}}\right)$
$u'_i, v'_i$	Fluctuation of velocity component from the time-averaged value, $\left(\frac{\text{m}}{\text{s}}\right)$
$U, V$	Velocity, $\left(\frac{\text{m}}{\text{s}}\right)$
$\bar{v}$	Velocity vector $\langle u, v, w \rangle$ , $\left(\frac{\text{m}}{\text{s}}\right)$
VTI	Velocity time integral (m)
$x$	Axial coordinate, (m)

$y$	Circumferential coordinate, (m)
$y^+$	Non dimensional viscous sub layer height

### Greek symbols

$\theta$	Angular velocity, ( <i>radians</i> )
$\varepsilon$	Turbulent dissipation rate, $\left(\frac{m^2}{s^3}\right)$
$\gamma$	Ratio of specific heats, $\gamma = c_p/c_v$
$\nu$	Kinematic viscosity, $\left(\frac{m^2}{s}\right)$
$\mu$	Dynamic viscosity, $\left(\frac{kg}{m \cdot s}\right)$
$\mu_t$	Turbulent viscosity, $\left(\frac{m^2}{s}\right)$
$\rho$	Density, $\left(\frac{kg}{m^3}\right)$
$\bar{\tau}, \tau_{ij}$	Stress tensor, ( <i>Pa</i> )
$\tau$	Shear stress, ( <i>Pa</i> )
$\omega$	Specific dissipation rate, $\left(\frac{1}{s}\right)$
$\Omega_{ij}$	Vorticity tensor, $\left(\frac{1}{s}\right)$

## **Subscripts**

LVOT	Left ventricle outflow tract
<i>rms</i>	Root mean square
Dop	Doppler
Cat	Catheterization
<i>w</i>	Wall

## **Abbreviations**

ALE	Arbitrary Lagrangian-Eulerian approach
AoA	Cross-sectional area of the proximal ascending aorta
AS	Aortic stenosis
BMHV	Bileaflet mechanical heart valve
BPV	Bioprosthetic heart valve
CT	Computed tomography
CW	Continuous wave
DES	Detached eddy simulation approach
DNS	Direct numerical simulation
DPIV	Digital particle image velocimetry
DVI	Doppler velocity index
$E_LCo$	Energy loss coefficient
EOA	Effective orifice area
FSI	Fluid structure interaction

MHV	Mechanical heart valve
MRI	Magnetic resonance imaging
LDA	Laser Doppler anemometry
LVOT	Left ventricle outflow tract
PW	Pulsed wave
PIV	Particle image velocimetry
RES	The aortic valve resistance
RRS	Reynolds shear stress
SGS	Sub-Grid-Scale
TEE	Transesophageal echocardiography
TPG	Transvalvular pressure gradient
TSS	Turbulent shear stress
TTE	Transthoracic echocardiography
TVSS	Turbulent Viscous Shear Stress
UDF	User defined function
URANS	Reynolds-average Navier-Stokes approach
VSS	Viscous shear stress

## **Introduction**

According to the American Heart Association, the prevalence of valve disease in the United States reached 2.5% in 2000, amounting to approximately 7 million people. The major problem associated with valve function is their failure to either open fully to allow blood to pass smoothly (stenosis) or to close completely to prevent regurgitation of flow to the ejection side (incompetence). In severe cases, heart valve replacement is the ultimate solution to restore normal function of the heart's valves.

More than 280,000 heart valve replacements are conducted world-wide each year. Almost half of the implanted valves are mechanical heart valves (MHVs) (mainly bileaflet mechanical heart valves (BMHVs)) while the remaining half are bioprosthetic heart valves (Pibarot and Dumesnil, 2009). Despite the marked improvement in prosthetic heart valve design and functionality, implanted prosthetic heart valves are not completely free of complications (i.e., thromboembolism, structural failure, endocarditis, and hemolysis) (Vesey and Otto, 2004). In MHVs, thrombus and/or pannus formation are major causes of functional stenosis and/or regurgitation (Rizzoli et al., 1999; Roudaut et al., 2003). Prosthetic heart valve dysfunction, in most cases, is lethal, and an early diagnosis for prosthetic valve dysfunction is essential for better outcome and successful treatment (i.e. heparin, fibrinolysis and reoperation) (Aoyagi et al., 2000; Roudaut et al., 2007).

Most numerical and experimental studies of BMHVs have focused on normally functioning valves with an emphasis on the velocity field, transvalvular pressure drop and

blood components damage. In previous numerical studies, the flow downstream of a normal BMHV was investigated under steady state flow conditions (Ge et al., 2003) and pulsatile flow conditions with or without Fluid-Structure Interaction (FSI) (Grigioni et al., 2005; Pedrizzetti and Domenichini, 2006; Alemu and Bluestein, 2007). It should be noted that in most studies where FSI was considered, the flow through the BMHV was assumed to be laminar (Redaelli et al., 2004; Guivier et al., 2007; Dumont et al., 2007). Recently, Direct Numerical Simulation (DNS) with fully coupled FSI was performed by Dasi et al. (2007), Nobili et al. (2008) and De Tullio et al. (2009). It should be noted, however, that the application of DNS to clinical problems is limited due to its high computational cost.

Flow disturbances downstream of a normal BMHV are magnified in the presence of leaflet prosthesis dysfunction. There are very few *in silico*, *in vitro* or *in vivo* studies examining the effects of BMHV dysfunction on flow patterns (Baumgartner et al., 1993; Aoyagi et al. 2001; Montorsi et al. 2003; Smadi et al., 2009).

In the clinical setting, Doppler echocardiography, cinefluoroscopy and computed tomography (CT) are the most commonly used modalities for the assessment of prosthetic heart valve performance. Due to the risks associated with X-ray exposure, Doppler echocardiography is routinely used as a first choice in the evaluation of prosthetic heart valve performance. Only patients suspected of prosthetic valve dysfunction in Doppler echocardiography are sent to cinefluoroscopy or CT for

visualization of prosthetic valve leaflet morphology and mobility (Montorsi et al., 2003, Cianciulli et al., 2005; LaBounty et al., 2009).

The main challenge in echocardiography is the limited capacity of visualization. In the aortic position, the clear visualization of aortic prosthetic valves using transthoracic Doppler echocardiography (TTE) and/or transesophageal Doppler echocardiography (TEE) is limited due to intense echo reverberations and shadowing caused by valve components. (Khandheria et al., 1991; Mohr-Kahaly et al., 1993; Maslow et al. 2000; Aslam et al., 2007). Therefore, the prosthetic valve evaluation process, using TTE as a first choice modality, can only rely on Doppler-derived parameters (peak velocity/gradient, mean pressure gradient, effective orifice area (EOA) and Doppler velocity index (DVI)) (Vesey and Otto, 2004; Zoghbi et al., 2009; Bach, 2010).

## **Motivation**

Bileaflet MHVs have been the subject of many recent studies due to their wide use. Bileaflet MHVs produce non-physiological flow due to their design compared to natural valves (three orifices instead of one orifice in the natural heart valve). Most studies have focused on investigating the performance of normal (healthy) MHVs.

One of the main issues that have not been investigated is the probability and the severity of clinical complication (i.e. thrombus formation, left ventricle function) associated with the presence of bileaflet MHV dysfunction. In addition, current *in-vitro* methods appear to be inferior at predicting flow or acquiring quantitative information within the valve housing or near the wall. Thus, there is a need to perform numerical simulations in order to better understand the dynamics of blood flow through MHVs. Furthermore, there is a

need to assess the diagnostic accuracy and the limitations of current non-invasive hemodynamic parameters.

## **Objective and Organization**

Based on the literature review presented in chapter 1, the main objectives for the current study are:

1. To investigate the relationship between blood flow patterns downstream of the dysfunctional BMHV and levels of hemolysis and/or thrombus formation.
2. To evaluate the limitations of the hemodynamic parameters and cutoff values suggested by the American Society of Echocardiography (ASE) guidelines.
3. To improve the accuracy of current diagnostic methods using the same clinical modalities and settings.

The thesis is comprised of five chapters. The first chapter consists of a literature review of the main published works on mechanical heart valves (clinical and engineering articles) as well as current ideas and challenges in the field. In chapter two, potential clinical complications associated with the dysfunction of bileaflet mechanical heart valves using 2-D two phase numerical simulations and *in vitro* tests are investigated. The impact of the simplifications made in chapter two on the clinically-related results are addressed in chapter three by simulating 3-D FSI models with a realistic aortic root. In chapter four, the performance of different Doppler-echocardiographic parameters suggested by the guidelines of the American Society of Echocardiography (ASE) on identifying the dysfunction of mechanical prosthetic valves in the aortic position is investigated. For this purpose, intensive *in vitro* studies were performed using a custom-

made cardiac simulator and a clinical echocardiography machine. In addition, *in vivo* data was acquired to validate the *in vitro* findings. In chapter five, a mathematical model that is able to predict the normal reference values of Doppler-derived parameters by considering flow conditions, valve size, and valve type is proposed. The theoretical results are validated against *in vitro* results. Moreover, *in vivo* data from a combined echocardiography/fluoroscopy study are extracted and analyzed to validate the theoretical predictions. The conclusion of our study and recommendations for future work are presented at the end of the thesis.

# Chapter 1

## Literature Review

Numerous studies have been conducted on mechanical heart valves (MHV) to determine the nature of blood flow and potential medical complications. The results of these studies are presented in this chapter and analyzed in terms of material, design, hemodynamic parameters, medical complications and performance diagnosis.

The studies are divided into two main categories: numerical studies and experimental studies.

### 1.1 Numerical Studies

Computational Fluid Dynamics (CFD) are widely used to investigate blood flow through MHVs. Currently available MHVs do not mimic the native heart valve (fig. 1.1), and generally produce non-physiological flow. Due to the complex nature of the non-physiological flow produced by MHVs, different assumptions have been considered. The laminar assumption has been used to simulate the pulsatile nature of the cardiac cycle due to the absence of a numerical model capable of covering the laminar, transitional and turbulent regimes. The development of the low Reynolds Wilcox ( $k-\omega$ ) model (Wilcox 1998) encouraged researchers to simulate the pulsatile flow under the turbulent regime assumption. In addition, the fluid-structure interaction (FSI) between valve leaflets and blood flow has been studied to include the effect of blood flow on the leaflet and vice

versa. Due to the dramatic increase in the computational power and memory of computers, Direct Numerical Simulations (DNS) were recently introduced to simulate blood flow through the entire cardiac cycle with strongly coupled FSI simulation (De Tullio et al., 2009).

### 1.1.1 Laminar Blood Flow

A comparison between 3-D numerical simulations for a bileaflet valve and experimental studies using Laser Doppler Anemometry (LDA) measurements was performed by King et al. (1997). The group considered only a quarter of the geometry by applying two planes of symmetry. The nature of flow was unsteady and laminar. The aim of this study was to validate the CFD solution and to get the optimal opening angle for the leaflet. Significant differences between CFD and LDA were found and were explained by limitations in CFD itself. However, good agreement was found between the numerical and the experimental results in terms of the quality and behaviour of the flow, including the existence of vortex shedding downstream of the valve and the presence of slow moving fluid in the sinus area. Finally, the authors concluded that numerical simulations were able to predict the flow characteristics downstream of a MHV and can be used to improve the design of future MHVs.

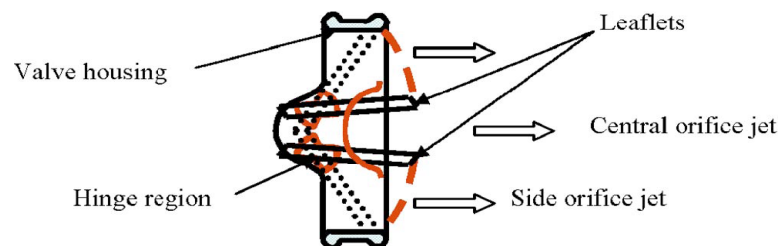


Figure 1.1 Schematic of the St. Jude Medical valve with leaflets shown in open and closed (dotted line) positions (Dasi et al., 2007).

A new technique for moving mesh was proposed by using multi-zone unstructured moving grid schemes by Shi et al. (2003). In short, the mesh was created for the entire geometry without considering the solid domain (the leaflets) and once the leaflet position was calculated, the nodes in contact with the solid phase were considered as a moving boundary for the solid phase. The CFD results showed that the leaflet tip is the most sensitive region for hemolysis due to high velocity and the presence of a velocity gradient near the tip.

The Arbitrary Lagrangian Eulerian method (ALE) was used by Dumont et al. (2004). They used FLUENT (commercial software) and the ALE method to implement FSI to MHV 2-D unsteady (pulsatile) laminar flow conditions. They compared their results with a CCD camera to record the valve positions at different instants. User defined function (UDF) was used to write an external code to describe the leaflet motion and a dynamic mesh was used to redefine the mesh with each small movement of the solid boundaries. The authors concluded that the simulation gave good agreement with the experimental results.

3-D pulsatile blood flow through a St. Jude HP 27 bileaflet valve was simulated by Redaelli et al. (2004). Only a part of the systolic phase was considered to simulate the valve opening process. They used a user defined function and a laminar model to implement FSI using FLUENT. In parallel, experimental work using a high speed camera was performed to validate the numerical simulations of the MHV opening process by considering the same valve design and the same inlet condition. A good agreement was found between numerical and experimental results. Further improvements to the current

model were suggested including the consideration of normal flowrate and the transitional and turbulent effects in the simulation by using an appropriate turbulence model.

Ge et al. (2003) investigated grid resolution and flow symmetry, focusing mainly on grid resolution and its effect on the accuracy of the results obtained using CFD. For this purpose, 3-D, steady and fully developed flow through a St. Jude bileaflet mechanical heart valve was simulated for different Reynolds (Re) numbers. They concluded that the results are very sensitive to mesh independence under physiological conditions. Furthermore, they questioned the validity of a symmetrical model assumption, since they found that asymmetry in the flow can appear for Re as low as 120, even though the flow was assumed laminar and steady.

The flow through a St. Jude bileaflet heart valve in the aortic position with co-existing subaortic stenosis was investigated by Guivier et al. (2007). 2-D laminar and pulsatile flow simulations were performed by taking into account the fluid-structure interaction effect. The study concluded that, under such conditions, the major jet flow moves towards the lateral orifice rather than the centre. Furthermore, the leaflet close to the subaortic stenosis will not work properly. Therefore, more awareness should be considered by clinicians to align the echo-Doppler beam to avoid an underestimation of the effective orifice area of the valve.

Recently, Guivier-Curien et al. (2009) extended their 2-D model to a 3-D fluid-structure interaction model. They simulated blood flow through a 27 mm St. Jude prosthetic heart valve and validated the numerical results using 2-D PIV. However, the study had one important limitation which is adapting a maximum flowrate equal to only one third ( $\sim 8$  L/min) of the actual normal flowrate ( $\sim 25$  L/min). This modification was necessary in order to obtain a laminar flow that is far from the physiological blood flow, especially when MHV is present. A strongly coupled FSI was adapted. Five different time instants including, acceleration, deceleration and peak of the systolic phase were analyzed. The axial velocity vectors and the leaflet dynamics (opening and closure) from the experimental and numerical measurements were compared and good agreement was found between both studies.

### **1.1.2 Turbulent Flow**

Peacock et al. (1997) investigated the onset of turbulence under pulsatile flow conditions in a straight tube and correlated the results to flow conditions in the human aorta downstream of the aortic heart valve. They suggested that the onset of turbulence in the human aorta is highly possible. However, by implanting the mechanical heart valves, the flow downstream of the mechanical heart valve was highly disturbed and the turbulent flow became dominant during the peak and deceleration stages of the systolic phase (Liu et al., 2000). Therefore, in order to extract useful clinical information (i.e., threshold of platelet activation and/or blood hemolysis), simulating turbulent blood flow through the mechanical heart valve is essential, especially at the physiological flowrate.

## **Turbulence Simulation**

Bluestein et al. (2000) numerically and experimentally investigated the occurrence of thromboembolic complications caused by normally functioning bileaflet mechanical heart valves. A time dependent numerical study was performed using Wilcox  $k-\omega$  turbulence model for internal flow with low Reynolds number. Digital Particle Image Velocimetry (DPIV) was also conducted under the same conditions. The comparison between numerical and experimental results showed the ability of the Wilcox  $k-\omega$  model to simulate blood flow through a bileaflet mechanical heart valve. In addition to blood contact with foreign material, non-physiological blood flow through the three valve orifices introduced vortex shedding downstream of the valve leaflets which in turn played an important role in cerebrovascular micro emboli formation. Moreover, the shedded vortices could cause platelets to aggregate. Long residential times with high levels of shear stress were noticed during the vortex shedding process.

The effects of surgical implantation techniques and valve orientation on blood hemodynamics in the valve's wake position were studied by Bluestein et al. (2002). Time dependent Computational Fluid Dynamic (CFD) simulations using the Wilcox  $k-\omega$  model for blood flow with low Reynolds number was conducted on commercial software (FLUENT). The mesh quality near the wall was made fine to maintain  $y^+ \leq 1$  ( $y^+$  is the non-dimensional viscous sub layer height). The simulation did not consider fluid-structure interactions between the leaflets and the blood, and the valve leaflets were fixed in the fully open position. The study concluded that heart valve misalignment has an important effect on elevating platelet activation and thrombembolism formation.

An *in-vitro* study was conducted by Yin et al. (2004) on two different MHVs: Bileaflet (CarboMedics) and monoleaflet (Bjork-Shley) valves. In addition, numerical simulations using Wilcox  $k-\omega$  model for transitional/turbulent flow under pulsatile flow were conducted. To measure the shear stress histories of the platelets, numerically, the Lagrangian approach for particulate two phase flow was used to calculate, approximately, the separated trajectories of platelets that were close to the valve leaflets. Thromboembolism phenomenon in both MHVs was noticed. Experimentally, the platelet activation states were two times higher in bileaflet valve than in the monoleaflet valve. Furthermore, the numerical results showed that the shear stress magnitude could be more than four times higher in bileaflet valves.

In 2005, Ge et al. extended their previous work (Ge et al., 2003) by increasing the flowrate to near-peak systole flowrates. The flow was fully turbulent with Re as high as 6000. Two Re numbers were chosen to be modeled,  $Re = 750$  and  $Re = 6000$ . For laminar flow, the Direct Numerical Simulation (DNS) was employed. For turbulent flow, two different models were used (the Reynolds-average Navier-Stokes approach (URANS) and the Detached Eddy Simulation approach (DES)). The DES method is a hybrid technique proposed as a precise approach for predicting separated flows. It combines two concepts: URANS for the entire boundary layer and Large Eddy Simulation (LES) for the separated regions.

To validate their numerical results, they performed experimental measurements using Particle Image Velocimetry (PIV) under the same conditions. For laminar flow, good agreement between numerical and experimental results was observed and the unsteadiness of flow was noticed as early as for  $Re = 350$ . The DES approach was

recommended to study flow in the sinus region as opposed to the URANS approach. URANS showed steady, stable and ring-shaped vortices. On the other hand, DES showed a very complex flow with multiple eddies. The damaging of red blood cells has a direct relation with the number and the form of eddies generated downstream of the valve. For DES results, red blood cells remain for less time inside the vortical field and therefore cause lower blood elements damage.

### **Direct Numerical Simulation (DNS)**

Dasi et al. (2007) studied blood flow through a 23 mm regent St. Jude medical heart valve assuming DNS model and using 10 million nodes and a time step of 0.1 ms. An immersed boundary method was used to track the leaflet movements. The numerical results were validated against 2-D PIV measurements. The comparison was made about the vorticity magnitude and its evolution during the systolic phase. Good agreement was found during the acceleration part of the systolic phase. In the meantime, less accurate agreement was found during the peak and deceleration periods of the systolic phase where the turbulent nature persisted until the late stage of deceleration.

In order to confirm the accuracy of the simulations numerically, the dynamics of the valve leaflets, Nobili et al. (2008) were studied using the ALE method with commercial software (FLUENT) and user-defined functions in order to simulate the flow through a model of 27 mm St. Jude HP mechanical heart valve using strongly coupled FSI. The validation for the numerical simulations was done for the leaflet dynamics and the instantaneous transvalvular pressure gradient through the valve. The simulation

consisted of 2.1 million elements and a time step of 0.2 ms. Furthermore, only two cycles were simulated to guarantee cycle independence.

Recently, De Tullio et al. (2009) simulated blood flow through a 27 mm Sorin-Bicarbon bileaflet mechanical heart valve using the immersed boundary method with Direct Numerical Simulation (DNS). Even though 2.5 million nodes had good accuracy, 6.6 million nodes were adapted for the entire domain. Also, the angular velocity of the leaflets was used to check the convergence with a residual error of approximately  $10^{-4}$ . This could raise questions on the validity of such criteria during the stationary status of the leaflets (around the peak of the systolic phase and during the complete diastolic phase). However, different time instants were depicted during the systolic phase to validate the numerical results using 2-D PIV measurements. Good agreement was found during early stage acceleration, while a less comparative agreement was observed during the deceleration phase. This could be interpreted as a shortcoming of the statistical average for the numerical simulation as, only, 10 cycles were averaged compared to 200 cycles in the PIV measurements. The opening and closure dynamics in the numerical simulations were in very good agreement with the experimental findings. The leaflets were allowed to move in two axial and rotational directions. The asymmetric orientation for the valve and the sinuses create a significant difference between the two leaflets dynamics (the upper leaflet (close from the sinus valsalva) had a 20 ms closing delay time compared to the lower one). Finally, the authors found that the 2-D turbulent shear stress calculations underestimated the turbulent shear stress magnitude especially in the sinus area where the flow is highly three dimensional.

## **1.2 Experimental Studies**

Various clinical *in-vivo* techniques have been introduced to explain the nature of flow and to evaluate heart valve performance including echocardiography, catheterization and Magnetic Resonance Imaging (MRI). Catheterization is an inadequate method to be used for MHV flow analysis (Fukumoto et al., 2003), while echocardiography and MRI represent appropriate techniques for diagnosis. Moreover, these techniques, as well as more advanced techniques such as Particle Image Velocimetry (PIV) and Laser Doppler Anemometry (LDA) have been used *in-vitro* to verify the accuracy of *in-vivo* diagnosis methods and to clarify the nature of the flow downstream of MHVs (Liu et al., 2000; Grigioni et al., 2001; Brucker et al., 2002).

Validation of different techniques through *in-vitro* studies has been studied by different authors. Browne et al. (2000) attempted to demonstrate the difference between LDA and PIV. Steady flow measurements near peak systole were carried out through a St. Jude bileaflet MHV in the aortic position. In addition, maximum turbulent shear stress and maximum turbulent principal stress were studied and compared. Large differences in values and trends (up to 200%) between the two methods were shown. A combination of the two techniques was recommended by using PIV to describe the general flow patterns and using LDA in specific areas to get more detailed and accurate results.

### **1.2.1 Laser Doppler Anemometry (LDA)**

Laser Doppler Anemometry (LDA) was used experimentally to investigate turbulent flow characteristics downstream of different types of bileaflet valves by Liu et al. (2000). St. Jude Medical valves, in addition to CarboMedics and Edwards Tekna valves, were

selected for investigation. The maximum turbulent normal and shear stresses were found to be 7.8 mm downstream of the valve. For the St. Jude bileaflet valve, the maximum Reynolds normal stress was  $1250 \text{ dyn/cm}^2$  (125 Pa) and the maximum Reynolds shear stress was  $510 \text{ dyn/cm}^2$  (51 Pa). Higher values for the CarboMedics bileaflet valve were measured; the magnitude of Reynolds normal and shear stress was  $1780 \text{ dyn/cm}^2$  (178 Pa) and  $680 \text{ dyn/cm}^2$  (68 Pa), respectively. The highest value for Reynolds stress was obtained from the Edwards Tekna bileaflet valve, where the Reynolds normal stress was  $2630 \text{ dyn/cm}^2$  (263 Pa) and the Reynolds shear stress was  $770 \text{ dyn/cm}^2$  (77 Pa). The valve's exposure time was very similar for all three types, and ranged from 1-10 ms. Moreover, the Kolmogorov length scale (the size of the smallest eddies that are responsible for dissipating the energy) of the three valves ranged from  $20\text{-}70 \mu\text{m}$ . As the size of the smallest eddy is significantly larger than the size of a red blood cell, it creates less damage than eddies of sub-cellular scale. Finally, the authors concluded that such combination of turbulent stress, exposure time and Kolmogorov scales could initiate blood cells damage.

Lu et al. (2001) re-evaluated and discussed the reference work by Sallam and Hwang (1984). Sallam and Hwang (1984) claimed that hemolytic thresholds for red blood cell damage in turbulent flow were equal to  $400 \text{ N/m}^2$  and 1 ms for turbulent shear stress and exposure time, respectively. However, by using the same method and two-component LADA, the new suggested values by Lu and co-workers for hemolytic thresholds were found to be  $800 \text{ N/m}^2$  and 1 ms. Moreover, Kolmogorov length scales were estimated to be around  $9 \mu\text{m}$  which is on the same order of magnitude as the size of red blood cells.

Grigioni et al. (2001) focused on the leaflet design in bileaflet valves in terms of flow characteristics and turbulent shear stress levels. The authors studied a Sorin Bicarbon (SB) valve (curved leaflet) and a St. Jude valve (straight leaflet). The same diameter and flow conditions were considered and the velocity profiles for four different positions downstream of the valves were measured. Laser Doppler Anemometry (LDA) was used to measure the velocity profiles downstream of the valves. Significant differences for velocity profiles were observed between the two valves. High shear rates were observed for the SB, but for shorter duration compared to the St. Jude valve, in which lower shear rates with longer residency time are observed. They suggested that the design of the SB valve should be improved to reduce thrombus formation.

### **1.2.2 Particle Image Velocimetry (PIV)**

Brucker (1997) was able to measure a relatively high velocity magnitude using a dual-camera DPIV. The two cameras (master and slave) record a specific illuminated plane with a controlled time delay between both of them. Then, a frame-by-frame cross correlation is made. This method is good when the pulsed and synchronized illumination is not available and the method is also independent of recording frequency. Two different prosthetic valves were tested under the same flow conditions. One valve is the Bjork Shiley monoleaflet mechanical heart valve and the other is the Sorin-Bicarbon bileaflet mechanical valve. A frame rate of 50 Hz and a time delay of 0.2-0.3 ms, was enough to capture the strain rate as well as the vortex formation downstream of the valves.

A new tri-leaflet MHV in aortic position was studied by Bucker et al. (2002) using 2-D Digital Particle Image Velocimetry (DPIV). In addition, a high speed camera was used to capture the leaflet motion during the cardiac cycle. The study showed good consistency between the new MHV and the native valve in terms of flow nature and leaflet closing and opening phases.

The flow patterns downstream of an artificial bileaflet heart valve were investigated by Balducci et al. (2004). A 2-D PIV with Particle Tracking Velocimetry (PTV) was used to estimate the level of shear stress and the particle residential time, respectively. The mean flowrate was 1 L/min ( $V_{max} = 0.625$  m/s). The authors confirmed the importance of combining PTV with the PIV in order to calculate the blood elements' residential time as well as the level of shear stress. The level of shear stress was found to be below the threshold for red blood cells damage.

Using Viscous Shear Stress (VSS) and/or Reynolds Shear Stress (RSS), to investigate the damage of blood elements, is controversial. Therefore, Ge et al. (2008) attempted to study the physical differences between both parameters. Their study was conducted using 2-D high-resolution velocity measurements with a PIV system. The PIV results were compared with 3-D FSI numerical results extracted from Dasi et al. (2007). The blood hemodynamics through a St. Jude 23 mm regent bileaflet mechanical heart valve were investigated. The highest Reynolds Shear Stress (RSS) and Viscous Shear Stress (VSS) values were found during the acceleration phase. The minimum Kolmogorov scale was 42  $\mu\text{m}$ . This is significantly larger than the red blood cells scale ( $\sim 7$   $\mu\text{m}$ ). A significant

difference, in terms of magnitude and location, between the RRS and VSS downstream of the bileaflet valve were found. The study concluded that the RRS is not an adequate physical representative to the level of blood elements damage.

The levels of turbulent and viscous shear stress, for the region downstream of a St. Jude Medical 27 mm bileaflet valve, was investigated by Li et al. (2010) using 2-D DPIV. Due to the limitation in the spatial resolution of the DPIV measurements, the dynamic equilibrium between the resolved and the Sub-Grid-Scale (SGS) energy flux was adopted. The Turbulent Viscous Shear Stress (TVSS), which is proportional to the square root of Reynolds Shear Stress (RSS), was calculated. The magnitude of both RSS and TVSS were 80 and 12 N/m<sup>2</sup>, respectively. They found the shear stress values were significantly lower than the threshold for damaging red blood cells.

Kaminsky et al. (2007) studied the importance of the out-of-plane velocity component downstream of two different prosthetic heart valves (ATS bileaflet valve and monoleaflet valve) using 3-D time resolved (3000 images /second) PIV measurements. They showed that the third velocity component had a minimal impact on the velocity magnitude. However, the third velocity component was more significant in the mono-leaflet case compared to the bileaflet valve, especially around the trailing edges of the leaflets and inside the valsalva sinuses.

### 1.2.3 *In Vivo* Diagnostic Parameters

A list of the most important parameters for evaluation of bileaflet MHVs was given in the recent review papers by Zoghbi et al. (2009) and Bach (2010). In both papers, the authors gave the definition for each parameter and proposed a new procedure for evaluating MHVs (Table 1.1).

Effective Orifice Area (EOA) and Energy Loss Coefficient ( $E_LCo$ ) are parameters for calculating the area of the heart valve. The  $E_LCo$  parameter is associated with the effective orifice area as it includes the pressure recovery phenomenon (Garcia et al., 2000):

$$E_LCo = \frac{(EOA * AoA)}{(AoA - EOA)} \quad (2.1)$$

where AoA is the cross-sectional area of the proximal ascending aorta.

Doppler Velocity Index (DVI) is the ratio of the left ventricle outflow tract velocity to the maximum velocity through the heart valve.

It is worth noting that the parameters being used for evaluating bileaflet MHVs (3 orifices) are exactly the same as for the native heart valves (single orifice). Therefore, all parameters and equations are derived based on assuming the existence of only one orifice (the central orifice) for the MHV as well as for the native valve.

Some remarks on the use of current diagnostic techniques are highlighted below.

Most parameters are valve size dependent except the Doppler Velocity Index (DVI). Generally, the Effective Orifice Area (EOA) and the Energy Loss Coefficient ( $E_LCo$ ) are proportional to valve size. Therefore, only the combination of valve size and the parameter value are useful. However, published works on the reference values for

different parameters are inconsistent with each other. (Zoghbi et al., 2009; Rosenhek et al., 2003). Moreover, the two lateral orifices are not included in the calculations or taken into account in the evaluation process. Hence, the physical flow through the complete MHV is not accurately represented in the current methods. Therefore, revisiting the assumptions and the theory behind current methods are critical in order to include the flow through the two lateral orifices and to investigate its influence on the measurements' accuracy.

Table 1.1 List of the most used diagnosis parameters for MHV.

<b>Parameter</b>	<b>Lateral Orifices in Calculations</b>	<b>Flow Dependence</b>	<b>Valve Size Dependence</b>	<b>Note</b>
<b>Peak and Mean Pressure Gradient</b>	Not considered	Dependent	Dependent	-Peak pressure gradient is less accurate than the mean ( left ventricle contractility and the transvalvular flow)
<b>EOA</b>	Not considered	Independent	Dependent	-EOA < 0.8 cm <sup>2</sup> ( significant stenosis ) -Depends on the ability of measuring the left ventricle outflow tract area.
<b>Doppler Velocity Index (DVI)</b>	Not considered	Independent	Less dependent	-DVI < 0.25 (significant obstruction). -Sensitive only to severe stenosis. -No need to measure LVOT area
<b>Energy Loss Coefficient (E<sub>L</sub>Co)</b>	Not considered	Independent	Dependent	-Accounts for pressure recovery phenomenon. - Usually > EOA (Garcia et al., 2000)

The main conclusions of the literature review could be addressed based on the used methods (numerical studies and experimental studies).

The main conclusions from the numerical studies could be addressed as follows:

1. Among different prosthetic heart valves, bileaflet MHV was the main subject of recent studies (the most implanted prosthetic valves).
2. The laminar assumption is not adequate for representing the physiological flow. Although it can be included to depict the features of the main flow features, the results cannot be used to give an accurate correlation between the pathological conditions and the simulated flow. Therefore, it is highly recommended to avoid using the laminar assumption when possible.
3. The turbulence models (especially  $k-w$  and LES models) were significantly better at simulating physiological flowrate range compared to the laminar model. The models are often used for validation against PIV, LDA and MRI.
4. Recently, with a significant improvement in computer technology and parallel computing, the DNS became achievable with reasonable accuracy.
5. It is worth noting that the majority of the studies are dedicated to investigate the performance of normal (healthy) MHVs. However, it is important to evaluate the dysfunctional MHVs as well.

The main conclusions from the experimental studies can be addressed as follows:

1. Clinical complications (i.e., thrombus formation, left ventricle function) due to the presence of bileaflet dysfunction in mechanical heart valves have not been investigated yet.

2. The above *in-vitro* methods appear to be inferior in predicting flow or acquiring quantitative information within the valve housing or near the wall and the need for numerical simulation arises as a promising tool for better understanding the dynamics of blood flow through MHVs.
3. The diagnostic parameters for the native aortic heart valve are being used for the mechanical valves as well. However, using the parameters for MHVs is not as accurate as using them with the native heart valves. Many limitations (i.e., flow and valve size dependence) were mentioned in the literature and the need for new diagnostic parameters is essential.
4. Using 3-D PIV for testing a dysfunctional mechanical heart valve is necessary (the out of plane velocity component is expected to have a significant contribution to velocity magnitude compared to healthy mechanical heart valves).

## Chapter 2

### **Potential Clinical Complications Associated With Dysfunction of Bileaflet Mechanical Heart Valve: CFD and *In Vitro* Study**

In the current chapter, the clinical consequences of the presence of Bileaflet Mechanical Heart Valve (BMHV) dysfunction was explored in terms of level of damage for the bloods elements (e.g, platelet activation), and also, the impact of such dysfunction on the accuracy of Doppler measurements (peak velocity, mean pressure gradient, and peak pressure gradient). The current point of research was approached numerically considering two phase flow and using pulsatile 2-D turbulence model. Also *in vitro* test was conducted using custom-made cardiac simulator with a Doppler echocardiographic measurements.

#### **2.1 Introduction**

Dysfunction of Bileaflet Mechanical Heart Valve (BMHV) is a serious and potentially fatal complication. The incidence of dysfunction with this type of prosthesis is 0.2–6% patients/year (Montorsi et al., 2003). The restriction of the motion of the leaflet(s) may be due to pannus in-growth (prevalence 0.14–0.65% patients/year (Sakamoto et al., 2006)) and/or thrombus formation. Several non-invasive medical imaging modalities, including Doppler echocardiography, magnetic resonance, computed tomography, and

cindefluoroscopy may be used to detect BMHV dysfunction and quantify its severity. However, these modalities have important limitations from theoretical, technical, and logistic standpoints. In particular, it is often difficult or impossible to discriminate with the currently available diagnosis techniques, a normally functioning BMHV from a dysfunctional BMHV with mild severity that may become life-threatening in the short-term (Pibarot and Dumesnil, 2009). Moreover, the potential impact of a dysfunctional BMHV on blood components (red blood cells, platelets and coagulation factors) remains relatively unexplored.

Most previous numerical and experimental studies of BMHVs have focused on normally functioning valves with an emphasis on the velocity field, transvalvular pressure drop and blood components damage. In previous numerical studies, the flow downstream of a normal BMHV was investigated under steady state flow conditions (Ge et al., 2003) and pulsatile flow conditions with or without Fluid-Structure Interaction (FSI) (Grigioni et al., 2005; Pedrizzetti and Domenichini, 2006; Alemu and Bluestein, 2007). It should be noted that in most studies where FSI was considered, the flow through the BMHV was assumed to be laminar (Guivier et al., 2007; Redaelli et al., 2004; Dumont et al., 2007). Recently, Direct Numerical Simulation (DNS) with fully FSI was performed by Dasi et al. (2007) and Nobili et al. (2008). It should be noted, however, that application of DNS to clinical problems is limited due to its high computational cost.

Most numerical and experimental studies on BMHV showed that the flow is characterized by trailing vortices arising from the leaflets and high levels of turbulent and wall shear stresses, usually many times higher than the physiological ones (Ge et al.,

2005; Ge et al., 2008; Dasi et al., 2007), potentially leading to blood component damage.

The disturbances of flow downstream of a normal BMHV should be magnified in the presence of leaflet prosthesis dysfunction. There are very few *in silico* or *in vitro* studies examining the effect of BMHV dysfunction on flow pattern. Baumgartner et al. (1993) showed, *in vitro*, that a dysfunctional BMHV (Carbomedics valve with one leaflet blocked) leads to an increase in the energy loss through the valve and a significant difference between Doppler and catheter gradients. This was confirmed numerically in a recent study performed by Smadi et al. (2009).

The objective of this study is to numerically and experimentally investigate the pulsatile turbulent flow downstream of a dysfunctional BMHV in terms of velocity field, diagnosis limitations and potential negative effect on blood components.

## **2.2 Models and Methods**

### **2.2.1 Numerical Method**

Five 2-D 25 mm St. Jude Medical Hemodynamic Plus valve models were created for the purpose of this study. The restriction of the leaflet motion was applied only on one of the 2 leaflets (as it often occurs in the clinical setting). The position of the leaflet was varied from the fully opened position (opening angle =  $85^{\circ}$ ; normal function) to the fully closed position (angle =  $30^{\circ}$ ; 100% dysfunction) with three equally spaced intermediates. It should be noted that the current study focuses only on dysfunction affecting only one leaflet, given that this is the most frequent situation in the clinical setting and that it is

more difficult to detect when compared to the situation where both leaflets have restricted motion (Montorsi et al., 2003).

The simulations were performed under unsteady state conditions with an experimental pulsatile flow as inlet condition (Fig. 2.1) and ambient pressure at the outlet. The mean cardiac output was 5 L/min and the heart rate was 70 bpm (systolic phase duration 0.3 s). Blood was simulated as a Newtonian fluid with a density of  $1060 \text{ kg/m}^3$  and a dynamic viscosity of  $0.0035 \text{ Pa s}$ . The assumption of a Newtonian fluid behavior is realistic for blood flow in large arteries such as the aorta (Morris et al., 2005). The inlet conditions corresponded to a  $Re_{\text{max}} = 7969$ ,  $Re_{\text{average}} = 3820$  and Womersley number = 16.2.

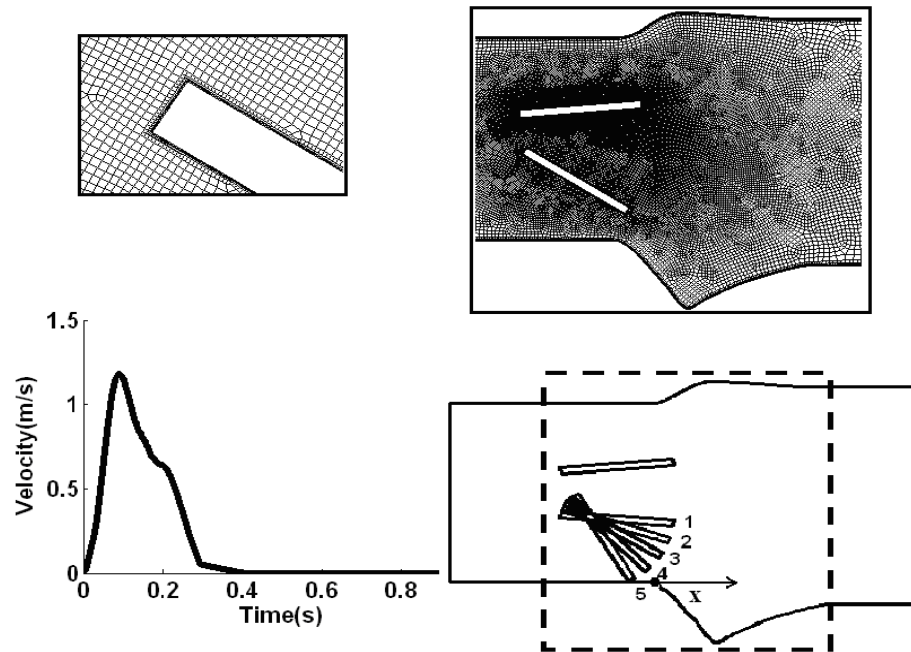


Figure 2.1 Models for the five different cases: 1) 0% dysfunction; 2) 25% dysfunction; 3) 50% dysfunction; 4) 75% dysfunction; 5) 100% dysfunction.

The Wilcox's low-Reynolds model (Wilcox, 1998) was used to simulate the flow during the complete cardiac cycle. However, the interaction between the valve leaflets and the fluid was not considered. As a consequence, the opening and closure dynamics were not simulated properly in this study. Therefore, only the fully opening period (from 60 ms to 250 ms) was analyzed in the results section (Alemu and Bluestein, 2007).

Commercially available software (Fluent 6.3.26 - Fluent Inc.; Lebanon; NH; USA) was used to perform the numerical simulations. Although blood flow through a BMHV is characterized with laminar-transitional-turbulent behavior, the Wilcox's low-Reynolds model was found able to accurately predict its main flow characteristics (Bluestein et al., 2000).

### **Turbulence Model**

In the present study, time-averaging or Reynolds averaging has been used as a mean of analyzing turbulence by separating fluctuating properties with their time-mean values. Thus, the true velocity ( $u_i$ ) is defined by:  $u_i = \bar{u}_i + u'_i$ , where the overbar refers to time-average and prime refers to fluctuation from this average. When this is substituted in the general Navier-Stokes equations, a new term will be introduced, i.e., the Reynolds stresses ( $-\rho \overline{u'_i u'_j}$ ). To close the governing equations with the new extra variables, two-equation transitional  $k - \omega$  model was used through which these Reynolds stresses are approximated using the Boussinesq relation for incompressible flow (Wilcox, 1998)

$$-\rho \overline{u'_i u'_j} = \mu_t \left( \frac{\partial u_i}{\partial x_j} + \frac{\partial u_j}{\partial x_i} \right) - \frac{2}{3} \left( \rho k + \mu_t \frac{\partial u_i}{\partial x_i} \right) \delta_{ij} \quad (2.1)$$

where  $u_i$  is the average velocity in  $i$  direction,  $\mu_t$  is the turbulent eddy viscosity and  $k$  is the turbulent kinetic energy.

A second-order upwind scheme was selected to be the discretization scheme for the convection terms of all governing equations. For all transient calculations, a second-order temporal discretization scheme was used. The mass-momentum equations were solved using the COUPLED solver and all results were converged to residuals of  $< 10^{-4}$ , unsteady simulation in general required 15-25 iterations per time step. Moreover, additional care was taken close to the wall and leaflet surfaces to maintain  $y^+ \ll 1$ . The time step was set to 0.25 ms to satisfy time step independency. Three cycles were simulated before starting extraction of the results in order to reach the periodicity.

### **Discrete Phase Model**

In order to calculate the level of platelet activation ( $\sum \tau * \Delta t$ ) (summation of shear stress magnitude multiplied by the exposure time) across different paths, a Lagrangian approach of particulate two phase flow was used. This model has been used and described in details by Bluestein et al. (2000).

Briefly, at each time instant, the absolute value of total shear stress (laminar and turbulent) was taken into account using Boussinesq approximation ( $\tau = \mu \partial u / \partial y - \rho \overline{u'v'}$ ) and multiplied by the exposure time ( $\Delta t$ ), then the summation of the results of all time instants during the selected period was calculated.

In order to show the effect of valve dysfunction on the platelet activation level, the calculations were carried out during the deceleration phase (0 - 50 ms after the peak and 100 - 150 ms after the peak). Therefore, the results did not depict the platelet activations in the entire diastolic phase but rather depicted the platelet activation level wherein flow conditions predispose to platelet aggregation (Alemu et al., 2007).

## Numerical uncertainties

Steady flow simulations were conducted first to establish the grid density. The uncertainty and error in the study was found following the recommendations suggested by Celik et al. (2008). Table 2.1 and figure 2.2 show the calculations for the discretization error of the maximum velocity value in the entire field and velocity profile at the vicinity of the valve, respectively.  $N$  is the number of elements,  $r$  is the refinement ratio,  $p$  is the apparent order,  $\phi_{ext}$  is the extrapolated value,  $e_a$  is the apparent error,  $e_{ext}$  is the extrapolated error and  $GCI_{fine}$  is the fine-grid convergence index. According to the maximum velocity in the entire field,  $GCI_{fine}$  was 0.09% which does not account for modeling errors. In addition, figure 2.2 shows the axial velocity profile at the vicinity of the valve. The local order of accuracy  $p$  ranges from 0.5 to 11 with a global  $p$  average 1.6. The maximum discretization uncertainty was 6% in the area close from the dysfunctional leaflet.

### 2.2.2 Experimental Method

In order to investigate the accuracy of the conventional Doppler-echocardiographic measurements in detecting the dysfunction of BMHV and also to validate and compare some of the results obtained with the numerical study, Doppler echocardiographic measurements were performed in a mock flow model incorporating a BMHV with various degrees of dysfunction.

The mock flow circulation model used in this *in vitro* study has been described and validated (Garcia et al., 2003) (Fig. 2.3). The model is mainly made up of a reservoir, a compliant aortic chamber and a valve resistance. The flow was provided by a computer

Table 2.1 Calculations of discretization error  
 $\phi = \text{Maximum velocity in the entire field (m / s)}$

$N_1, N_2, N_3$	299,848, 177,650, 100,450
$r_{21}$	1.299
$r_{32}$	1.3300
$\phi_1$	2.844237
$\phi_2$	2.849587
$\phi_3$	2.879322
$p$	5.8921
$\phi_{ext}^{21}$	2.8422
$e_a^{21}$	0.19%
$e_{ext}^{21}$	0.072%
$GCI_{fine}^{21}$	0.09%

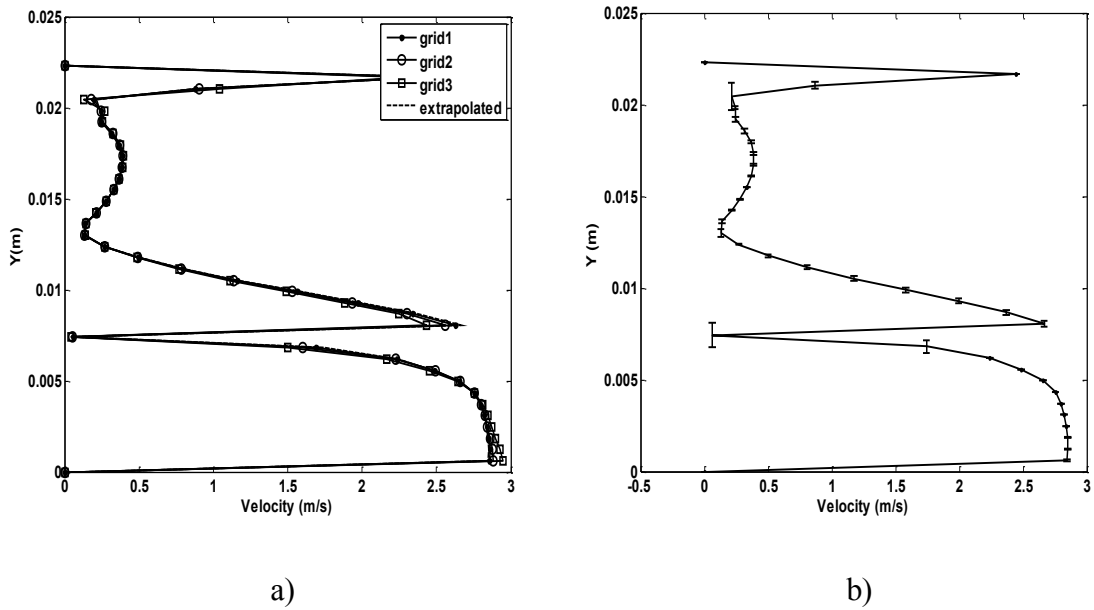


Figure 2.2 (a) Velocity profile at the vicinity of the valve for different grid solutions; (b) Fine-grids solution with discretization error bars.

controlled DC motor coupled to a gear pump (Vi-CORR, Viking Pump). The left ventricular outflow tract and the aorta were both circular and rigid (cross sectional area =  $8 \text{ cm}^2$ ). The compliant chamber was located immediately downstream of the proximal rigid aorta. The fluid was composed of 2/3 water and 1/3 of glycerol so that its density ( $1080 \text{ kg/m}^3$ ) and viscosity (3.5 cP) were similar to that of blood under high shear rate conditions. The flowrate was measured by an electromagnetic flowmeter (Cliniflow II, Carolina Medical Electronics, accuracy 5% full scale) and the ventricular and aortic pressures with Millar catheters (model MPC 500, accuracy 0.5% full scale) under a sampling frequency of 1000 Hz. For each experiment, 10 cycles were recorded and the average was used to calculate the hemodynamic parameters.

For all experiments, the transvalvular flowrate was maintained at 5 L/min, corresponding to a stroke volume of approximately 70 mL for a heart rate of 70 bpm (ejection phase: 0.3 s). Systolic and diastolic pressures were maintained under normal conditions: 120 mmHg and 80 mmHg, respectively.

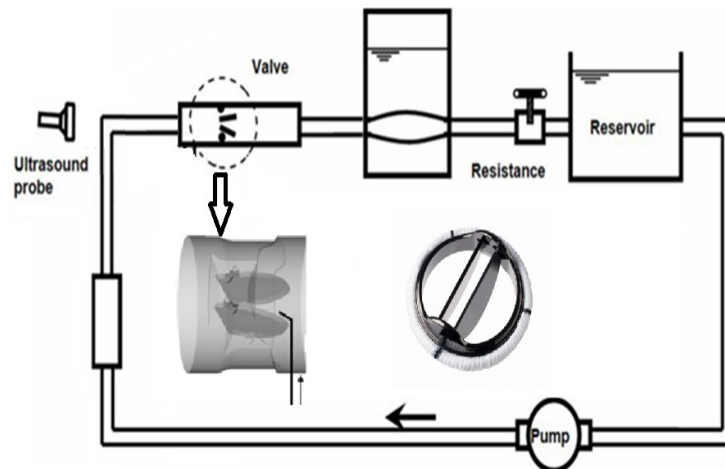


Figure 2.3 (a) Schematic representation of the mock flow model and the alteration mechanism of the lower leaflet opening position using a small stop pin.

### **3.2.2.1 Doppler Echocardiographic Measurements**

Doppler echocardiographic velocity measurements were performed using a Sonos 5500 (Philips Medical Systems/Agilent Technologies, Andover, Massachusetts) with a probe of 2.25 MHz. The probe was oriented to obtain optimal alignment of Doppler beam and flow across the central orifice of the BMHV. In order to avoid aliasing, the continuous-wave Doppler mode was used. The measurements were performed over five to seven cycles and averaged. Maximal Doppler-echocardiographic velocity, mean and maximal transvalvular pressure gradients (determined using simplified Bernoulli equation) were evaluated for the BMHV with 0%, 50% and 100% degrees of dysfunction. These results were compared to the ones obtained from the numerical study.

## **2.3 Results**

### **2.3.1 Doppler-echocardiographic Measurements**

Figure 2.4a shows the maximum velocity magnitude at the peak of systolic phase for different degrees of dysfunction using Doppler-echocardiographic velocity measurements and numerical simulation. It should be mentioned that for Doppler-echocardiography, the ultrasound beam is usually conically-shaped and its axis was aligned with the central orifice (the traditional method). As a consequence, the results obtained using Doppler-echocardiography for the maximum instantaneous velocities were compared with the maximum instantaneous velocity obtained numerically through the entire domain.

In the healthy model, there was a good agreement between numerical and experimental results with percentage of difference less than 1.3%. When a dysfunction was induced on the lower leaflet, a discrepancy, proportional to the severity of the dysfunction, appeared

between the experimental (Doppler-echo) and numerical results for maximum velocity. This difference reached up to 15% for 100% dysfunction.

Figure 2.4b shows the maximum transvalvular pressure gradient ( $TPG_{max}$ ) and mean transvalvular pressure gradient ( $TPG_{mean}$ ), for different percentage of dysfunction. The TPGs were determined using the standard simplified Bernoulli equation ( $TPG = 4V^2$ ).

$TPG_{max}$  is a function of the square of maximum velocity ( $TPG = 4V_{max}^2$ ). Therefore, the numerical and experimental  $TPG_{max}$  results have the same trend as for the maximum velocity but with a magnification of the percent difference (2.6%-32.2%). On the other hand, in both 0% and 50% dysfunctions, the numerical  $TPG_{mean}$  magnitude was lower than the echo-Doppler  $TPG_{mean}$  magnitude. This could be explained as a result of the absence of FSI in the current numerical simulation. For 100% dysfunction, the FSI effect was limited due to movement of only one leaflet and as a consequence the numerical  $TPG_{mean}$  magnitude was higher than the echo-Doppler one.

### **2.3.2 Platelet Activation**

Figure 2.5 shows estimated platelet trajectories for different percentages of dysfunction downstream of the BMHV during two different periods of the deceleration phase. Figure 2.5.a shows platelets paths from 0-50 ms after peak systole instant and figure 2.5.b shows platelets paths from 100-150 ms after peak systole instant. Eighteen equally spaced positions across the valve were selected to inject the platelets at 0 and 100 ms after the peak and the results were depicted after 50 ms from the injection time.

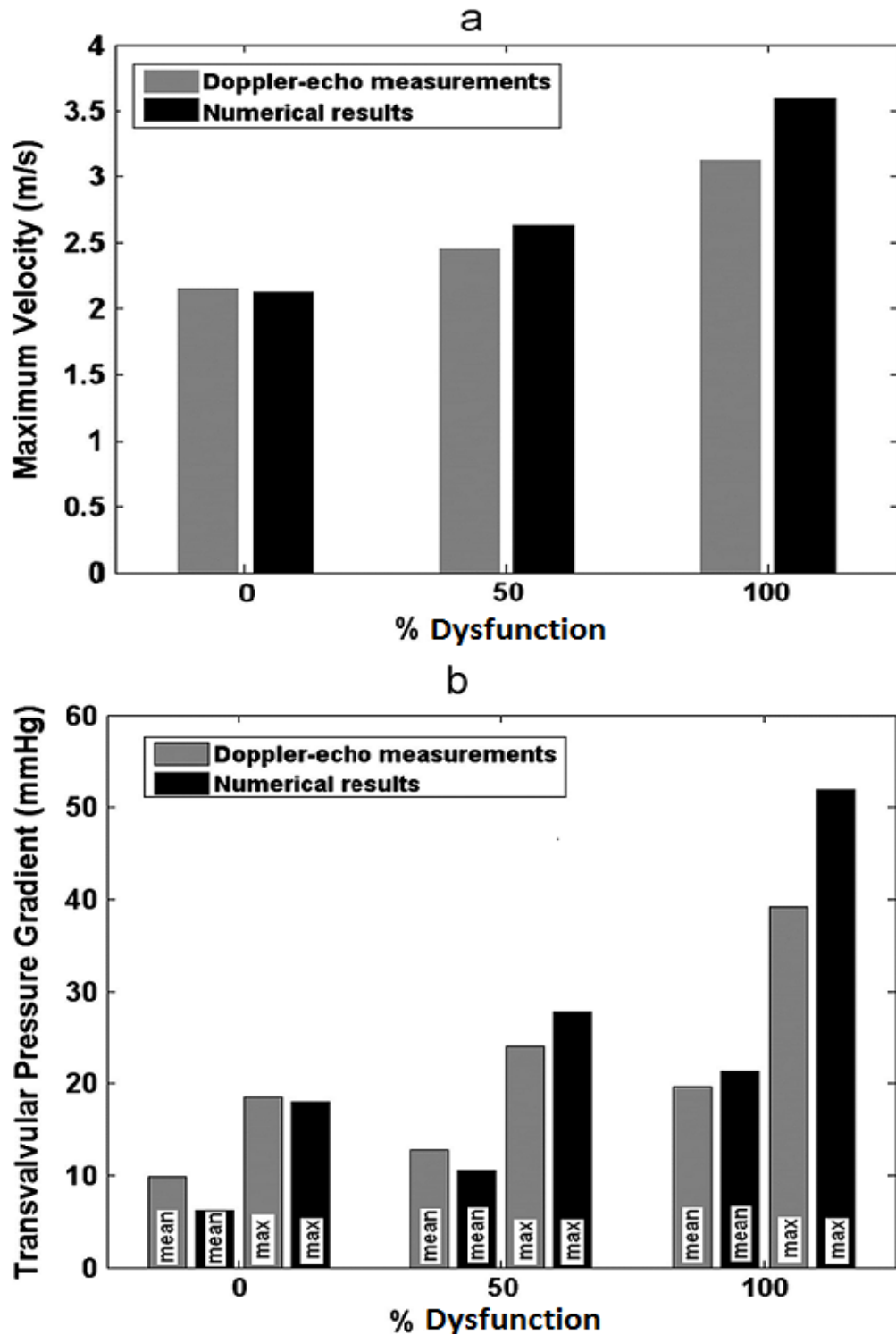
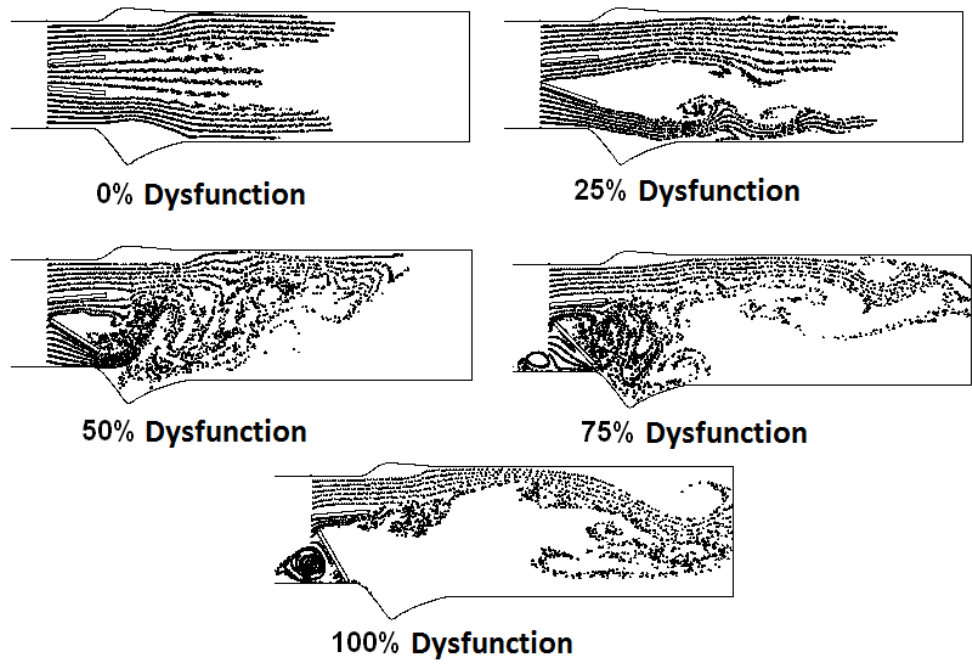
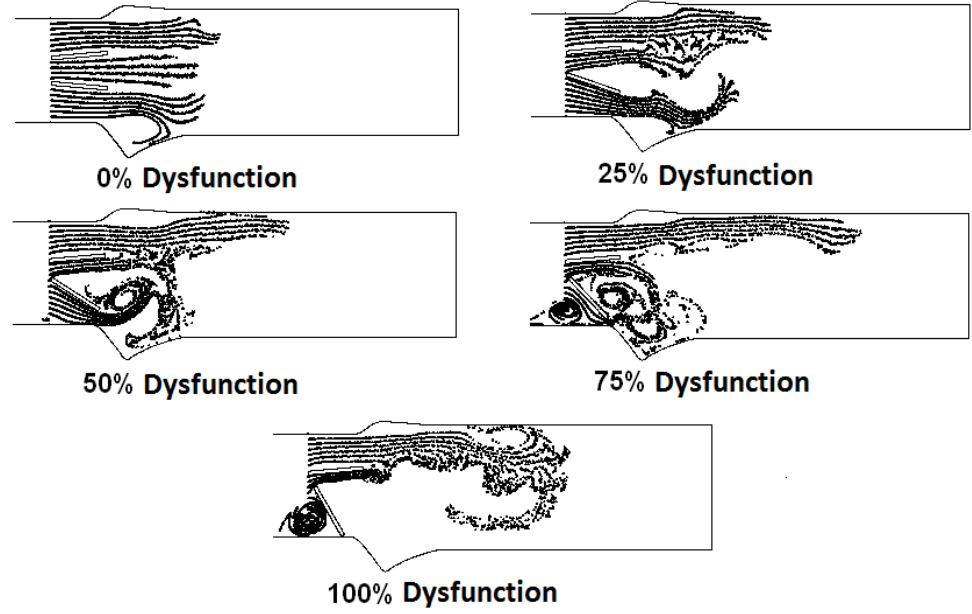


Figure 2.4 Comparisons between numerical and Doppler-echocardiographic results; (a) maximum velocity; (b) the mean and the maximum transvalvular pressure gradients (TPG).



a)



b)

Figure 2.5 Comparison of platelets paths downstream of the valve during the deceleration phase a) 0-50 ms after the peak b) 100-150 ms after the peak and for different percentages of dysfunction.

Platelet paths changed significantly with increasing the percentage of BMHV dysfunction. As a consequence of the development of a more vortical flow due to bottom leaflet dysfunction, platelets might be trapped in some regions of the domain, thereby increasing significantly the residential time. Hence, even if the turbulent shear stress is generally low in these regions, the level of platelets activation may be significant. Another important result is that with increasing valve dysfunction, the platelets on the normal leaflet side travel farther in the domain (due to a higher velocity), except for a 100% dysfunction, where the interaction between the upper-lateral jet and the recirculation zone developed downstream of the valve limits the displacement of the platelets by redirecting them to the regions of lower turbulent shear stresses.

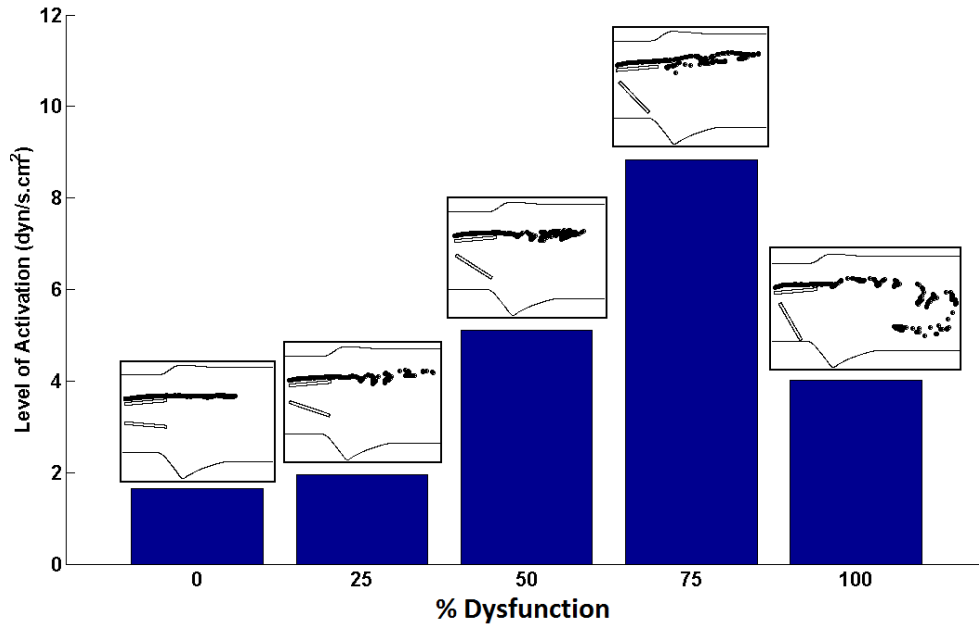
Figure 2.6a and 2.6b show the level of platelet activation as calculated by  $(\sum \tau * \Delta t)$  during the deceleration phase (100 ms to 150 ms after the peak of the systolic phase) for particles released near the outer edge of the upper leaflet (normal leaflet) (Fig. 2.6a) and near the inner edge of the bottom leaflet (dysfunctional leaflet) (Fig. 2.6b). The level of platelets activation was determined for different dysfunction severities (from 0% to 100%). For the particles released near the outer edge of the upper leaflet, the highest level of activation was obtained for a 75% dysfunction (8.7 dyne.s/cm<sup>2</sup>). This value is five times higher than that of the healthy case and it is higher than that of a fully closed leaflet. This can be explained by the fact that in a partially blocked leaflet, the platelets were trapped in the wake of the trailing edge where the level of shear stress is relatively high. On the other hand, in the fully dysfunctional leaflet, the platelets escaped away from the wake of the leaflet region to the core of the flow where the shear stress is relatively lower.

## 2.4 Discussion

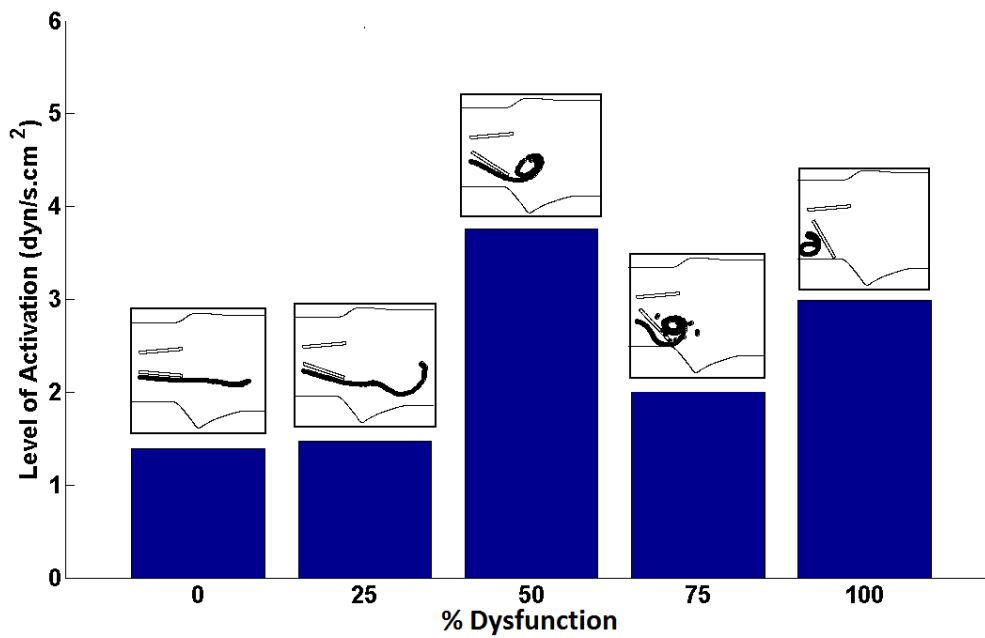
### 2.4.1 Clinical Diagnosis

In the clinical setting, the evaluation of BMHV function is usually performed using Doppler echocardiography. Maximum velocity of the forward flow is measured by positioning the ultrasound wave beam through the valve. Only the instantaneous maximum velocity is used to determine the transvalvular pressure gradient and effective orifice area (EOA). However, in order to get accurate measurements, it is very important to align the ultrasound beam with the flow direction (Doppler Effect). Furthermore, clinicians usually tend to position the axis of the Doppler beam within the center of the valve. In the case of normally functioning BHMV, the maximum velocity is similar in the 3 orifices. However, in the case of a completely dysfunctional leaflet, the flow is shifted towards the normal leaflet and the maximal velocity is through the lateral orifice along the wall. The Doppler beam aligned on the central orifice may miss the maximum velocity that is displaced laterally. This may explain the discrepancy between peak gradient measured by Doppler echocardiography and that obtained by numerical simulation in the case of severe prosthesis dysfunction (Fig. 2.4).

In contrast, the difference in  $TPG_{\text{mean}}$  was the highest in the healthy case. This could be explained by the fact that the fluid-structure interaction has not been simulated in this study, and as the  $TPG_{\text{mean}}$  is calculated through the whole systolic phase, as a result, a percentage of error is expected during the opening and closure of the valve. For this reason, the effect of neglecting FSI on  $TPG_{\text{mean}}$  is less significant with higher percentage of dysfunction.



(a)



(b)

Figure 2.6 Platelets level of activation during the deceleration phase (100-150 ms after the peak) for different percentages of dysfunction. (a) Particles released from the upper valve orifice, (b) Particles released from the lower valve orifice.

Consequently, clinicians should pay attention to seek the maximum velocity by shifting the Doppler beam from central to lateral, and this should be done on both sides

#### **2.4.2 TSS and Residential Time (Platelet Activation)**

Turbulent shear stress level and position will change in the case of a dysfunctional BMHV. In 50% dysfunction of one leaflet, the relatively high shear stress areas covered most of the domain downstream of the valve. Therefore, the number of blood elements that will be exposed to high shear stress level is higher in the case of partially dysfunctional leaflet than in the case of normal function or of a leaflet blocked in the fully closed position. Furthermore, the increase in the number and scale of vortices downstream of the valve will lead to an increase in the residential time of blood elements in these high shear stress regions. As a result, the level of platelet activation and thrombus formation can increase significantly. Interestingly, this study shows that the level of platelet activation is markedly increased at moderate levels of dysfunction, which may predispose to worsening of thrombosis or de novo thrombosis. Hence, this could lead to a vicious cycle where the abnormal flow pattern caused by mild or moderate degrees of dysfunction creates favorable conditions for thrombus formation on the valve, which in turn worsens the valve dysfunction.

It is worth to mention that the potential of blood hemolysis was considered early in the study conducted by smadi et al. (2009) where they concluded that the maximum shear stress in the presence of 100% dysfunction (205 Pa) did not reach the hemolytic threshold (400 N/m<sup>2</sup> and 1 ms) that suggested by Sallam and Hwang (1984). Therefore, only platelet activation state was depicted.

## **2.5 Conclusion**

In conclusion, this study showed that the flow upstream and downstream of a dysfunctional mechanical heart valve was highly influenced by dysfunction severity and this resulted in discrepancies between the Doppler echocardiographic and numerically derived transvalvular pressure gradients. Moreover, the flow downstream of the dysfunctional valve was characterized by abnormally elevated shear stresses and large-scale vortices. These characteristics can predispose to blood components damage. Finally, from a clinical point of view, clinicians should try, when possible, to check the maximal velocity position not only at the central orifice but also through the lateral orifices. Finding the maximal velocity in the lateral orifice could be an indication of valve dysfunction.

## Chapter 3

### **Bileaflet Prosthetic Heart Valve Disease: Numerical Approach Using 3-D Fluid-Structure Interaction Model with Realistic Aortic Root**

Certain assumptions were made in the numerical simulations in chapter two, including two-dimensional flow (2-D), immobile leaflets, and non-realistic valsalva sinuses. The impact of such simplifications on clinically-related outcomes has not been clarified yet. In this chapter, three-dimensional (3-D) blood flow in the presence of fluid-structure interactions was simulated. Realistic aortic root geometry was created for this purpose.

#### **3.1 Introduction**

Valve stenosis or incompetence at severe levels reduce the performance of the heart and place additional stress and strain upon it. In many cases, surgical replacement of the diseased valve with a bioprosthetic or mechanical heart valve is necessary to restore normal heart function. Due to their longer lifespan, around 50% of valve replacements worldwide are mechanical heart valves. Usually, a patient with a Bileaflet Mechanical Heart Valve (BMHV) must take lifelong anticoagulant medication due to the risk of thromboembolic complications, which can restrict leaflet movement. Another potential complication associated with mechanical valves is pannus formation (Montorsi et al., 2003). Non-invasive diagnosis and evaluation of the severity of BMHV dysfunction using Doppler echocardiography and magnetic resonance imaging is not straight forward, usually due to theoretical, technical or accessibility limitations. It is important, therefore,

to investigate the flow downstream of a dysfunctional BMHV and to investigate the limitations of current diagnostic techniques.

Most numerical and experimental studies on BMHVs have focused on normal functioning valves with high emphasis on the velocity field, transvalvular pressure drop and blood components damage. Numerically, different approaches were considered. For the geometry, 2-D and 3-D analysis were conducted with simple or realistic aortic root. Also, a simple aortic arch (straight tube) and a realistic curved arch were considered. In addition, both steady and pulsatile flows were simulated. Generally, steady flow was used to study flow at the peak of the systolic phase, while pulsatile flow was concentrated more on the whole cardiac cycle with more than one of the three phases (acceleration, peak and deceleration phases) (Yoganathan et al., 2004; Bluestein et al., 2010).

Recently, Direct Numerical Simulations (DNS) with full FSI were performed by Dasi et al. (2007), Nobili et al. (2008) and De Tullio et al. (2009). However, the high computational cost required for DNS, limits its applicability to practical clinical problems.

Finally, few studies investigated the blood flow through an obstructed BMHV. Baumgartner et al. (1993) showed, *in vitro*, that a dysfunctional BMHV (Carbomedics valve with one leaflet blocked) led to an increase in energy loss through the valve resulting in a significant discrepancy between catheter and Doppler echocardiographic transvalvular pressure gradients. This reduction resulted from a less significant pressure recovery downstream of the dysfunctional BMHV. This was confirmed numerically, in a recent study performed by Smadi et al. (2009) where the authors also suggested new

diagnostic parameters to investigate non-invasively the severity of BMHV dysfunction using Doppler echocardiography and magnetic resonance imaging.

In the current study, blood flow patterns downstream of healthy and dysfunctional BMHVs is investigated by conducting 3-D FSI simulations and using realistic aortic roots. In addition, the development of coherent structures is investigated. Clinically, the maximum pressure gradient is compared to 2-D numerical simulation and *in vitro* measurements.

### **3.2 Numerical Method**

A 3-D model for 25 mm St. Jude Medical Hemodynamic Plus valve was created and implanted in a 3-D realistic aortic root. The restriction on leaflet motion was applied only to one of the two leaflets (Smadi et al., 2010). The position of the leaflet was varied from the fully opened position (normal function) to the fully closed position (100% dysfunction) with one intermediate position (50% dysfunction) (Fig. 3.1).

The dysfunction was present only during the leaflet opening phase (stenosis) while the leaflet is functioning properly during the closure (no extra regurgitation). This is consistent with *in vivo* findings by Aoyagi et al. (2000).

The simulations were performed under unsteady conditions with an experimental pulsatile flow as the inlet condition (Fig. 3.1) and ambient pressure at the outlet. The mean cardiac output was 5 L/min and the heart rate was 70 bpm (systolic phase duration 0.3 s). Blood was simulated as a Newtonian fluid with a density of 1060 kg/m<sup>3</sup> and a dynamic viscosity of 0.0035 Pa s. The assumption of a Newtonian fluid behavior is

realistic for blood flow in large arteries such as the aorta (Morris et al., 2005). The inlet conditions corresponded to a  $Re_{max} = 8934$ ,  $Re_{average} = 3820$  and Womersley number = 16.2.

### 3.2.1 Turbulent-FSI Approach

The current simulation was carried out using commercial software (FLUENT) and adapted the Arbitrary Lagrangian Eulerian method (ALE) for re-configuring the mesh of the fluid domain after the solid part (the leaflets) moved to a new position. Meshing the geometry was done by GAMBIT 2.4 (Fluent Inc.) and by using 2.5 million elements. This method was used and validated by Dumont et al. (2004), Dumont et al. (2007) and Nobili et al. (2008).

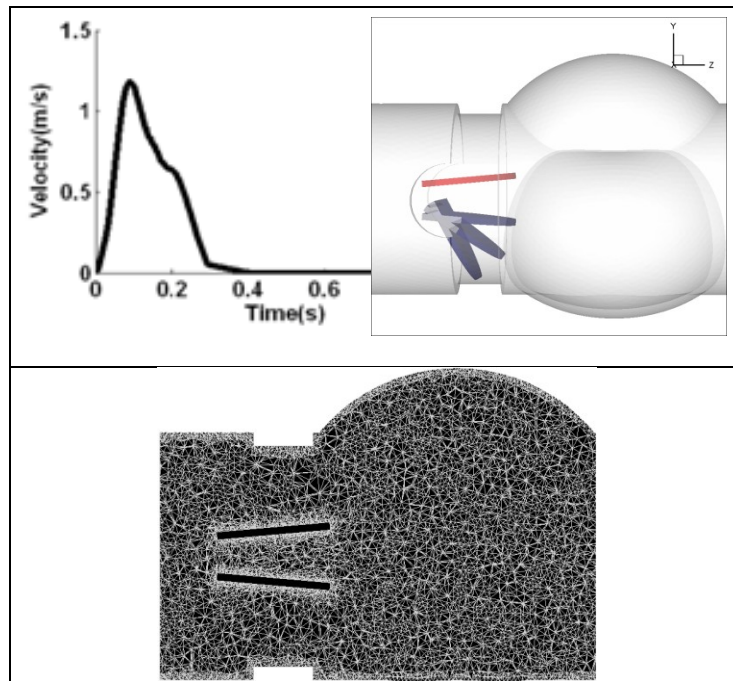


Figure 3.1 The geometry (high right corner) and the mesh quality (lower part) of 25 mm St. Jude hemodynamic Plus (SJHP) with the instantaneous velocity (high left corner) as an inlet condition.

In the present study, two-equations transitional  $k-\omega$  model was used to capture the laminar-transitional-turbulent flow phenomenon (See chapter two). A second-order upwind scheme was selected to be the discretization scheme for the convection terms of all governing equations. For all transient calculations, a second-order temporal discretization scheme was used. The mass-momentum equations were solved using the PISO solver and all results converged to residuals of  $< 10^{-4}$ . Unsteady simulations generally required 5-10 iterations per time step. Moreover, additional care was taken close to the wall and leaflet surfaces to maintain  $y^+ \ll 1$ . The time step was set to 0.05 ms and two cycles were simulated before starting extraction of the results.

The motion for the leaflets is assigned and controlled by an external subroutine based on experimental data extracted from a high-speed camera. The angular velocity for the leaflets was kept the same for all cases. The full nonlinear fluid-structure interaction was not considered. Moreover, the scope of the current study was to evaluate the influence of valve dysfunction on the blood flow downstream of the MHV and to compare the healthy and the dysfunctional cases with each other.

### **3.3 Results and Discussion**

#### **3.3.1 Velocity Contours**

Figure 3.2 shows axial velocity contours for three different percentages of dysfunction and at two different instants. In the healthy model (0% dysfunction), the orientation of the valve leaflets in the flow field created two wakes and three jets (one central and two laterals). Also, a circulation zone within the sinus area was detected and represented with a negative value for the axial velocity.

The strength of rotation within the sinus area was proportional to the percentage of dysfunction. The negative axial velocity magnitude reached the maximum with the 100% dysfunction case ( $V_{\text{axial}} = -1.5$  m/s). Moreover, more circulation zones appeared with increased dysfunction severity.

Introduction of a 50% dysfunction to one leaflet significantly disturbed the flow downstream of the MHV. Although the three jets still existed, the velocity profile distribution was different from the healthy model. The central and upper lateral jets moved closer to each other by shifting the central jet peak velocity towards the upper lateral side, while the lower lateral jet moved towards the wall. For 100% dysfunction, the flow behavior is close to the 50% dysfunction case except with only two dominant central and upper lateral jets instead of the three jets. It was clear that the central common flow is no longer dominant in the presence of the dysfunction and the lateral orifices gained greater importance as the majority of the flow passed through one of them.

The maximal velocity increased dramatically (from  $\sim 2.3$  m/s for healthy case to  $\sim 4$  m/s for 100% dysfunction), which in turn increased the Doppler peak pressure gradient (from 21 mmHg to 64 mmHg). However, this dramatic change in pressure gradient was not clinically sufficient to confirm the presence of valve obstruction as other factors could lead to the same result (i.e., high flowrate, left ventricle outflow obstruction and prosthesis patient mismatch).

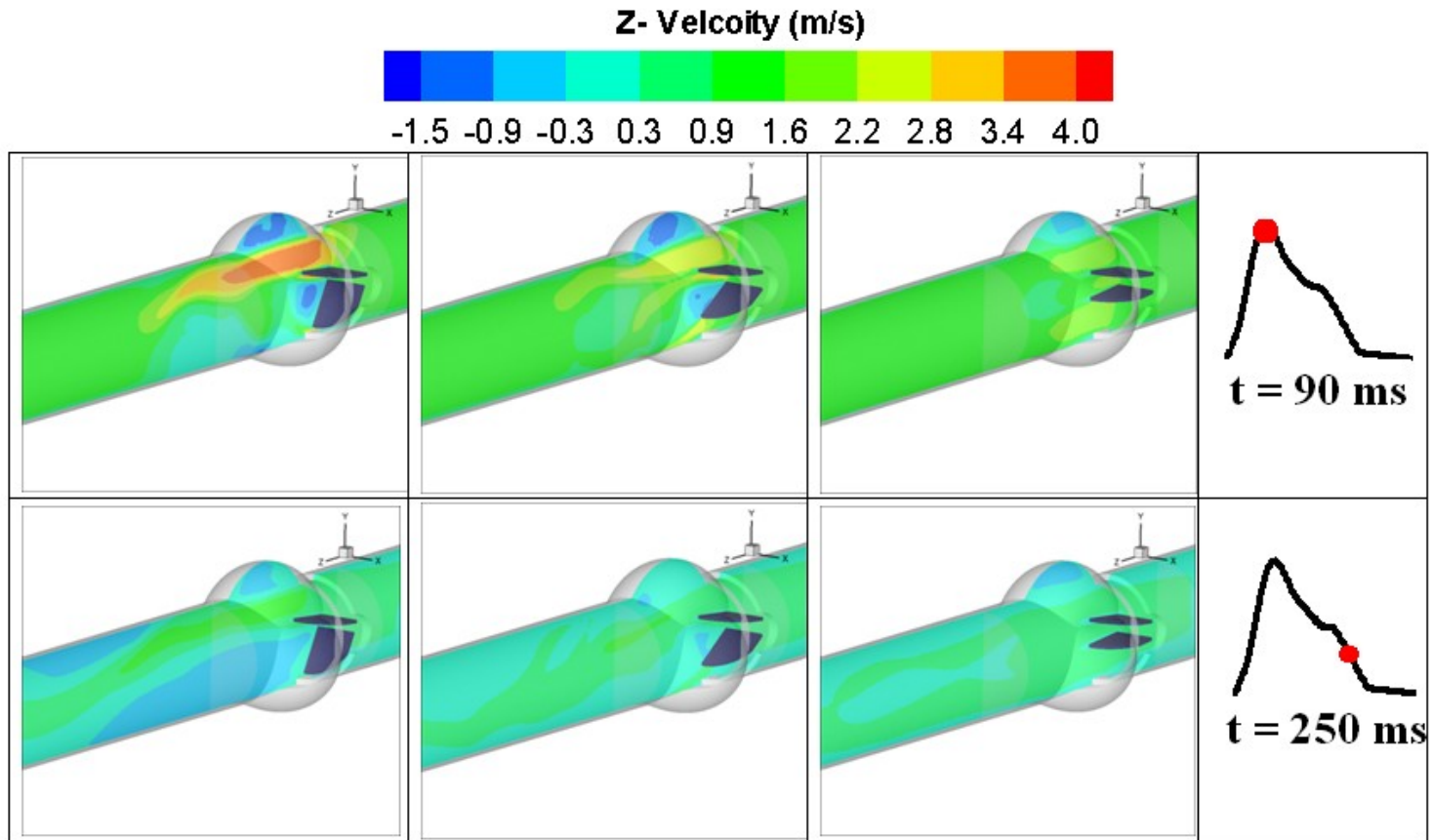


Figure 3.2 Contours for velocity magnitude through the bileaflet valve for different percentage of dysfunctions at two time instants (at the peak and late during the deceleration).

### 3.3.2 Coherent Structures

Figure 3.3 shows the isosurface considering Q-criterion downstream of the valve for three different dysfunctions and two different time instants.

$$Q = \frac{1}{2} \left( \frac{\partial U_i}{\partial U_j} \frac{\partial U_j}{\partial U_i} \right) = \frac{1}{2} \left( \Omega_{ij} \Omega_{ij} - S_{ij} S_{ij} \right) \quad (4.1)$$

where  $U$  is the velocity;  $S$  is rate of strain tensor by  $S_{ij} = \frac{1}{2} \left( \frac{\partial U_i}{\partial x_j} + \frac{\partial U_j}{\partial x_i} \right)$  and  $\Omega$  is the

rotation tensor by  $\Omega_{ij} = \frac{1}{2} \left( \frac{\partial U_i}{\partial x_j} - \frac{\partial U_j}{\partial x_i} \right)$ .

At the peak of the systolic phase, for the healthy case, three major vortex rings were observed within the three sinuses. This is consistent with the findings in the literature. However, introduction of the dysfunction significantly disturbed the flow downstream of the valve and the coherent structures were dominant through the entire aortic root. In the case of 100% dysfunction, the vortex structures traveled for the longest distance downstream of the valve compared to the other two cases. In the case of 50% dysfunction, the vortex structures covered more area within the sinuses compared to the other cases. In general, in healthy BMHVs, the maximum viscous and shear stresses were found at the peak instant and downstream of the trailing edge of the two leaflets where vortex shedding (von Kármán Vortex Street) occurs (Ge et al., 2007). On the other hand, in the dysfunctional BMHVs, the vortical flow covered a larger area. As a consequence, blood elements remained for longer periods in the region of elevated shear stress. Therefore, platelet activation and/or red blood cell damage could occur.

As the coherent structures in the partially dysfunctional valve (50%) were more dominant compared to the completely dysfunctional one (100%), the partially dysfunctional bileaflet MHV could be developed to a severe case (100% dysfunction) at a relatively high rate and within a short period. Therefore, detecting the dysfunction at early stages is crucial and any delay in diagnosis could have life threatening consequences.

An isosurface of  $Q$  criterion with a value of  $5000 \text{ s}^{-1}$  was chosen to depict the coherent structure during the deceleration phase just before the closure starts. Although, the strength of the coherent structure seemed to be decreasing, the disorganized vortical structure persisted. This can be attributed to the destabilizing effect of the deceleration phase (Dasi et al., 2007). However, the disorganized or chaotic-like coherent structure was more dominant in both cases of dysfunctional BMHV compared to the healthy one.

### **3.3.3 Velocity Magnitude (Two vs. Three Velocity Components)**

Figure 3.4 shows the discrepancy between using the three velocity components and using only the two in-plane velocity components to calculate the velocity magnitude. In the current study, only, B-datum plane is presented where the maximum discrepancy was found. In normally functioning BMHV, a minor discrepancy was found in the sinus area, which is in a good agreement with the findings of Kaminsky et al. (2007). However, in the presence of dysfunction, the discrepancy was more significant and covered larger areas (the central area between leaflets and the area downstream of the sinuses).

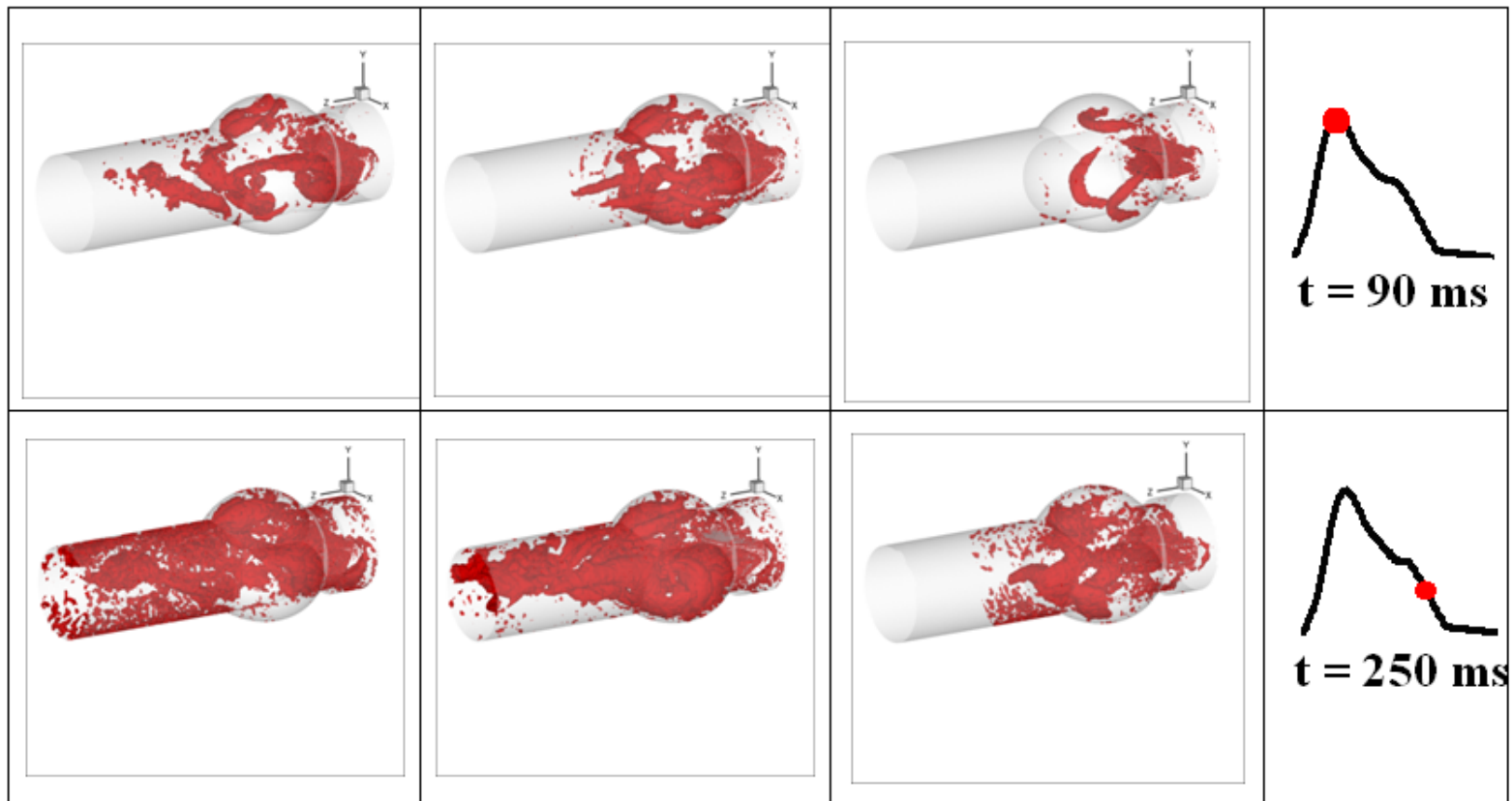


Figure 3.3 3-D coherent structure based on Q-criterion at peak and late during deceleration phase.

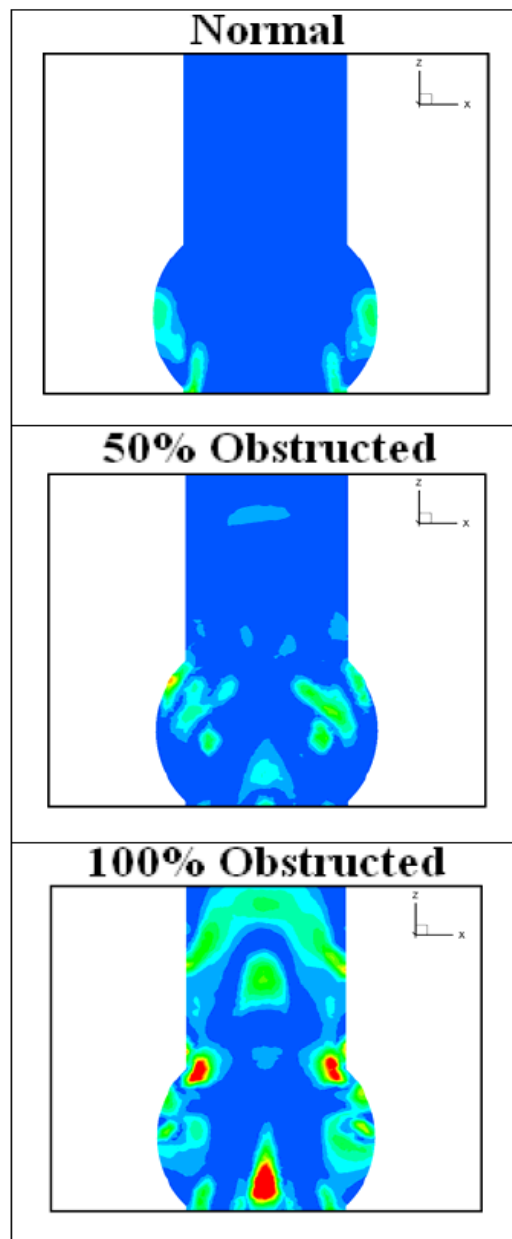
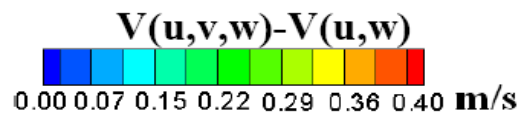


Figure 3.4 The difference between the two-component and three-component velocity magnitude ( $V(u,v,w)$  and  $V(u,w)$ ) at the central plane (B-datum) and the peak systole.

This discrepancy between 2-D and 3-D velocity magnitude might be explained by the presence and evolution of coherent structures downstream of BMHVs. The travelling path for the coherent structures at some regions was out of plane and volumetric as shown in fig. 3.3.. This, in turn, explains the increases in the magnitude of out of plane velocity component and affects the accuracy of 2-D assumption. Therefore, the maximum discrepancy between 2-D and 3-D velocity magnitude was proportional to the strength and presence of coherent structures. It is important to mention that the level of discrepancy between 2-D and 3-D velocity magnitudes was proportional to the percentage of valve dysfunction and considering 3-D PIV is important especially when the dysfunctional mechanical heart valve is the scope of the study.

### **3.4 Conclusion**

In conclusion, this study showed that the blood flow downstream of BMHV is strongly three-dimensional and time dependent, especially with the existence of valve dysfunction. Therefore, with the presence of valve dysfunction, pulsatile 3-D simulations should be adapted when the evolution of the vortical structure downstream of the BMHV is the objective of the study. As depicted above, the lateral flow is dominant in the presence of BMHV dysfunction. However, the two lateral orifices were not included in the calculations or taken into account in the process of clinical evaluation. Hence, the physical flow through the complete BMHV is not accurately represented in the current evaluation. Therefore, revisiting the assumptions and the theories behind the current clinical method is critical in order to include the flow through the two lateral orifices and to investigate its influence on the measurements' accuracy.

## Chapter 4

### **Performance of Doppler-echocardiographic Parameters for the Detection of Aortic Mechanical Prosthetic Valve Dysfunction**

Numerical simulations (chapters 2 and 3) revealed that the flow downstream of the dysfunctional valve was characterized by abnormally elevated shear stresses and large-scale vortices. These characteristics can predispose to blood components damage. And early detection of prosthetic valve dysfunction could be, then, a key factor for optimal medical management.

In this chapter, *in vitro* and *in vivo* studies were performed to evaluate the performance of different Doppler-echocardiographic parameters suggested by the American Society of Echocardiography (ASE) guidelines, to identify dysfunction of mechanical prosthetic valve in the aortic position.

#### **4.1 Introduction**

Replacing an aortic stenotic native heart valve with a prosthetic heart valve is the ultimate solution for symptomatic patients with severe aortic valve stenosis. Despite the marked improvement in prosthetic heart valve design and functionality, thromboembolism, structural failure, endocarditis and hemolysis are still possible complications. In such case, the native heart valve disease is replaced by a “prosthetic heart valve disease” (Vesey and Otto, 2004; Rahimtoola, 2010). The reported incidence of such serious and

life-threatening complications is between 0.2-6% (Montorsi et al., 2003; Aoyagi et al., 2000). Early detection of prosthetic valve dysfunction is then a key factor for successful treatment (i.e., heparin, fibrinolysis and reoperation) (Roudaut, 2007).

Transthoracic Doppler Echocardiography (TTE) is the primary screening technique to evaluate prosthetic valve dysfunction. However, visualization of the prosthetic valve, in many cases, is limited especially in aortic position (Khandheria et al.; 1991, Mohr-Kahaly et al., 1993; Maslow et al., 2000; Aslam et al., 2007). The assessment mainly relies, therefore, on hemodynamic parameters (aortic peak Doppler velocity, mean transvalvular pressure gradient, effective orifice area (EOA) and Doppler velocity index (DVI)) (Bach, 2010; Zoghbi et al., 2009; Vesey and Otto, 2004).

Recently, the American Society of Echocardiography (ASE) published its first *guidelines and standards* document about the assessment of prosthetic heart valve performance. Different cutoff values were suggested for the diagnosis of aortic valve dysfunction. (i.e., peak Doppler velocity > 3 m/s, mean transvalvular pressure gradient > 20 mmHg, Doppler velocity index < 0.3, effective orifice area < 1.2 cm<sup>2</sup>, aortic flow acceleration time > 80 ms). However, these fixed cutoff values suggested by ASE guidelines might not allow an accurate detection of prosthetic heart valve dysfunction under several conditions depending on valve type, valve size and transvalvular flowrate (Baumgratner 2009; Hage and Nanda, 2009; Aoyagi et al., 2000; Montorsi et al., 2003). Furthermore, current ASE guidelines do not differentiate between bioprosthetic and mechanical heart valves (MHV). While, the hemodynamic of bioprosthetic heart valves is close to the hemodynamic of native heart valves, the hemodynamic of MHVs is less physiological

(i.e. multiple jets, localized high gradient, pressure recovery, mechanism of opening and closure) (Baumgartner et al., 1992, Pibarot and Dumesnil, 2009).

The objective of this study is to evaluate under controlled experimental conditions the potential limitations of the parameters and cutoff values suggested by ASE guidelines. For this purpose extensive *in vitro* and retrospective *in vivo* studies were conducted on two commercially available bileaflet MHVs (St. Jude and On-X) with different sizes and for several flowrate conditions.

## **4.2 Methods**

### **4.2.1 *In Vitro* Study**

**Model.** BMHVs were mounted in an *in vitro* mock flow model already described and validated (Garcia et al., 2004) (Fig. 4.1). Briefly, the model is mainly made up of a reservoir, a compliant aortic chamber and a valve resistance. The flow was provided by a computer controlled DC motor coupled to a gear pump (Vi-CORR, Viking Pump). The left ventricular outflow tract and the aorta were both circular and rigid and their size was adjusted to be equal to the nominal size of the BMHV under evaluation. The compliant chamber was located immediately downstream of the proximal rigid aorta. The fluid was composed of 2/3 water and 1/3 of glycerol so that its density ( $1080 \text{ kg/m}^3$ ) and viscosity (3.5 cP) were similar to those of blood under high shear rate conditions. The ventricular and aortic pressures were measured with Millar catheters (model MPC 500, accuracy 0.5% full scale) under a sampling frequency of 1000 Hz. For each experiment, 10 cycles were recorded and the average was used to calculate the hemodynamic parameters.

**Test protocol.** Doppler echocardiographic measurements were performed on seven BMHVs: 4 different sizes of St. Jude HP aortic valves (21, 23, 25 and 27 mm) and 3 different sizes of On-X aortic valves (21, 23 and 25 mm). The dysfunction of the BMHV was introduced by restricting the movement of only one leaflet. This is because such condition is more difficult to detect clinically than when both leaflets have restricted motion (Montorsi et al., 2003). The position of the leaflet was varied from fully opened position (0% dysfunction) to fully closed position (100% dysfunction) with one intermediate position (50% dysfunction). All BMHVs were tested under five different transvalvular flowrates (3 to 7 L/min), corresponding to stroke volumes of 30 to 120 mL at a fixed heart rate of 70 bpm (ejection phase: 0.3 s). Aortic systolic and diastolic pressures were maintained under normal conditions: 120 mmHg and 80 mmHg, respectively.

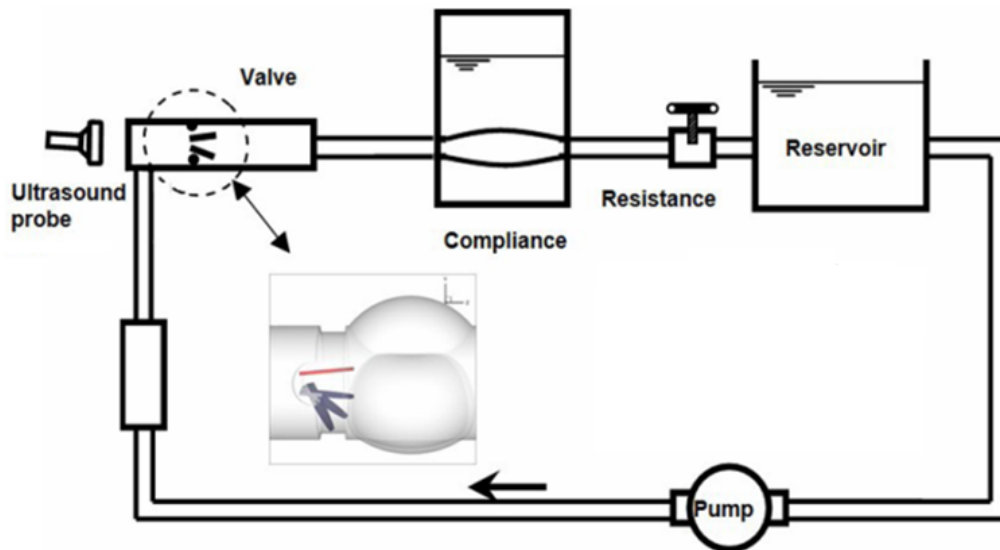


Figure 4.1 Sketch for the custom-made cardiac simulator.

**Echocardiography.** Doppler echocardiographic velocity measurements were performed in all cases using a Sonos 5500 (Philips Medical Systems/Agilent Technologies, Andover, Massachusetts) with a probe of 2.25 MHz. For measuring peak transvalvular velocity, the probe was placed at different locations on the measurement window to obtain the highest possible peak Doppler velocity reading through the three orifices of BMHV (one central and two lateral orifices). In order to avoid aliasing, the continuous-wave Doppler mode was used. The measurements were performed over 3 cycles and averaged. Peak Doppler velocity, mean transvalvular pressure gradients (determined using simplified Bernoulli equation), Doppler EOA (estimated using continuity equation) were evaluated for all BMHVs with 0%, 50% and 100% percentage of dysfunction. Peak flow velocity and Velocity Time Integral ( $VTI_{LVOT}$ ) in the Left Ventricular Outflow Tract (LVOT) was measured approximately 0.5 cm upstream from the prosthetic valve using pulsed-wave Doppler mode. The stroke volume was calculated as the product of the cross-sectional area of the LVOT and  $VTI_{LVOT}$ .

#### **4.2.2 In Vivo Study**

**Patient Population.** From March 2005 to July 2010, 31 patients were referred to cinefluoroscopy in the Quebec Heart and Lung Institute for the evaluation of aortic prosthetic heart valve performance. From this cohort, we included in the present study only the patients who had aortic BMHV and had their fluoroscopy test within two weeks from echocardiography evaluation. Among this cohort, 7 patients, with normally functioning prosthetic valves (as evaluated by cinefluoroscopy) were excluded from this study as Doppler measurements seemed not accurate.

The final cohort consisted then of 17 patients. These patients were then further subdivided into 2 groups depending on whether they had a normally functioning valve (n = 13) (Table. 4.1) or a valve dysfunction (in one or both leaflets, n = 4) (Table. 4.2). In our center, only patients with suspected obstruction (high mean pressure gradient ( $TPG_{\text{mean}} > 20$  mmHg), low EOA ( $EOA < 1$  cm<sup>2</sup>), or obstruction visualization by 2-D echocardiography are referred to a fluoroscopy test. The fluoroscopy test was considered to give a definite answer about the presence and severity of valve obstruction.

***Echocardiography and Cinefluoroscopy.*** Doppler echocardiographic velocity measurements were obtained by placing the transducer in the apical position. Peak flow velocity in the left ventricular outflow tract was measured approximately 0.5 cm upstream from the prosthetic valve. Cinefluoroscopy was performed to obtain a tangential view of the implanted BMHV. For each patient, the maximum opening and closing angles were determined by averaging three consequent cardiac cycles. In this study the determination of the opening and closing angles were successfully achieved in all the 17 patients.

***Inter-observer variability:*** To evaluate the inter-observer variability related to the *in vitro* study, all the measurements were repeated by two blinded observers with the use of the same experimental setup for SJHP21 and On-X 21.

***Statistical Analysis.*** Results are expressed as mean  $\pm$  SD. Variability was expressed as mean percent error, calculated as the absolute difference between the two observations divided by the mean of the observations and expressed as percent.

Table 4.1 *In vivo* Doppler-derived data for normal aortic bileaflet valves

Patient No.	Valve Size	LVOT Diameter (cm)	SV (ml)	Peak Velocity (m/s)	Mean Pressure Gradient (mmHg)	EOA (cm <sup>2</sup> )	Doppler Velocity Index (DVI)
<b>SJ</b>							
1	21-mm ST	2.1	69	2.41	15.4	1.28	0.41
2	25-mm ST	2.2	88	3.1	25	1.60	0.44
3	25-mm ST	2.4	68	2.04	9	2.13	0.44
4	25-mm ST	2.55	76	2.14	9.3	2.06	0.43
5	25-mm ST	2.3	79	2.15	9	1.88	0.40
<b>Carbomedics Top Hat</b>							
6	21-mm	2.1	87	3.51	27	1.23	0.34
7	23-mm	2.3	113	3.45	25	1.77	0.38
8	23-mm	2.2	114	3.75	30	1.90	0.40
9	23-mm	2.2	69	1.81	7	1.76	0.45
10	25-mm	2.4	107	2.89	24	1.78	0.36
<b>ADVANTAGE</b>							
11	21-mm	1.9	77	2.8	13	1.39	0.44
<b>On-X</b>							
12	19-mm	1.9	77	2.49	13	1.39	0.44
13	23-mm	2.25	84	1.87	7.36	2.20	0.62

*Hp*, Hemodynamic Plus; *ST*, Standard

Table 4.2 *In vivo* Doppler-derived data for dysfunctional aortic bileaflet valves

Patient No.	Prosthetic Valve	Diagnosis	LVOT Diameter (cm)	SV (ml)	Peak Velocity (m/s)	Mean Pressure Gradient (mmHg)	EOA (cm <sup>2</sup> )	(DVI)
14	23-mm SJ ST	Stenosis 35°-10°	2.2	61	3.26	20	0.97	0.22
15	25-mm SJ ST	Stenosis 56°-56°	1.9	47	4.30	42	0.52	0.18
16	27-mm SJ HP	Stenosis 35°-35°	2.3	100	3.29	17	1.56	0.35
17	27mm-Carbomedics Top Hat	Stenosis 22°-32°	2.1	94	4.08	41	1.14	0.29

*Hp*, Hemodynamic Plus; *ST*, Standard

## **4.3 Results**

### **4.3.1 *In Vitro* Results**

#### **Peak Doppler Velocity**

Figure 4.2 shows, for both types of BMHVs (St. Jude, On-X), the variation in peak Doppler velocity as a function of flowrate, valve size and percentage of dysfunction. As expected, peak Doppler velocity magnitude was proportional to transvalvular flowrate and inversely proportional to valve size.

For the majority (83%) of healthy cases (0% dysfunction), peak Doppler velocity magnitude did not exceed the peak Doppler velocity magnitude of 3 m/s (the suggested ASE threshold for possible dysfunction). Only the peak Doppler velocity downstream of the smaller valves: SJHP21 (3.8 m/s) and On-X21 (3.27 m/s) exceeded ASE guidelines threshold. After introducing a 50% dysfunction to one leaflet, the majority (71%) of peak Doppler velocity values still did not exceed ASE threshold, with the exception of 21 mm and 23 mm valve sizes (for flowrate > 6 L/min). After introducing a 100% dysfunction to one leaflet, the majority (70%) of peak Doppler velocity values measured through SJHP valves exceeded 3 m/s as well as all (100%) peak Doppler velocity values for On-X. The highest peak Doppler velocity measured for SJHP and On-X was 5.6 and 6 m/s, respectively.

#### **Mean Transvalvular Pressure Gradient**

Figure 4.3 shows, for both types of BMHVs (St. Jude, On-X), the variation of mean transvalvular pressure gradient ( $TPG_{\text{mean}}$ ) as a function of flowrate, valve size and percentage of dysfunction.

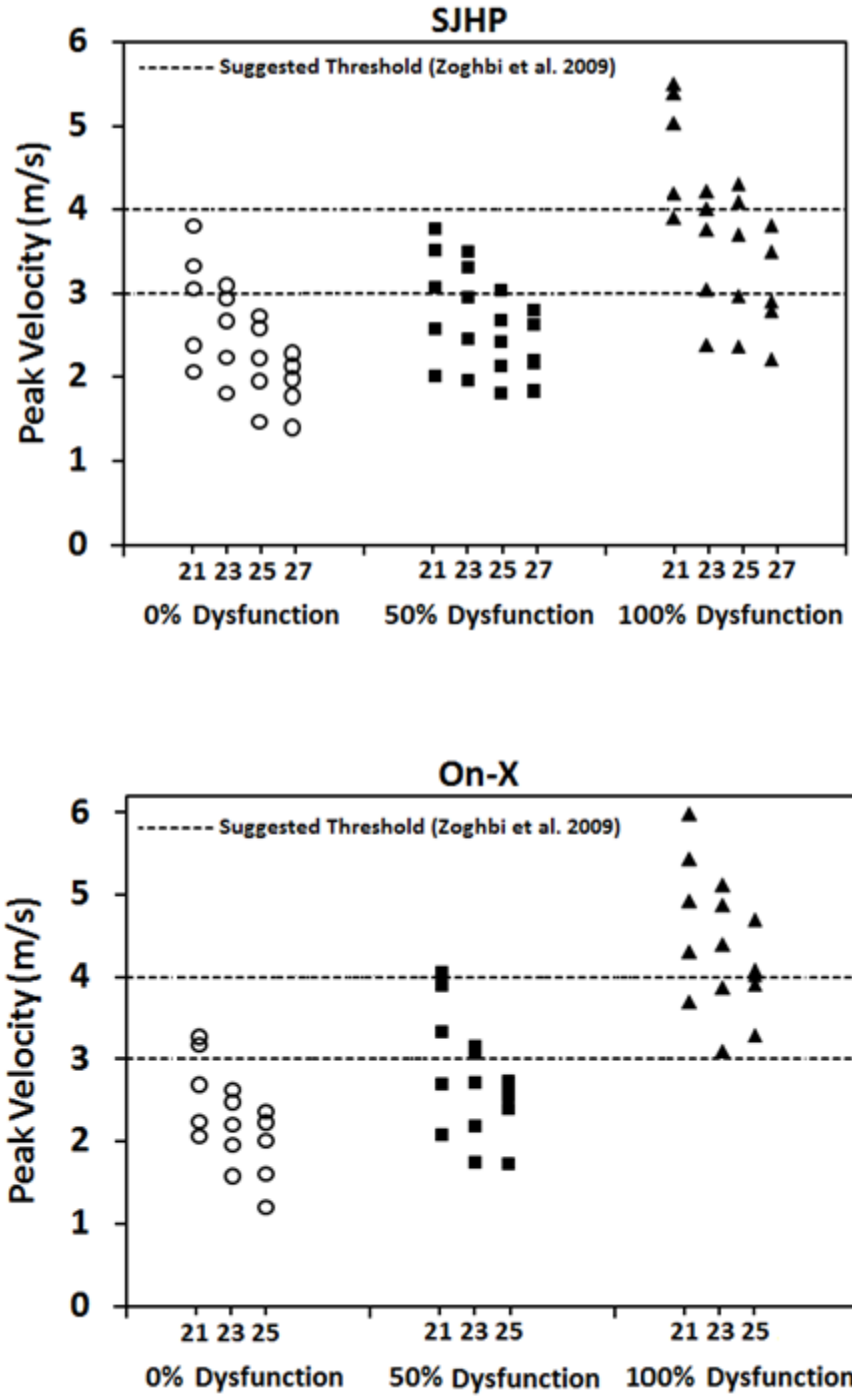


Figure 4.2 Measured peak Doppler velocity grouped by prosthetic valves' type, dysfunction and size.

As expected,  $TPG_{mean}$  was strongly flow dependent. It was also inversely proportional to valve size. For the majority of healthy cases (0% dysfunction),  $TPG_{mean}$  magnitude did not exceed 20 mmHg (the suggested ASE threshold for possible valve dysfunction). Only  $TPG_{mean}$  of SJHP 21 mm and On-X 21 mm at high cardiac output (7 L/min) reached up to 22 mmHg and 26.6 mmHg, respectively.

After introducing a 50% dysfunction to one leaflet, the majority (74%) of  $TPG_{mean}$  measured still did not exceed 20 mmHg. Only  $TPG_{mean}$  for SJHP and On-X with sizes of 21 mm and 23 mm exceeded 20 mmHg at normal and high cardiac flowrate conditions (flowrate  $\geq$  5L/min). It is worth noting that none of 0% and 50% dysfunction cases exceeded the higher limit of ASE for  $TPG_{mean}$  (35 mmHg).

After introducing a 100% dysfunction to one leaflet,  $TPG_{mean}$  for the majority (65%) of SJHP valves and all (100%) of On-X valves exceeded the ASE guidelines for lower cutoff value (20 mmHg). The highest  $TPG_{mean}$  measured were 64.0 mmHg and 73.6 mmHg for SJHP-21 mm and On-X 21 mm, respectively. While one leaflet was completely blocked,  $TPG_{mean}$  for the majority (80%) of SJHP valves did not exceed the ASE guidelines for higher cutoff value (35 mmHg). Interestingly, On-X valves showed an opposite trend and  $TPG_{mean}$  for the majority (53%) of 100% dysfunction cases exceeded 35 mmHg.

### **Doppler Velocity Index (DVI)**

Figure 4.4 shows, for both types of BMHVs (St. Jude, On-X), the variation of Doppler velocity index as a function of flowrate, valve size and percentage of dysfunction, valve size. For SJHP valves (normal and dysfunctional), there was no strong correlation ( $R = 0.02$ ) between valve size and DVI.

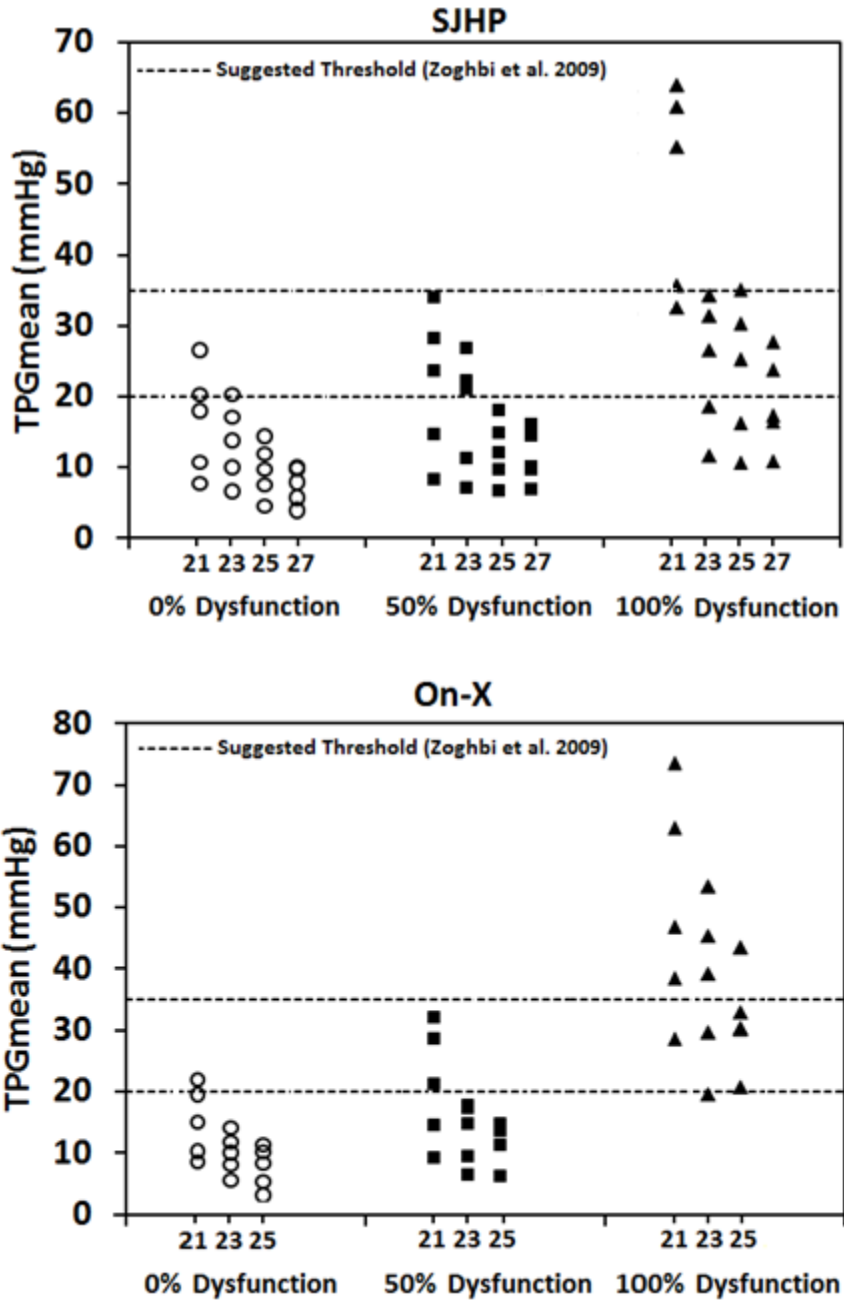


Figure 4.3 Measured mean pressure gradient grouped by prosthetic valves' type, dysfunction and size.

Whereas, for On-X valves, DVI negatively correlated with valve size ( $R = -0.89$ ).

For healthy cases (0% dysfunction), DVI ranged between 0.54 and 0.48 (mean,  $0.52 \pm 0.014$ ) for SJHP valves and ranged between 0.6 and 0.45 (mean,  $0.52 \pm 0.05$ ) for On-X valves. With 50% dysfunction, DVI ranged between 0.41 and 0.47 (mean,  $0.44 \pm 0.02$ ,  $p < 0.001$ , compared to healthy case) for SJHP and ranged between 0.37 and 0.47 (mean,  $0.41 \pm 0.03$ ,  $p < 0.001$ , compared to healthy case) for On-X. For all cases with 50% dysfunction, DVI did not reach ASE guidelines upper limit (DVI = 0.3) for possible dysfunction. With 100% dysfunction on one leaflet, DVI decreased significantly ranging between 0.29 and 0.34 (mean,  $0.31 \pm 0.017$ ,  $p < 0.001$ , compared to healthy case) for SJHP and between 0.24 and 0.29 (mean,  $0.265 \pm 0.014$ ,  $p < 0.001$ , compared to healthy case) for On-X. All DVI values for both SJHP and On-X with 100% dysfunction were lower than 0.3. However, none (0%) of the values for SJHP and only 20% of values for On-X reached ASE guidelines lower limit indicating significant valve dysfunction (DVI < 0.25).

### **Effective Orifice Area**

Figure 4.5 shows the variation of valve EOA as a function of flowrate, valve size and percentage of severity. As expected, EOA for mechanical heart valves demonstrated no significant variation with flowrate. The values of EOA were only a function of valve size and percentage of valve dysfunction. For healthy cases (0% dysfunction), EOA ranged between  $1.84 \text{ cm}^2$  and  $3.10 \text{ cm}^2$  (mean,  $2.38 \pm 0.40 \text{ cm}^2$ ) for SJHP valves, and between  $1.81 \text{ cm}^2$  and  $2.84 \text{ cm}^2$  (mean,  $2.28 \pm 0.31 \text{ cm}^2$ ) for On-X valves.

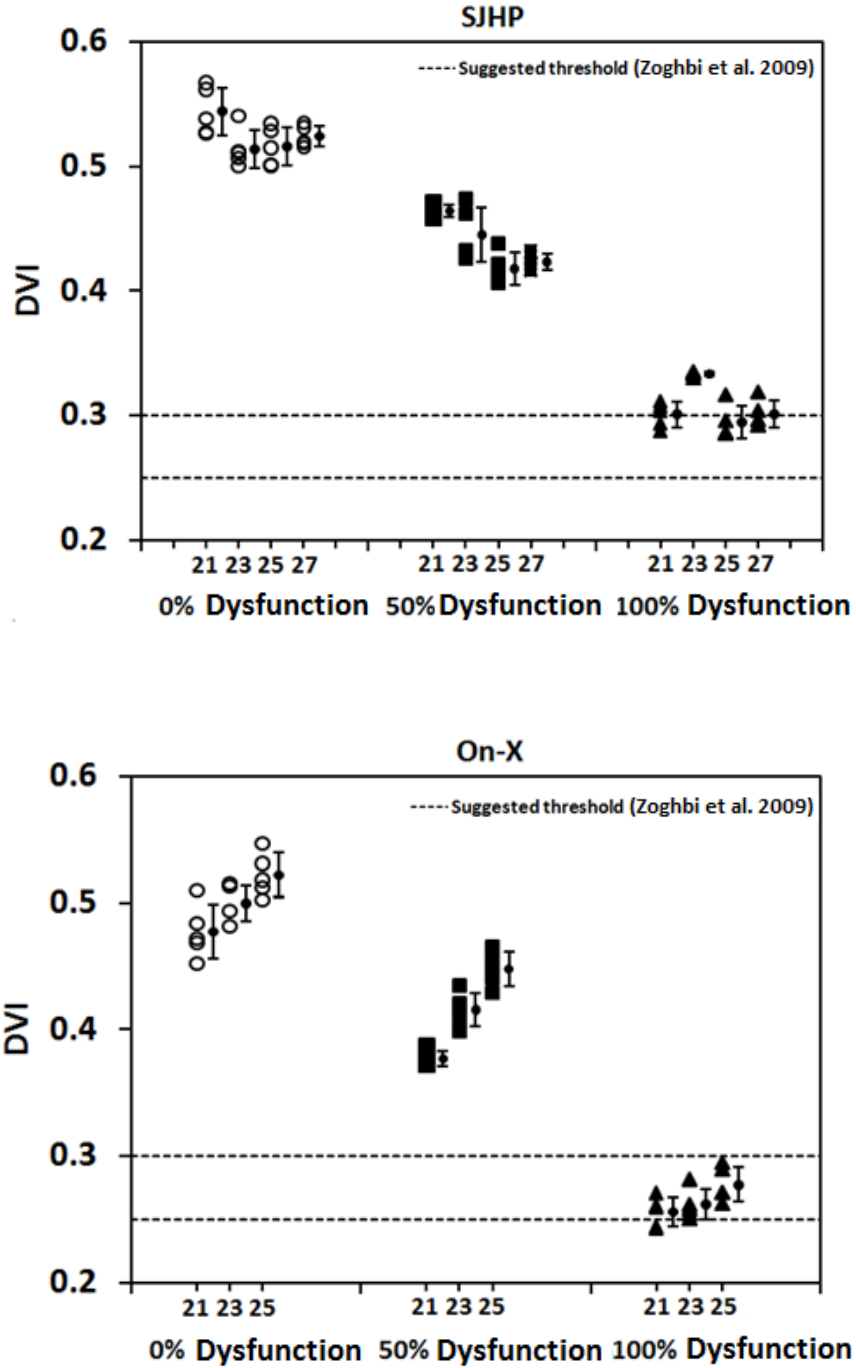


Figure 4.4 *In vitro* Doppler velocity index, calculated as the ratio of peak velocity in the left ventricle outflow tract to that of the transprosthetic peak velocity in 0% dysfunction, 50% dysfunction and 100% dysfunction of SJHP (left) and On-X (right) prosthetic valves and for different cardiac outputs. Bars, mean  $\pm$  SD of the measured values each valve size.

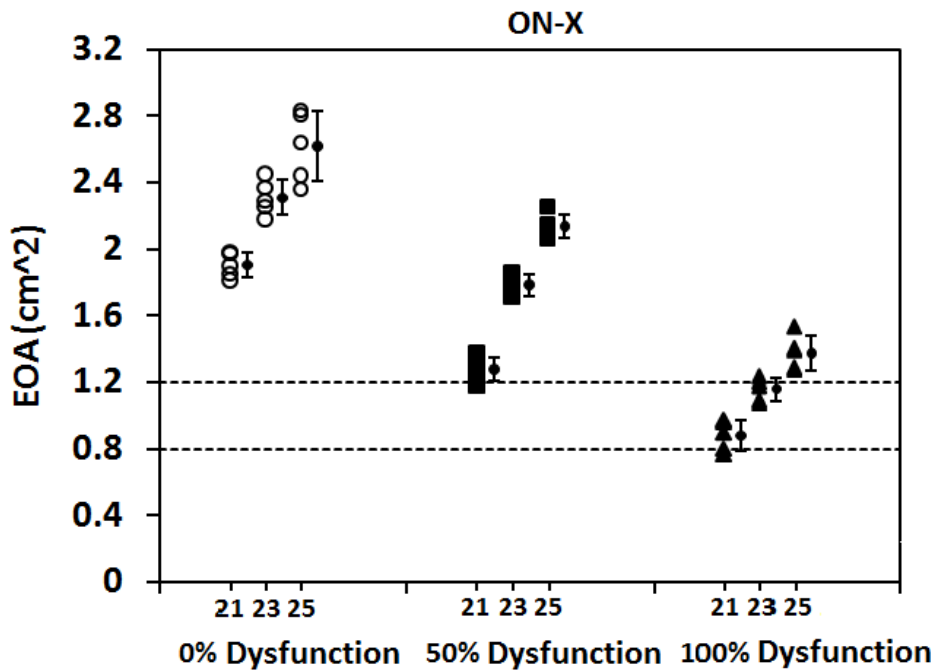
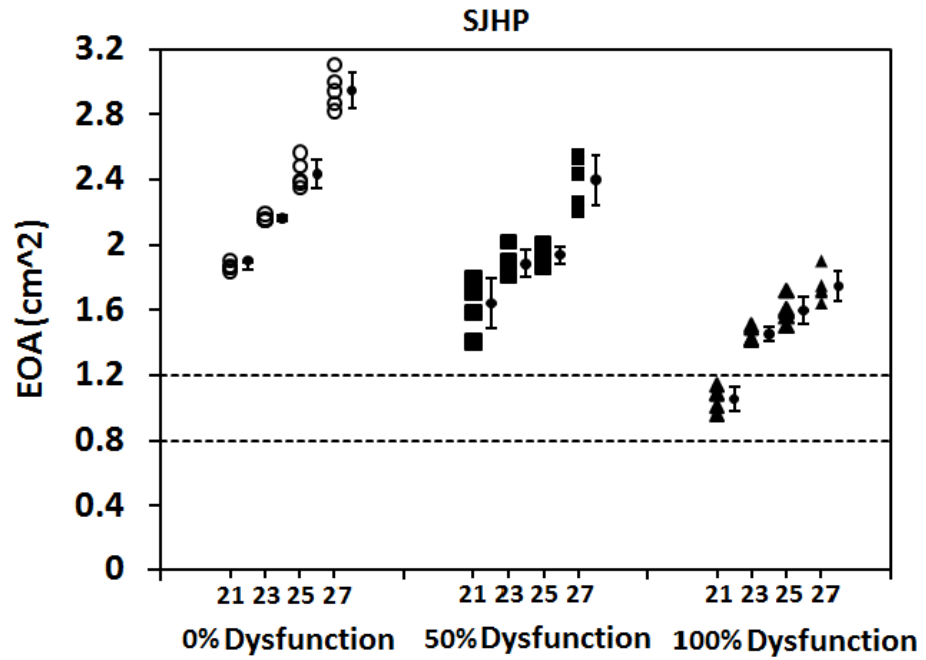


Figure 4.5 *In vitro* effective orifice area (cm<sup>2</sup>) in 0% dysfunction, 50% dysfunction, and 100% dysfunction of SJHP (upper) and On-X (lower) prosthetic valves and for different cardiac outputs. Bars, mean  $\pm$  SD of the measured values each valve size.

With 50% dysfunction, EOA decreased and ranged between 1.40 cm<sup>2</sup> and 2.55 cm<sup>2</sup> (mean, 1.99 ± 0.29 cm<sup>2</sup>,  $p < 0.001$ , compared to healthy case) for SJHP valves, and between 1.19 cm<sup>2</sup> and 2.26 cm<sup>2</sup> (mean, 1.76 ± 0.37 cm<sup>2</sup>,  $p < 0.001$ , compared to healthy case) for On-X valves. None of 50% dysfunction cases of SJHP and On-X valves reached ASE guidelines EOA cutoff value for possible dysfunction (EOA = 1.2 cm<sup>2</sup>). With 100% dysfunction in one leaflet, further decrease in EOA was achieved. EOA values ranged between 0.96 cm<sup>2</sup> and 1.90 cm<sup>2</sup> (mean, 1.46 ± 0.27 cm<sup>2</sup>,  $p < 0.001$ , compared to healthy case) for SJHP valves and between 0.76 cm<sup>2</sup> and 1.53 cm<sup>2</sup> (mean, 1.14 ± 0.22 cm<sup>2</sup>,  $p < 0.001$ , compared to healthy case) for On-X valves. Only 37% of EOA values for 100% dysfunction cases were lower than 1.2 cm<sup>2</sup>, and 5.7% of EOA values of 100% dysfunction cases were lower than ASE guidelines EOA cutoff value for significant dysfunction (EOA = 0.8 cm<sup>2</sup>).

### **Sensitivity and Specificity Analysis**

Sensitivity and specificity analysis are used to measure how often the correct diagnosis occurs in dysfunctional and normal BMHVs. The sensitivity of one diagnosis parameter is the probability that the dysfunction is diagnosed given that the patient has an actual BMHV dysfunction. And the specificity is the probability that there is no dysfunction is diagnosed given that the patient has normally functioning BMHV.

Sensitivity and specificity analysis was conducted in two different ways: 1) considering two groups: healthy (0% dysfunction) and dysfunctional (including both 50% and 100% dysfunction). The results are displayed in Table 4.3; 2) considering two extreme groups: healthy (0% dysfunction) and dysfunctional (including 100% dysfunction and excluding 50% dysfunction). The results are displayed in Table 4.4.

When considering healthy (0% dysfunction) and dysfunctional valves (including both 50% and 100% dysfunction), all the parameters suggested by ASE guidelines have a relatively high specificity. The lowest specificity was for peak Doppler velocity with 82.9%. However, their sensitivity was relatively low.  $EOA \leq 0.8 \text{ cm}^2$  and  $DVI \leq 0.25$  criteria showed the lowest sensitivity (2.9% and 4.3%, respectively) and  $V_{\max} \geq 3 \text{ m/s}$  criterion showed the highest sensitivity with only 57.1%.  $EOA \leq 1.2 \text{ cm}^2$  showed a sensitivity of 21.4%. Interestingly, when considered in this analysis the criterion suggested by (Wang et al., 1995, Girard et al., 2001, Pibarot and Dumesnil, 2009): a prosthetic heart valve is considered as dysfunction if the  $EOA_{\text{measured}} \leq EOA_{\text{normal}} - SD$ , the sensitivity reached 61.3%. Normal  $EOA$  values for most prosthetic valve and their standard deviations are tabulated in ASE guidelines and standards document. Also considering  $DVI \leq 0.35$ , as suggested by Pibarot and Dumesnil 2009, improved the sensitivity (50%).

Now, when considering only healthy valves (0% dysfunction) and valves with 100% dysfunction and excluding the 50% cases, there was a significant increase in sensitivity and specificity for all parameters.  $EOA \leq 0.8 \text{ cm}^2$  and  $DVI \leq 0.25$  criteria still showed the lowest sensitivity (5.7% and 8.6%, respectively). Both  $EOA \leq EOA_{\text{normal}} - SD$  and  $DVI \leq 0.35$  showed the highest sensitivity (100%). Also, peak Doppler velocity showed high sensitivity (82.9 %).

### **Measurement variability**

Inter-observer variability for peak LVOT Velocity, peak transaortic velocity,  $TPG_{\text{mean}}$ , and  $EOA$ , was  $1.8 \pm 1.3$ ,  $2.4 \pm 1.3$ ,  $5.6 \pm 4.4$ , and  $2.9 \pm 2.2$ , respectively.

**Table 4.3 Sensitivity and specificity analysis for different echo Doppler parameters**

<b>Diagnosis criteria for dysfunction</b>	<b>Sensitivity (%)</b>	<b>Specificity (%)</b>
$V_{\max} \geq 4\text{m/s}$	<b>28.6%</b>	<b>100%</b>
$V_{\max} \geq 3\text{m/s}$	<b>57.1%</b>	<b>82.9%</b>
$\text{TPG}_{\text{mean}} \geq 35 \text{ mmHg}$	<b>18.6%</b>	<b>100%</b>
$\text{TPG}_{\text{mean}} \geq 20 \text{ mmHg}$	<b>48.6%</b>	<b>88.6%</b>
$\text{DVI} \leq 0.35$	<b>50.0%</b>	<b>100%</b>
$\text{DVI} \leq 0.3$	<b>34.3%</b>	<b>100%</b>
$\text{DVI} \leq 0.25$	<b>4.3%</b>	<b>100%</b>
$\text{EOA} \leq 1.2 \text{ cm}^2$	<b>21.4%</b>	<b>100%</b>
$\text{EOA} \leq 0.8 \text{ cm}^2$	<b>2.9%</b>	<b>100%</b>
<b><math>\text{EOA} \leq \text{EOA}_{\text{normal}} - \text{SD}</math></b>	<b>61.3%</b>	<b>100%</b>

**Table 4.4 Sensitivity and specificity analysis for different echo Doppler parameters (excluding 50% dysfunction cases).**

<b>Diagnosis criteria for dysfunction</b>	<b>Sensitivity (%)</b>	<b>Specificity (%)</b>
$V_{\max} \geq 4\text{m/s}$	<b>51.4%</b>	<b>100%</b>
$V_{\max} \geq 3\text{m/s}$	<b>82.9 %</b>	<b>82.9%</b>
$\text{TPG}_{\text{mean}} \geq 35 \text{ mmHg}$	<b>31.4%</b>	<b>100%</b>
$\text{TPG}_{\text{mean}} \geq 20 \text{ mmHg}$	<b>77.1%</b>	<b>88.6%</b>
$\text{DVI} \leq 0.35$	<b>100.0%</b>	<b>100%</b>
$\text{DVI} \leq 0.3$	<b>71.4%</b>	<b>100%</b>
$\text{DVI} \leq 0.25$	<b>8.6%</b>	<b>100%</b>
$\text{EOA} \leq 1.2 \text{ cm}^2$	<b>40.0%</b>	<b>100%</b>
$\text{EOA} \leq 0.8 \text{ cm}^2$	<b>5.7%</b>	<b>100%</b>
<b><math>\text{EOA} \leq \text{EOA}_{\text{normal}} - \text{SD}</math></b>	<b>100%</b>	<b>100%</b>

### **4.3.2 *In Vivo* Results**

Some overlap in values of Doppler-derived parameters was observed in each of normal and dysfunctional BMHVs groups as shown in figure 4.6.

Peak Doppler velocity and  $TPG_{\text{mean}}$  was significantly higher in dysfunctional valves when compared to normal valves ( $2.85 \pm 0.89$  vs.  $3.7 \pm 0.46$  m/s) and ( $30 \pm 12$  vs.  $20 \pm 13$  mmHg), respectively (see Tables 4.3 and 4.4). It should be noted, however that peak Doppler velocity ranged from 1.81 m/s to 3.75 m/s for healthy valves and from 3.26 m/s to 4.3 m/s for dysfunctional valves, leading to an overlap between the intervals. This was the same for  $TPG_{\text{mean}}$  (healthy valves: 7 to 57 mmHg; dysfunctional valves: 17 to 42 mmHg). DVI was significantly higher in healthy valve compared to dysfunctional valves ( $0.41 \pm 0.08$  vs.  $0.26 \pm 0.07$ ). However, DVI for dysfunctional valve ranged between 0.18 and 0.35. EOA for healthy valves was significantly higher than the EOA for dysfunctional valves ( $1.7 \pm 0.3$  cm<sup>2</sup> vs.  $1.05 \pm 0.37$  cm<sup>2</sup>). However, EOA ranged from 2.2 cm<sup>2</sup> to 1.23 cm<sup>2</sup> for healthy valves and from 1.56 cm<sup>2</sup> to 0.52 cm<sup>2</sup> for dysfunctional valves, showing a certain overlap between the intervals.

## **4.4 Discussion**

### **4.4.1 Peak Doppler Velocity and Mean Transvalvular Pressure Gradient**

The most recent ASE guidelines and standards suggest fixed threshold values for the detection of prosthetic valve dysfunction. A peak Doppler velocity equal or higher than 3 m/s or mean transvalvular pressure gradient equal or higher than 20 mmHg should be, following these guidelines, an indicator of possible valve dysfunction.

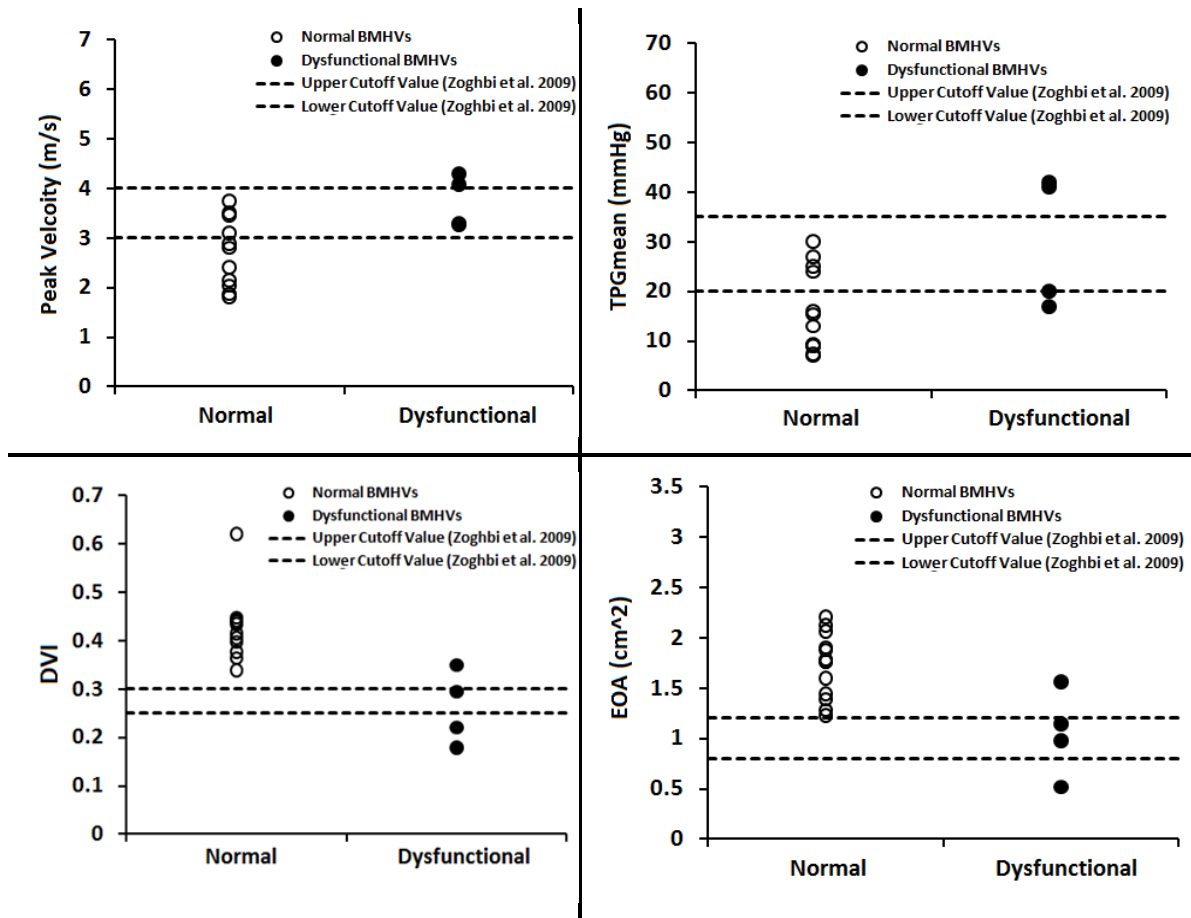


Figure 4.6 *In vivo* measurements for different Doppler derived parameters for normal and dysfunctional BMHVs.

The sensitivity analysis shows, based on the current guidelines for cutoff values, the difficulty of detecting the cases of 50% dysfunction (mild to moderate stenosis). However, it has already been demonstrated that Doppler-derived velocities and pressure gradients are strongly dependent on transvalvular flowrate, left ventricular function, valve size, and valve type (Baumgartner et al., 1990; Bottio et al., 2004). As a consequence, especially at low flowrate conditions, the sensitivity of peak Doppler velocity and  $TPG_{\text{mean}}$  for the detection of valve dysfunction is expected to be low. It was shown (fig. 4.6) that some dysfunctional BMHVs had peak Doppler velocity and values lower than the ASE suggested thresholds. This was mainly the case at low cardiac output and for relatively large valve size. These findings are in agreement with Aoyagi et al. (2000) where a wide range, with significant overlap, of values for peak Doppler velocities and  $TPG_{\text{mean}}$  was found for normal and dysfunctional BMHVs.

#### **4.4.2 Doppler Velocity Index**

Since DVI calculation does not rely on the determination of LVOT area or on the determination of valve size and type, it has been postulated that DVI is flow independent (Chafizadeh and Zoghbi 1991; Bach 2010). Few studies reported DVI values for dysfunctional BMHVs (Chafizadeh and Zoghbi, 1991; Aoyagi et al., 2000). Chafizadeh and Zoghbi (1991) found that in three severely dysfunctional BMHVs ( $EOA = 0.43 \pm 0.07 \text{ cm}^2$ ), DVI value was lower than 0.25. Aoyagi et al. (2000) investigated 16 obstructed BMHVs with mild to severe dysfunction and did not find DVI values lower than 0.25. In the current *in vitro* study, DVI showed a slow response to valve dysfunction and only under severe cases (100% dysfunction); DVI was found lower than

0.25. This led to a very low sensitivity: 4.3% with all cases and 8.6% when 50% dysfunction was excluded. Increasing DVI limit to 0.3 allowed a significant improvement in its sensitivity up to 34.3% for all cases and 71.4% when 50% dysfunction was excluded. Interestingly, by increasing DVI limit to 0.35 (Pibarot and Dumesnil, 2009; Aoyagi et al., 2000), DVI sensitivity reached up to 50% for all cases and 100% when 50% dysfunction was excluded.

Another important point is that since DVI relies on the upstream velocity, for a specific transvalvular flowrate and valve size, different LVOT areas will lead to different values of DVI (fig.4.7). Indeed, a large LVOT area will result in smaller upstream velocities and therefore smaller DVIs even for healthy valves. Similarly, any narrowing in the LVOT area will might lead to large DVIs even in the presence of dysfunction (See for example Patients #16 and #17 in Table 4.4). The relation between DVI and LVOT area is depicted in figure 4.7 for normally functioning SJHP 21 mm and SJHP 27 mm BMHVs.

#### **4.4.3 Effective Orifice Area**

It has already been demonstrated that valve EOA, mainly for BHMVs, is flow independent for a large range of flow variations (Baumgartner et al., 1992; Bech-Hanssen et al., 2001). However, EOA is highly dependent on valve design and valve size or valve geometrical orifice areas. As a consequence, using a constant threshold ( $EOA \leq 1.2 \text{ cm}^2$ ) for the detection of BMHV obstruction using Doppler derived EOA will be limited. One way to overcome this limitation is to consider valve-specific EOA thresholds. In this study, considering for each valve type and size its normal EOA reference value minus one standard deviation, as previously suggested (Wang al., 1995; Girard et al., 2001;

Pibarot and Dumesnil 2009) as a threshold resulted in a very high sensitivity of 84.5% for all cases. Normal reference values and their standard deviations are tabulated in ASE guidelines and standards document (Zoghbi et al., 2009). Reference values can also be found in other studies (Rosenhek et al., 2003; Pibarot and Dumesnil, 2009).

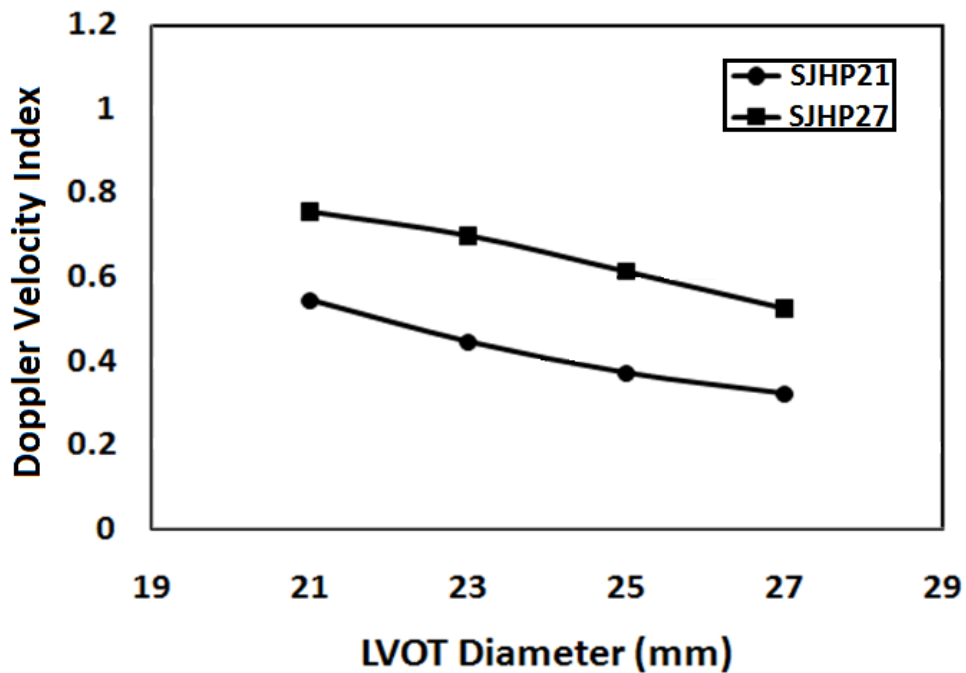


Figure 4.7 The effect of LVOT narrowing or dilatation on Doppler velocity index. Narrowing of LVOT diameter with the implantation of normal aortic prosthetic SJHP27 valve (■), and Dilatation of LVOT diameter with the implantation of normal aortic prosthetic SJHP21 (●).

#### **4.4.4 Low Cardiac Output State**

In the current *in vitro* study, including, only, low flowrate conditions (3-4 L/min) in the sensitivity analysis affected mainly flow dependent parameters (peak velocity and mean gradient). By including all cases, the sensitivity dropped from 57.1% to 32.1% and from 48.6% to 25% for peak Doppler velocity and mean transvalvular pressure gradient, respectively. The same trend persists when only 0% dysfunction and 100% dysfunction were included (50% dysfunction was excluded), as the sensitivity dropped from 82.9% to 64.3% and from 77.1% to 50% for peak Doppler velocity and mean transvalvular pressure gradient, respectively. Regardless the selection criterion (including or excluding 50% dysfunction cases), the sensitivity for both parameters was 100%.

However, the sensitivity and specificity did not change for DVI and EOA parameters (flow independent).

#### **4.5 Conclusion**

In the current study, good agreement was found between *in vitro* and *in vivo* concluded results. Sensitivity of the fixed cut-off values of different Doppler-echocardiographic diagnosis parameters suggested by the American Society of Echocardiography (ASE) guidelines was relatively low. In addition, some overlap in values of Doppler-derived parameters was observed in each of normal and dysfunctional BMHVs.

At low cardiac output, the measured flow dependent parameters (i.e., peak velocity and mean pressure gradient) did not exceed, mostly, the cut-off values which in turn could affect the accuracy of the detection of valve dysfunction. Therefore, when using peak Doppler velocity and mean transvalvular pressure gradient for evaluating mechanical

heart valve performance, valve type, valve size and flowrate conditions have to be considered.

Despite the fact that DVI is flow independent and simple to measure (no need to measure the diameter of the LV outflow tract), Doppler velocity index results should be interpreted with caution since they highly depend on LVOT area.

Considering reference effective orifice area minus one standard deviation as a cut-off value for a suspected valve dysfunction, as suggested by Pibarot and Dumesnil (2009), is a more stable and robust parameter for evaluating mechanical heart valve dysfunction.

## Chapter 5

### Theoretical Prediction of the Hemodynamic Performance of Bileaflet Mechanical Heart Valves

We demonstrated in the previous chapter that the fixed cut-off values for Doppler-derived parameters have relatively low sensitivity in detecting prosthetic valve dysfunction. Therefore, in this chapter, we propose a mathematical model capable of predicting the normal reference values of Doppler-derived parameters by considering flow conditions, valve size, and valve type. The theoretical results are validated against *in vitro* results. Moreover, *in vivo* data from a combined echocardiography/fluoroscopy study were extracted and analyzed to validate the theoretical predictions.

#### 5.1 Introduction

Nowadays, 7% of individuals above the age of 65 have a significant aortic stenosis. The number of heart valve replacements will dramatically increase in the coming years (Chenzbraun, 2010). Prosthetic heart valve dysfunction, in most cases, is lethal, and an early diagnosis for prosthetic valve dysfunction is essential for better outcome and successful treatment (i.e., heparin, fibrinolysis and reoperation) (Roudaut et al., 2007; Aoyagi et al., 2000).

Doppler echocardiography, cinefluoroscopy, and computed tomography (CT) are the most commonly used modalities for the assessment of prosthetic heart valve

performance. Due to the risks associated with X-ray exposure, Doppler/echocardiography is routinely used as a first choice in the evaluation of prosthetic heart valve performance. Only patients suspected of prosthetic valve dysfunction in Doppler/echocardiography are sent to cinefluoroscopy or computed tomography (CT) for visualization of prosthetic valve leaflet morphology and mobility (Montorsi et al., 2003; Cianciulli et al., 2005; LaBounty et al., 2009). However, in the aortic position, and in many cases, the clear visualization of aortic prosthetic valves using Transthoracic Doppler Echocardiography (TTE) and/or Transesophageal Doppler Echocardiography (TEE) is limited due to intense echo reverberations and shadowing caused by valve components (Khandheria et al., 1991; Mohr-Kahaly et al., 1993; Maslow et al., 2000; Aslam et al., 2007). Therefore, the prosthetic valve evaluation process, using TTE as a first choice modality, can only rely on Doppler-derived parameters (peak velocity/gradient, mean pressure gradient, Effective Orifice Area (EOA) and Doppler Velocity Index (DVI)) (Bach, 2010; Zoghbi et al., 2009; and Vesey and Otto, 2004). The recently published guidelines and standards by the American Society of Echocardiography (ASE) emphasized on the use of Doppler-derived parameters for the evaluation of aortic prosthetic valves (Zoghbi et al., 2009). For prosthetic valves in the aortic position, the guidelines suggested an algorithm using constant cut-off values for the previously mentioned Doppler-derived parameters not considering flow conditions, valve size and valve type.

We demonstrated in the previous chapter that the fixed cut-off values have a relatively low sensitivity in detecting valve dysfunction, especially for peak velocity and pressure gradient. Although the EOA reference value for each valve size and type was listed in the guidelines, the listed EOA values, in many cases, are inversely proportional to the valve

size (the larger the valve size the lower the EOA value) which is inconsistent with the fundamentals of fluid mechanics. In addition, the large standard deviation (over 30%) widens the range of expected normal reference value of a specific valve and hence reduces diagnostic accuracy.

A comprehensive study in precisely controlled environments was conducted to theoretically predict the normal reference values of Doppler-derived parameters by considering flow conditions, valve size, and valve type. Moreover, *in vivo* data from a combined echocardiography/fluoroscopy study were extracted and analyzed to validate the *in vitro* findings.

## **5.2 Methods Used for the Validation of the Proposed Theoretical Parameters**

### **5.2.1 Experimental Setup**

**Model.** BMHVs were mounted in an *in vitro* mock flow model previously described and validated (Garcia et al., 2003) (Fig. 5.1). The model is mainly made up of a reservoir, a compliant aortic chamber and a valve resistance. The flow was provided by a computer controlled DC motor coupled to a gear pump (Vi-CORR, Viking Pump). The left ventricular outflow tract and the aorta were both circular and rigid and their size was adjusted to be equal to the nominal size of the implanted valve. The compliant chamber was located immediately downstream of the proximal rigid aorta. The fluid was composed of 2/3 water and 1/3 glycerol so that its density ( $1080 \text{ kg/m}^3$ ) and viscosity (3.5 cP) were similar to that of blood under high shear rate conditions. The flowrate was measured by an electromagnetic flow-meter (Cliniflow II, Carolina Medical Electronics,

accuracy 0.5% full scale) and the ventricular and aortic pressures were measured with Millar catheters (model MPC 500, accuracy 0.5% full scale) under a sampling frequency of 1000 Hz. For each experiment, 10 cycles were recorded and the average was used to calculate the hemodynamic parameters. All valves were tested under five different transvalvular flowrates (3-7 L/min), corresponding to a stroke volume of 30-100 mL at a fixed heart rate of 70 bpm (ejection phase: 0.3 s). Systolic and diastolic pressures were maintained under normal physiological conditions: 120 mmHg and 80 mmHg, respectively.

***Test protocol.*** In order to investigate the accuracy of conventional Doppler-echocardiographic measurements in detecting BMHV dysfunction and to validate ASE suggested reference values, Doppler echocardiographic measurements were performed in a mock flow model incorporating seven BMHVs (4 different sizes of St. Jude HP aortic valves (21 mm-27 mm) and 3 different sizes of On-X aortic valves (21mm-25mm)) under a wide range of cardiac outputs (3-7 L/min) and with various degrees of dysfunction. The dysfunction of the prosthetic valve was introduced by restricting the movement of only one leaflet. This is because it is more difficult to detect when compared to the situation where both leaflets have restricted motion (Montorsi et al., 2003). The position of the leaflet was varied from the fully opened position (0% dysfunction) to the fully closed position (100% dysfunction) with one intermediate position (50% dysfunction).

***Echocardiography.*** Doppler echocardiographic velocity measurements were performed in all cases using a Sonos 5500 (Philips Medical Systems/Agilent Technologies,

Andover, Massachusetts) with a probe of 2.25 MHz. The probe was placed at different locations on the measurement window to obtain the highest possible peak velocity reading through the three BMHV orifices (one central and two lateral orifices). In order to avoid aliasing, the continuous-wave Doppler mode was used. The measurements were performed over three cycles and averaged. Peak Doppler-echocardiographic velocity, mean transvalvular pressure gradients (determined using simplified Bernoulli equation) and prosthetic EOA (estimated using continuity equation) were evaluated for the BMHVs with 0%, 50% and 100% dysfunction. Inter-observer variability for different parameters was evaluated by recording the measurements of all SJHP21 and On-X 21 cases by 2 of the authors (Table 5.1). Their observations were then compared with one another. Variability was expressed as mean percent error, calculated as the absolute difference between the two observations divided by the mean of the observations and expressed as a percentage.

Table 5.1 Variability of *in vitro* extracted Doppler-derived parameters for St. Jude and On-X Prosthetic Valves

	Interobserver (%)
Peak LVOT Velocity m/s	1.8 ± 1.3
Peak transprosthetic Velocity m/s	2.4 ± 1.3
EOA cm <sup>2</sup>	2.9 ± 2.2
TPG <sub>mean</sub> mmHg	5.6 ± 4.4

Values are given as mean±SD

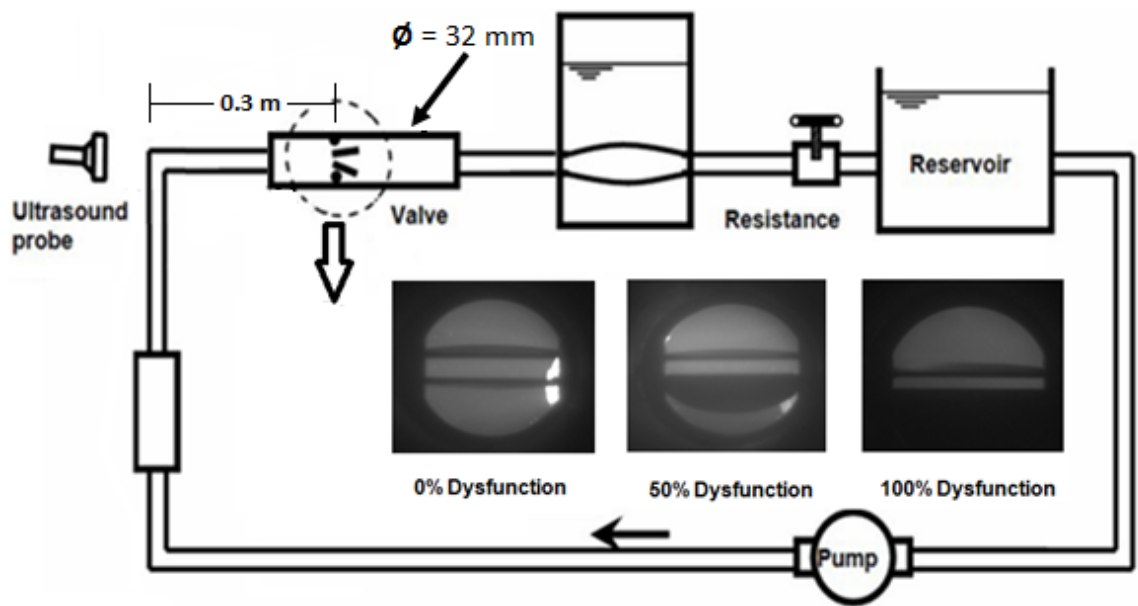


Figure 5.1 Sketch for the custom-made cardiac simulator, and the maximum opening position for the leaflets.

### **5.2.2 *In Vivo* Data**

***Patient Population.*** From March 2005 to July 2010, 31 patients underwent both a Doppler-echocardiographic exam and a valve cinefluoroscopy within a period of 2 weeks at the Quebec Heart and Lung Institute. The patients were referred to cinefluoroscopy due to suspected valve dysfunction on the Doppler-echocardiographic exam. Among these patients, 4 had a valve dysfunction confirmed by the visualization of abnormal motion of one or two leaflets on cinefluoroscopy. Seven patients with normally functioning prosthetic valve at cinefluoroscopy were excluded as Doppler-echocardiographic data was incomplete. The final cohort thus consisted of 17 patients: 13 with normal valve function (Table 5.3) and 4 with valve dysfunction (Table 5.4).

***Echocardiography and Cinefluoroscopy.*** In echocardiography, the magnitude of the velocity across the prosthetic valves was obtained by placing the transducer in the apical position. For continuous wave Doppler measurements, the transmitted beam was placed as close to the perpendicular plane of the valve ring as possible. Doppler velocity in the left ventricular outflow tract was measured approximately 0.5 cm upstream from the prosthetic valve. Cinefluoroscopy was performed to obtain a tangential view of the implanted prosthetic valve. The maximum opening and closing angles were determined by averaging 3 consequent cardiac cycles for each patient. In this study the determination of the opening and closing angles was possible in all 17 patients.

### **5.2.3 Mathematical Model for Proposed Parameters**

In the current model, theoretical reference values for Doppler-derived parameters

(e.g., peak velocity, mean velocity, TPGmean, and EOA), in normally functioning bileaflet mechanical heart valves, are predicted. Any significant difference between the theoretically predicted and accurately measured parameter can be interpreted as a dysfunction in the valve. The current theoretical predictions follow the standard clinical settings by considering the flow through the central orifice (between the two leaflets) for calculating Doppler-derived parameters.

### 5.2.3.1 Predicted Peak and Mean Velocities

The main assumption in the current approach is that the fraction of total flow crossing a specific orifice (central or lateral) is proportional to its area over the geometrical orifice area (Bech-Hanssen et al., 2001) (Fig. 5.2).

$$\frac{Q_{central}}{Q_{LVOT}} = \frac{A_{central}}{GOA} \quad (5.1)$$

Where  $Q_{central}$  is the flowrate through the central orifice ( $m^3/s$ ),  $A_{central}$  is the area of the central orifice ( $m^2$ ), and  $GOA$  is the total geometric valve orifice area (inner area) ( $m^2$ ).

Flowrate through the central orifice can be directly calculated as shown in equation 5.2:

$$Q_C = V_{central} * A_{central} * C_C \quad (5.2)$$

where  $V_{central}$  is the measured transvalvular velocity ( $m/s$ ),  $A_{central}$  is the area of the central orifice ( $m^2$ ),  $C_C$  is the contraction coefficient.

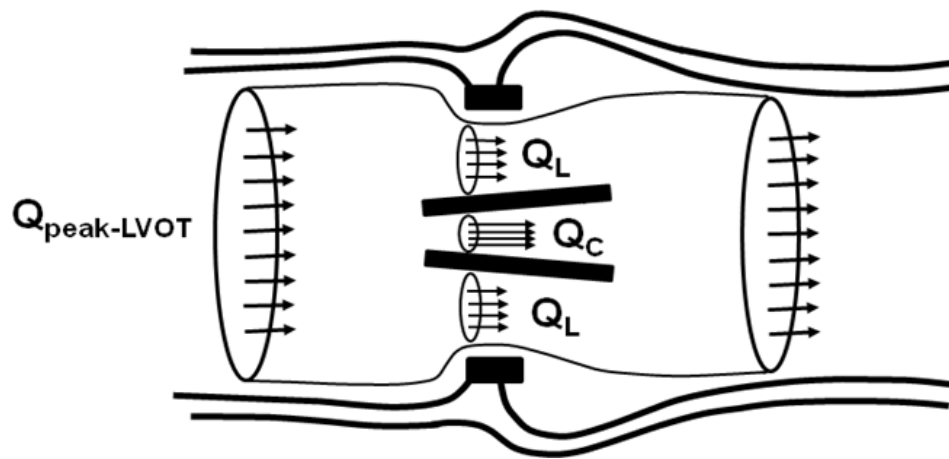


Figure 5.2 Schematic representation for blood flow through bileaflet mechanical heart valve, where  $Q_{\text{peak-LVOT}}$  is peak systolic flowrate (L/min) at the left ventricle outflow tract location,  $Q_C$  is the flowrate (L/min) through the central orifice, and  $Q_L$  is the flowrate (L/min) through the lateral orifice.

Equations 5.1 and 5.2 can be combined to give the following equation:

$$V_{central - predicted} = \frac{1}{GOAC_C} * Q_{LVOT} \quad (5.3)$$

From equation 5.3, we can predict peak transvalvular velocity as well as the mean transvalvular velocity as shown in equations 5.4 and 5.5, respectively.

$$V_{peak - predicted} = \frac{1}{GOAC_C} * Q_{peak - LVOT} \quad (5.4)$$

$$V_{mean - predicted} = \frac{1}{GOAC_C} * Q_{mean - LVOT} \quad (5.5)$$

$$Q_{peak - LVOT} = V_{peak - LVOT} * \frac{\Pi}{4} D_{LVOT}^2 \quad (5.6)$$

$$Q_{mean - LVOT} = V_{mean - LVOT} * \frac{\Pi}{4} D_{LVOT}^2 \quad (5.7)$$

where  $V_{peak - predicted}$  is the predicted peak transvalvular velocity (m/s),  $V_{mean - predicted}$  is the predicted mean transvalvular velocity (m/s);  $Q_{peak - LVOT}$  is the measured peak LVOT flowrate (m<sup>3</sup>/s),  $Q_{mean - LVOT}$  is the measured mean LVOT flowrate (m<sup>3</sup>/s), and  $D_{LVOT}$  is the measured LVOT diameter (m).

It is obvious that equations 5.5 and 5.6 rely, mainly, on accurate LVOT measurements (i.e., diameter, velocity spectrum), and prosthetic valve GOA to accurately predict the normal values of mean and peak transvalvular velocity.

### 5.2.3.2 Predicted Mean Pressure Gradient

Doppler derived pressure gradient is traditionally calculated as an average of

instantaneous pressure gradient  $\left( TPG_{mean} = \frac{\sum_1^n TPG_i}{n} = \frac{\sum_1^n (4 * V_i^2)}{n} \right)$ . Therefore,

considering the mean velocity for calculating  $TPG_{mean}$  ( $TPG_{mean} = 4 * V_{mean}^2$ ) will underestimate the  $TPG_{mean}$  normal value by a certain percentage (Const.) as shown in equation 5.8:

$$TPG_{mean - predicted} = \frac{4 * V_{mean - predicted}^2}{Const.} \quad (5.8)$$

However, this percentage changes according to the type of commercial echocardiography machine used for the measurements. In the current study *Sonos 5500* echocardiography machine was used and the constant value was 0.85.

### 5.2.3.3 Predicted Effective Orifice Area ( $EOA_{predicted}$ ):

$$EOA_{predicted} = \frac{Q_{LVOT}}{V_{central - predicted}} \quad (5.9)$$

Manipulating  $V_{central - predicted}$  by using equation 5.3:

$$EOA_{predicted} = GOA * C_C \quad (5.10)$$

## 5.3 Results

In the current results, a contraction coefficient of 0.7 was adapted for the theoretical prediction of normal reference values of Doppler-derived parameters. The previously

reported values for the contraction coefficient ranged from 0.6 to 0.8 ( $C_c \approx 0.6-0.8$ ) (Izzat et al., 1996; Chandas et al., 2000; Kadir et al., 2001; Bech-Hanssen et al., 2001; Guivier-Curien et al., 2009). However, different BMHVs have different designs (i.e., different maximum opening angle). Moreover, reported *in vivo* maximum opening angles might be lower compared to *in vitro* ones (Cianciulli et al., 2005). To compensate for such limitations, an additional 20% of the predicted values were considered to estimate the *in vivo* cut-off values of Doppler derived parameters.

$$V_{\text{Peak cut-off value}} = V_{\text{Peak-Predicted}} + 20 \% V_{\text{Peak-Predicted}}$$

$$\text{TPG}_{\text{mean cut-off value}} = \text{TPG}_{\text{mean-predicted}} + 20 \% \text{TPG}_{\text{mean-predicted}}$$

$$\text{EOA cut-off value} = \text{EOA}_{\text{Predicted}} - 20 \% \text{EOA}_{\text{Predicted}}$$

### 5.3.1 Validation Against *In Vitro* Data

#### Peak and Mean Velocities

Figures 5.3 and 5.4 show, for different sizes of SJHP and On-X BMHVs, variation in peak and mean Doppler velocities as a function of flowrate and percentage of BMHV dysfunction. Theoretically predicted peak and mean Doppler velocities for normally functioning BMHVs (0% dysfunction) are also shown.

Peak and mean Doppler velocity magnitudes were proportional to transvalvular flowrate and inversely proportional to valve size. The highest measured peak Doppler velocity in normally functioning valves was achieved for the smallest valve size and highest flowrate and reached up to 3.8 m/s and 3.27 m/s for SJHP21 and On-X21, respectively. Moreover, the highest measured mean Doppler velocity in normally functioning valves was achieved at the smallest valve size and highest flowrate and reached up to 2.30 m/s and

2.18 m/s for SJHP21 and On-X21, respectively. Furthermore, peak and mean Doppler velocities were proportional to the percentage of dysfunction. The highest peak velocity was found with the presence of 100% dysfunction and reached up to 5.6 and 6 m/s for SJHP21 and On-X21, respectively. The highest mean Doppler velocity was 3.7 m/s and 3.97 m/s for SJHP21 and On-X21, respectively.

Introducing 50% of dysfunction to one leaflet (25% reduction in total GOA), did not significantly alter the peak and mean Doppler velocity values. Compared to normal cases, peak and mean Doppler velocities of 50% dysfunctional cases increased by  $17.00\% \pm 10.72\%$  and  $18.15\% \pm 9.10\%$ , respectively.

Introducing 100% dysfunction to one leaflet (50% reduction in total GOA) significantly increased the peak and mean Doppler velocity by  $71.8\% \pm 31.14\%$  and  $71.92\% \pm 26.55\%$ , respectively.

As shown in Figures 5.5.a and 5.6.a, the correlation between theoretical and *in vitro* measurements of peak/mean Doppler velocities was excellent ( $R^2 = 0.96$  and  $R^2 = 0.93$ , respectively). In addition, good agreement was observed between predicted and measured peak and mean velocity values where fitting lines almost coincide with the line of equality. The good agreement was also observed in the Bland-Altman plots (Figures 5.5b and 5.6b).

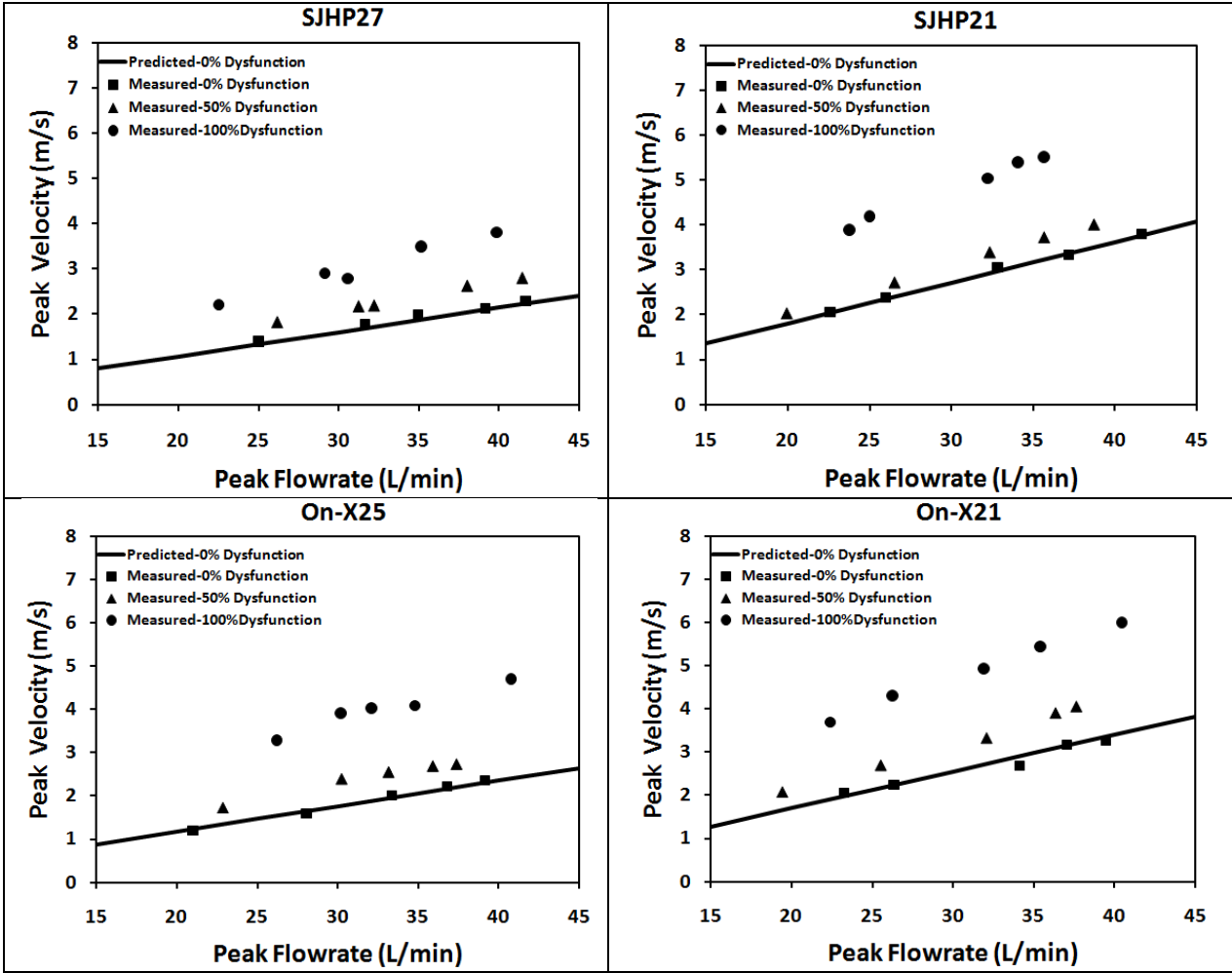


Figure 5.3 Measured peak transvalvular velocity for different flowrates and different percentages of valve dysfunction. Theoretically predicted peak velocity of normally functioning valve (0% dysfunction) for different flowrates is also plotted.

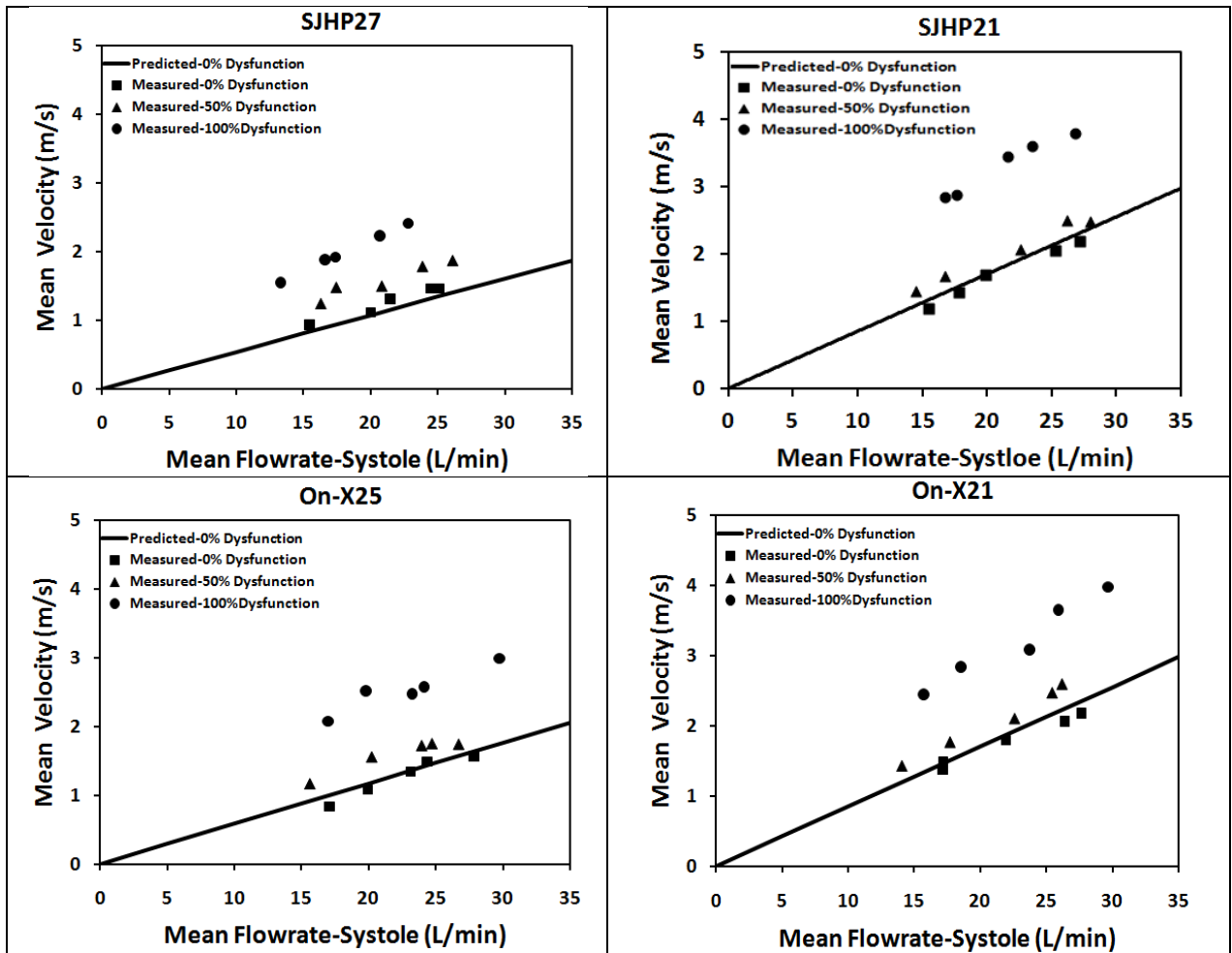
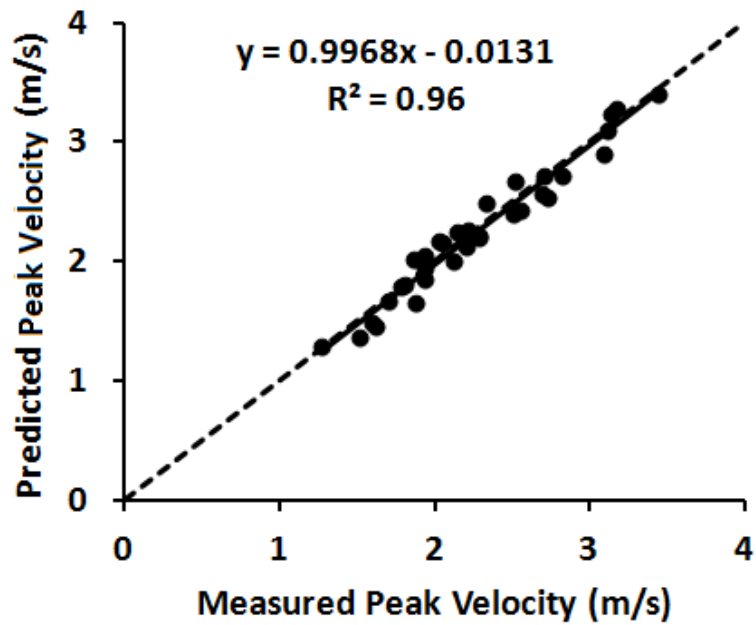
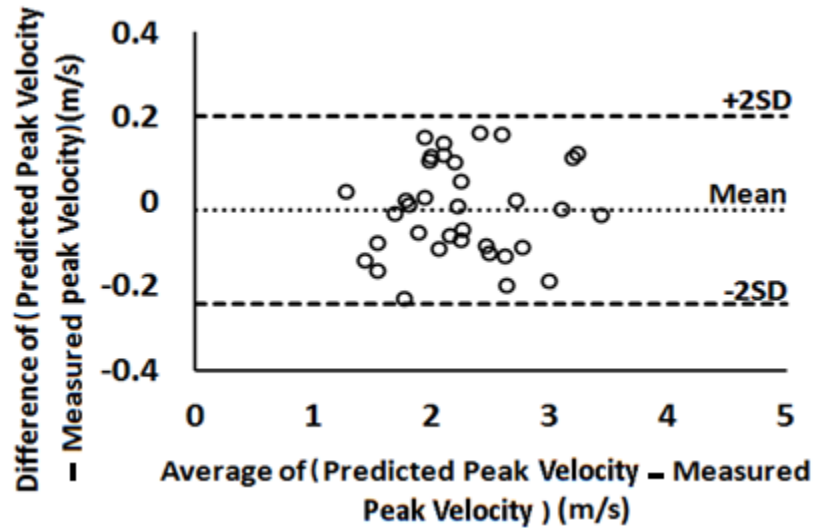


Figure 5.4 Measured mean transvalvular velocity for different flowrates and different percentages of valve dysfunction. Theoretically predicted mean velocity of normally functioning valve (0% dysfunction) for different flowrates is also plotted.

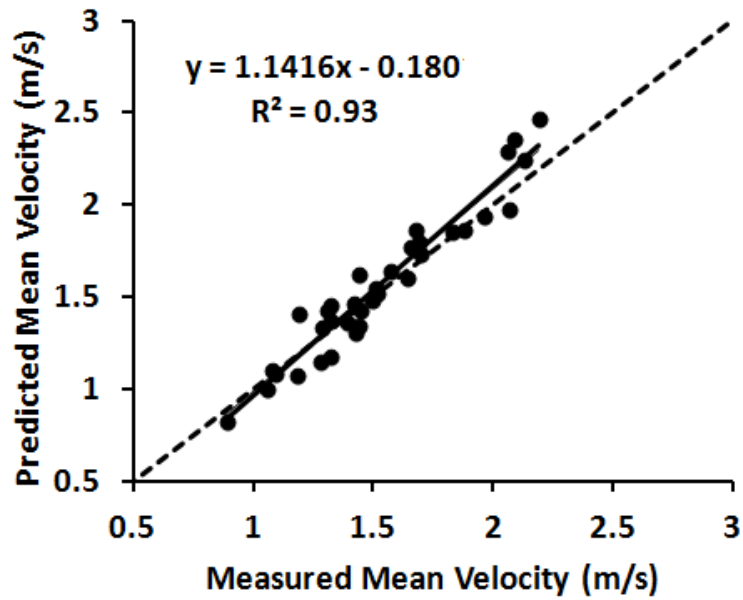


(a)

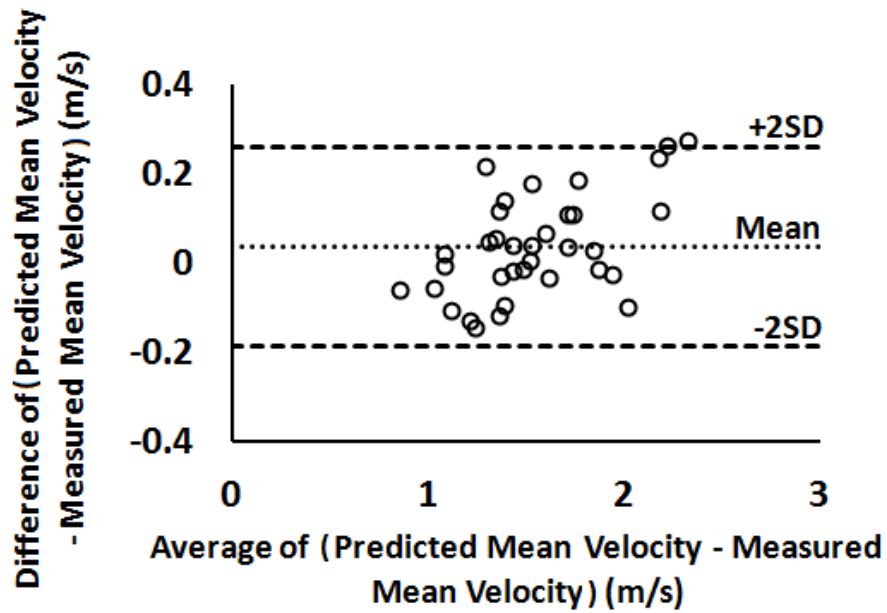


(b)

Figure 5.5 (a) *In vitro* correlations between predicted and measured peak Doppler velocity. (b) Differences between predicted and measured peak Doppler velocity are presented on a Bland-Altman plot.



(a)



(b)

Figure 5.6 (a) *In vitro* correlations between predicted and measured mean Doppler velocity. (b) Differences between predicted and measured mean Doppler velocity are presented on a Bland-Altman plot.

## Mean Pressure Gradient

Figure 5.7 shows, for the largest and the smallest sizes of SJHP and On-X BMHVs, variation in  $TPG_{\text{mean}}$  as a function of flowrate and percentage of dysfunction. The theoretically predicted  $TPG_{\text{mean}}$  for normally functioning BMHV (0% dysfunction) is also shown.

The  $TPG_{\text{mean}}$  magnitude was proportional to transvalvular flowrate and inversely proportional to valve size. The highest measured  $TPG_{\text{mean}}$  in normally functioning valves was achieved at the smallest valve size and highest flowrate and reached up to 26.6 mmHg and 22.0 mmHg for SJHP21 and On-X21, respectively. Furthermore,  $TPG_{\text{mean}}$  was proportional to percentage of dysfunction. The highest  $TPG_{\text{mean}}$  was found with the presence of 100% dysfunction and reached up to 64 mmHg and 73.63 mmHg for SJHP21 and On-X21, respectively.

Introducing 50% dysfunction to one leaflet (25% reduction in total GOA), did not significantly alter  $TPG_{\text{mean}}$  values. Relative to normal cases,  $TPG_{\text{mean}}$  increased by  $40\% \pm 23.27\%$  in the presence of 50% dysfunction,. Introducing 100% dysfunction to one leaflet (50% reduction in total GOA) significantly increased the percent difference for  $TPG_{\text{mean}}$  up to  $210.36\% \pm 103.20\%$ .

As shown in Figure 5.8a, the correlation between theoretical and *in vitro*  $TPG_{\text{mean}}$  was excellent ( $R^2 = 0.94$ ). Also, good agreement was found between predicted and measured  $TPG_{\text{mean}}$  values where the fitting lines almost coincide with the line of equality. The good agreement could be shown in the Bland-Altman plots as well (Figure 5.8b).

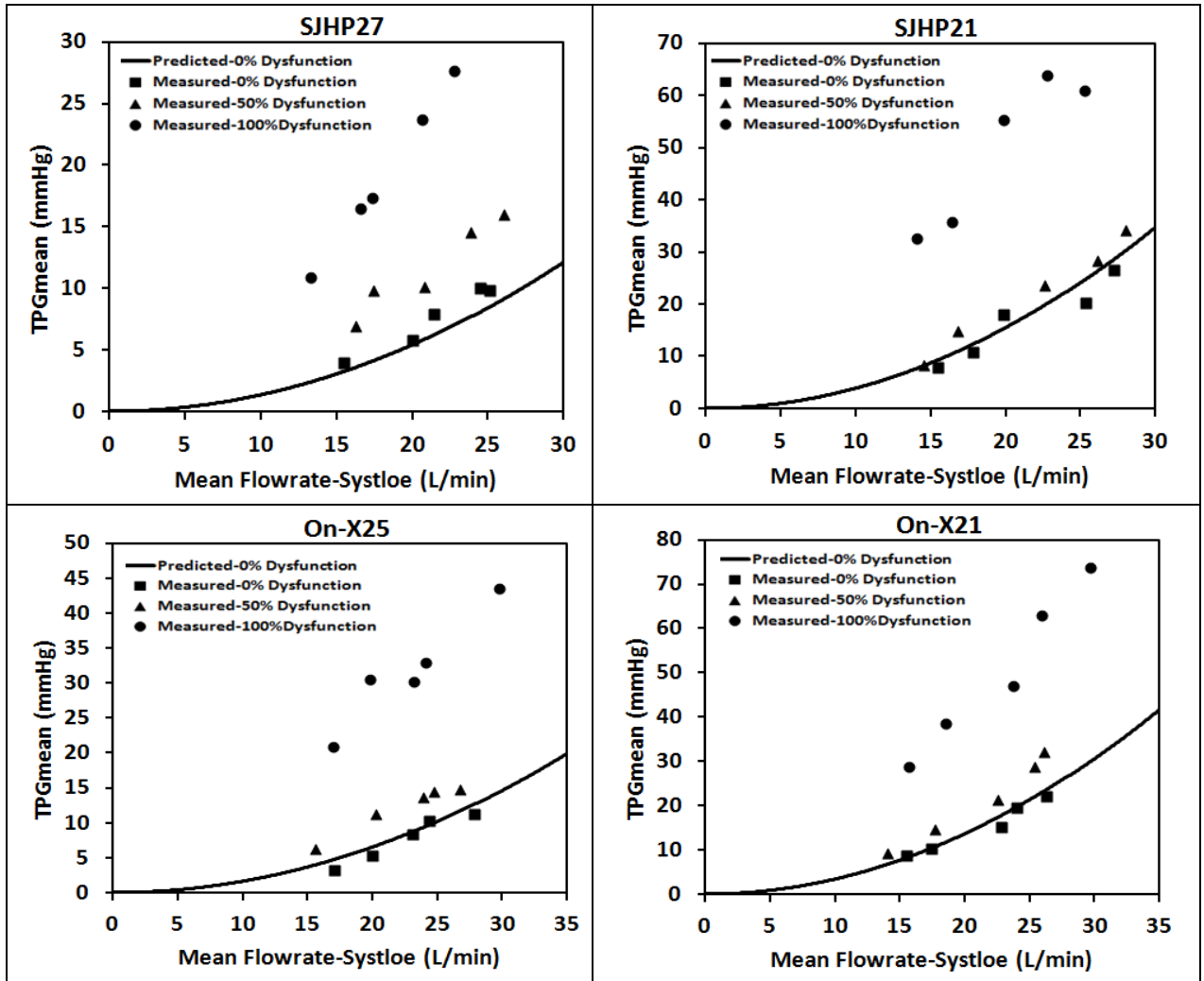
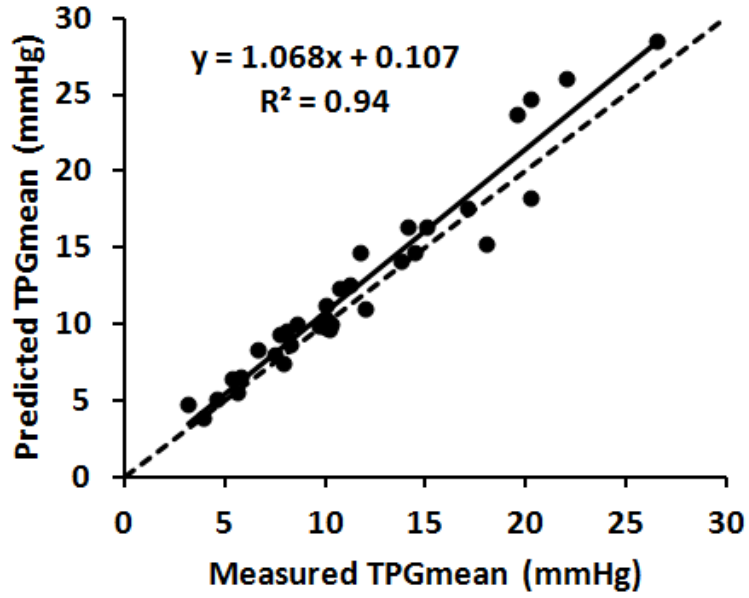
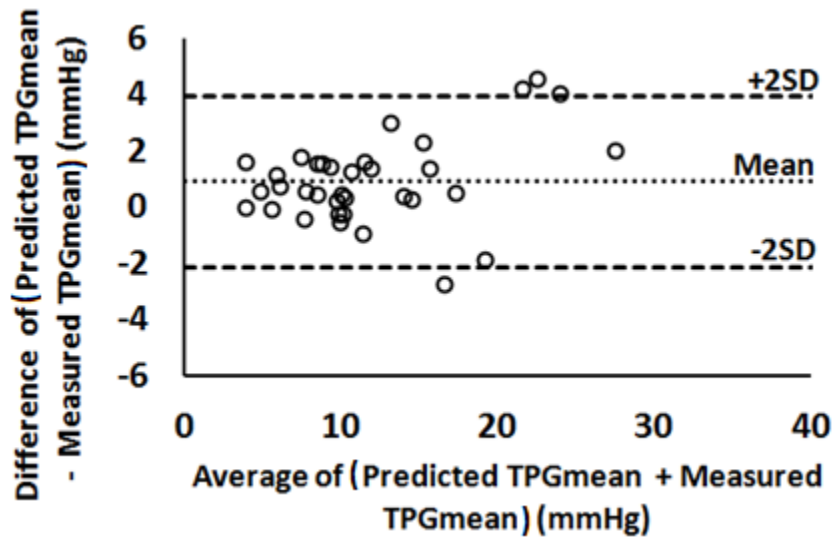


Figure 5.7 Measured  $TPG_{mean}$  for different flowrates and different percentages of dysfunction. The theoretically predicted  $TPG_{mean}$  of normally functioning valve (0% dysfunction) for different flowrates is also plotted.



(a)



(b)

Figure 5.8 (a) *In vitro* correlation between predicted and measured  $TPG_{\text{mean}}$ ; (b) Differences between predicted and measured  $TPG_{\text{mean}}$  are presented on a Bland-Altman plot.

### **Effective Orifice Area (EOA)**

Table 5.2 shows good agreement between current *in vitro* EOA values and the theoretical EOA, as well as the reported *in vivo* EOA values in the literature (Zoghbi et al. 2009; Pibarot and Dumesnil 2009). The reference values in these articles are extracted from different previous publications and not the results of one comprehensive study.

Figure 5.9 shows, for different sizes of SJHP and On-X BMHVs, the variation in EOA as a function of flowrate and percentage of dysfunction. Also, the theoretical EOA for normal-functioning BMHV (0% dysfunction) was shown.

EOA magnitude was found to be flowrate independent and only proportional to valve size and type. The highest measured EOA in normally functioning valves was achieved at the largest valve size and reached up to  $2.95 \pm 0.10 \text{ cm}^2$  and  $2.62 \pm 0.19 \text{ cm}^2$  for SJHP27 and On-X25, respectively. Furthermore, EOA was inversely proportional to percentage of dysfunction. The lowest EOA was found with the presence of 100% dysfunction and dropped to  $1.06 \pm 0.06 \text{ cm}^2$  and  $0.88 \pm 0.08 \text{ cm}^2$  for SJHP21 and On-X21, respectively.

However, reduction percentage in measured Doppler EOA was close from the reduction percentage in GOA. Compared to normal cases, EOA decreased by  $17.92\% \pm 6.1\%$  after the introduction of 50% dysfunction. Introducing 100% dysfunction to one leaflet (50% reduction in total GOA) decreased the measured Doppler EOA by  $41.78\% \pm 6.48\%$ .

As shown in Figure 5.10a, the correlation between theoretical and *in vitro* EOA was high ( $R^2 = 0.88$ ). Also, good agreement was found between predicted and measured EOA values as shown in the Bland-Altman plot (Figure 5.10b).

Table 5.2 Validation of measured EOA normal reference values

Valve Type *	GOA	Current ( <i>In vitro</i> )	Current (Theoretical)	Zoghbi et al., 2009 ( <i>In vivo</i> )	Pibarot & Dumesnil 2009 ( <i>In vivo</i> )
SJ-HP27/ SJ- ST29	4.18	2.95 ± 0.10	2.93	2.8 ± 0.5 (ST)	3.2 ± 0.3 (ST)
SJ-HP25/ SJ- ST27	3.56	2.44 ± 0.08	2.50	2.5 ± 0.4 (ST)	2.7 ± 0.6 (ST)
SJ-HP23/ SJ- ST25	3.00	2.16 ± 0.01	2.10	1.7 ± 0.5 (HP)	2.1 ± 0.4 (ST)
SJ-HP21/ SJ- ST23	2.46	1.87 ± 0.02	1.72	1.8 ± 0.5 (HP)	1.5 ± 0.5 (ST)
ON-X25	4.05	2.62 ± 0.19	2.84	2.4 ± 0.6	2.4 ± 0.8
ON-X23	3.43	2.00 ± 0.07	2.19	1.9 ± 0.6	2 ± 0.6
ON-X21	2.80	1.69 ± 0.05	1.96	1.7 ± 0.4	1.7 ± 0.4

SJHP valve has the same GOA as the SJ-ST, which is one size larger (SJHP25=SJST27)

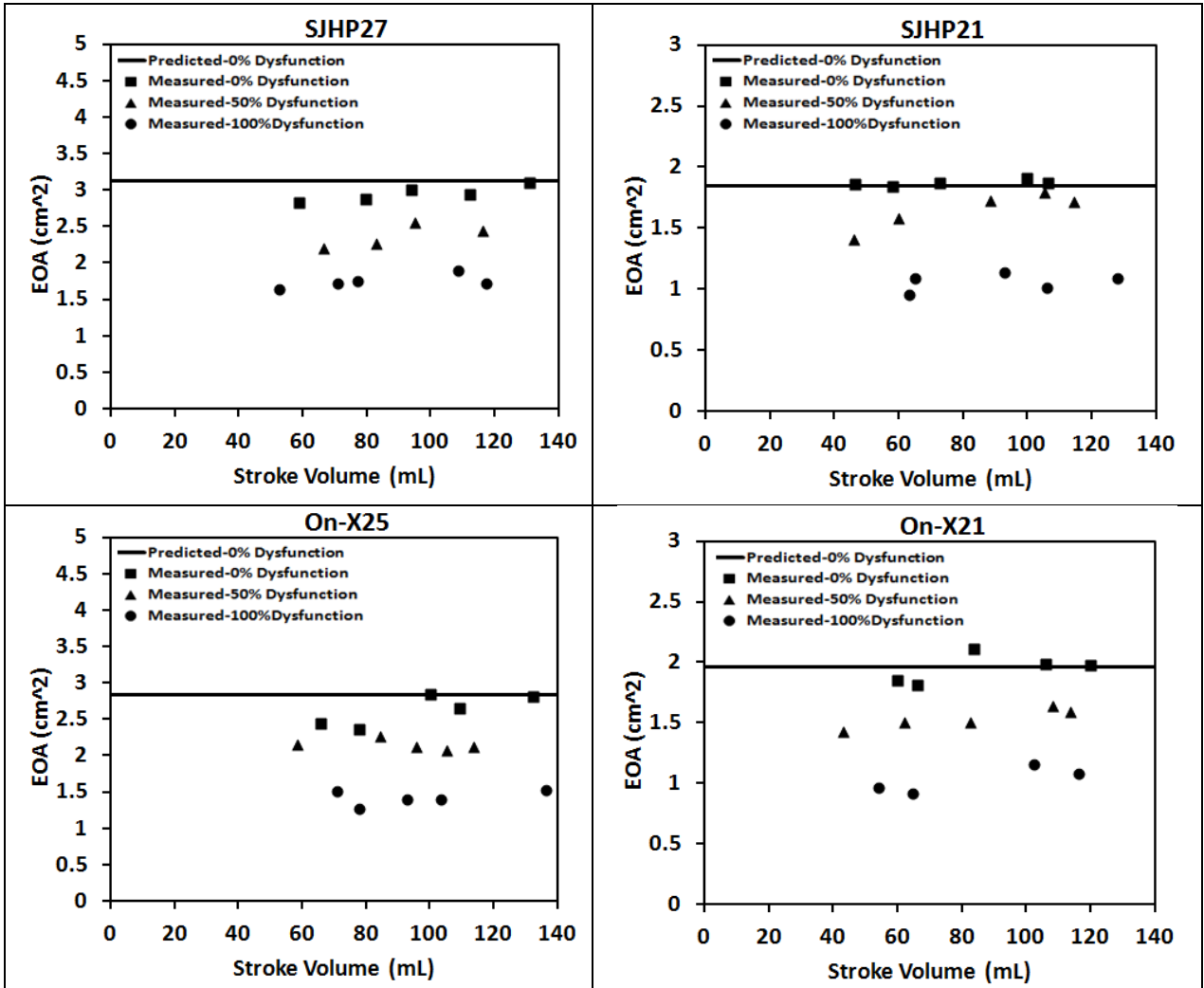
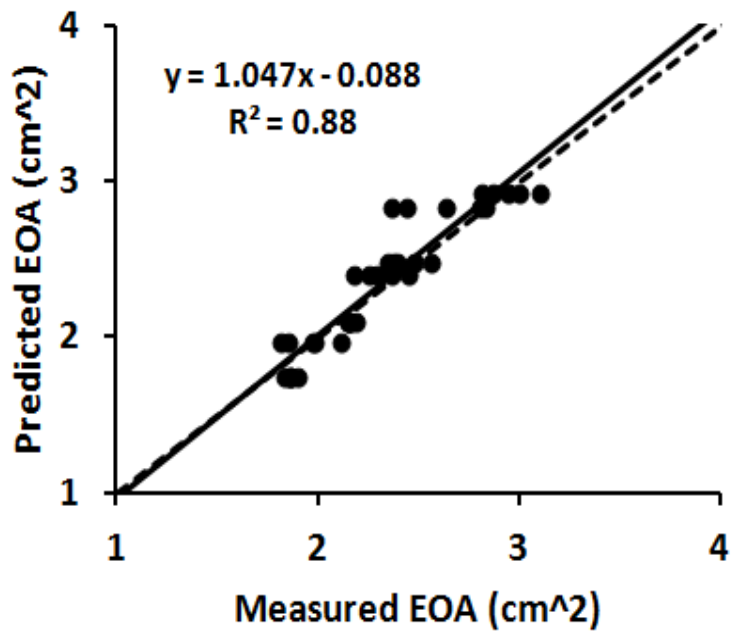
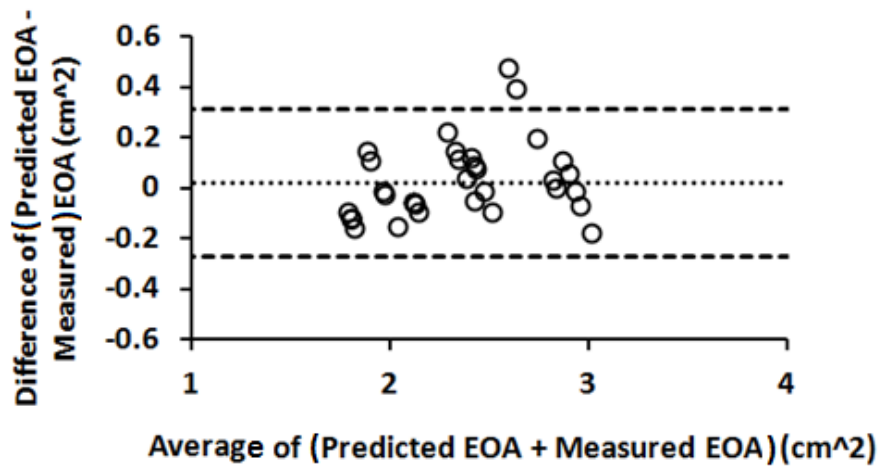


Figure 5.9 Measured EOA for different flowrates and different percentages of dysfunction. The theoretically predicted EOA of normally functioning valves (0% dysfunction) for different flowrates is also plotted.



(a)



(b)

Figure 5.10 (a) *In vitro* correlations between predicted and measured EOA. (b) Differences between predicted and measured EOA are presented on a Bland-Altman plot.

### 5.3.2 Validation Against *In-Vivo* Data

Tables 5.3 and 5.4 show the *in vivo* measured Doppler parameters and their corresponding theoretically predicted values (peak velocity,  $TPG_{\text{mean}}$ , and EOA) for normal and dysfunctional BMHVs, respectively. Good correlation ( $R^2 = 0.89$ ) was found between the predicted and measured peak velocity as shown in Fig. 5.11.a and on the Bland-Altman plot in Fig. 5.11b.

The mean values of the Doppler derived peak velocities and mean pressure gradients of dysfunctional valves were  $2.85 \pm 0.89$  m/s and  $30 \pm 11.6$  mmHg, respectively.

These values were higher than those of normal valves ( $3.7 \pm 0.46$  m/s and  $19.6 \pm 13$  mmHg). However, there was a wide range of peak velocities and gradients, and the peak velocity and gradient of some healthy valves was higher than the value for some dysfunctional valves. For healthy valves, EOA values ranged between 2.2 and 1.23 (mean,  $1.7 \pm 0.3$ ) and were higher than EOA values for dysfunctional valves which ranged between  $1.56 \text{ cm}^2$  and  $0.52 \text{ cm}^2$  (mean,  $1.05 \pm 0.37 \text{ cm}^2$ ). However, there was a wide range of peak velocities, gradients, DVI and EOA.

Additional validation against *in vivo* data for the obstructed St. Jude bileaflet valve, extracted from Aoyagi et al. (2001) was also conducted (Table 5.5). The EOA values for all listed cases were significantly lower than the suggested cut-off value.

## 5.4 Discussion

Early detection of valve dysfunction can save patients from lethal consequences. We demonstrated in the previous chapter that the fixed cut-off values for Doppler-derived parameters have relatively low sensitivity in detecting valve dysfunction. Although the

EOA reference value for each valve size and type was listed in the guidelines, these values, in many cases, were not in agreement with the fundamentals of fluid mechanics (the larger the valve size, the lower the EOA value!). In addition, the large standard deviation (over 30%) widens the range of expected normal reference values for a specific valve and thus reduces the diagnostic accuracy.

Predicting the normal values of Doppler-derived parameters (peak velocity, mean pressure gradient, and EOA) based on flow conditions and valve type, for each patient, would be extremely useful in improving the diagnostic accuracy of valve dysfunction.

#### **5.4.1 Velocities and Pressure Gradients**

Velocity and pressure gradients showed strong dependency on flowrate and BMHV size (Baumgartner et al., 1992). Of note is that accurate valve size relies on the actual inner GOA not the labelled size (Chambers et al., 2003). Therefore, detecting BMHV dysfunction using a fixed cut-off value for peak velocity and mean gradient without considering flow conditions or valve size/type, as suggested by ASE guidelines, can reduce in the sensitivity of diagnosing valve dysfunction. This is especially important for low flowrates through a large BMHV where the peak velocity and mean gradient could be less than the cut-off value. In contrast, high flowrate through normally functioning small BMHV could elevate the peak velocity and the mean pressure gradient above the cut-off values (figs. 5.3, 5.4, and 5.7).

The theoretically predicted peak velocity and mean pressure gradient proposed in this work take into account flowrate and valve size/type. Therefore, each patient can have a customized reference value based on the cardiac output and the implanted BMHV.

Table 5.3 Doppler-derived data for normal aortic bileaflet valves

No.	Valve Size	LVOT Dia. (cm)	SV (ml)	Peak Velocity (m/s)	Peak Velocity Cut-off Value (m/s)	Mean Pressure Gradient (mmHg)	EOA (cm <sup>2</sup> )	EOA Cut-off Value (cm <sup>2</sup> )
<b>SJ</b>								
1	21-mm ST	2.1	69	2.41	2.46	15.4	1.28	1.15
2	25-mm ST	2.2	88	3.10	2.55	25.0	1.60	1.73
3	25-mm ST	2.4	68	2.04	2.00	9.0	2.13	1.73
4	25-mm ST	2.55	76	2.14	2.33	9.3	2.06	1.73
5	25-mm ST	2.3	79	2.15	1.77	9.0	1.88	1.73
<b>Carbomedics Top Hat</b>								
6	21-mm	2.1	87	3.51	2.84	27.0	1.23	1.17
7	23-mm	2.3	113	3.45	3.01	25.0	1.77	1.43
8	23-mm	2.2	114	3.75	3.69	30.0	1.90	1.43
9	23-mm	2.2	69	1.81	2.00	7.0	1.76	1.43
10	25-mm	2.4	107	2.89	2.33	24.0	1.78	1.77
<b>ADVANTAGE</b>								
11	21-mm	1.9	77	2.80	2.43	13.0	1.39	1.15
<b>On-X</b>								
12	19-mm	1.9	77	2.49	2.23	13.0	1.39	1.24
13	23-mm	2.25	84	1.87	1.91	7.36	2.2	1.92

HP, Hemodynamic Plus; ST, Standard

Table 5.4 Doppler-derived data for obstructed aortic bileaflet valves

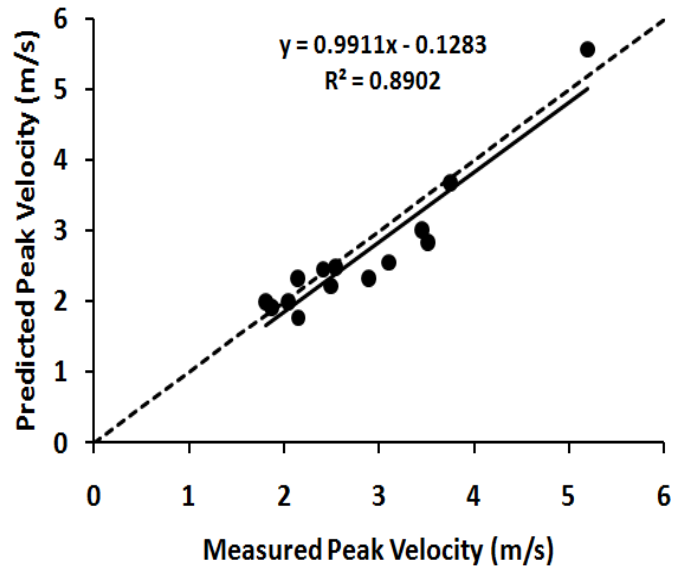
<b>Patient No.</b>	<b>Prosthetic Valve</b>	<b>Diagnosis</b>	<b>LVOT Diameter (cm)</b>	<b>SV (ml)</b>	<b>Peak LVOT Velocity (m/s)</b>	<b>Peak Velocity (m/s)</b>	<b>Peak Velocity (Cutoff value) (m/s)</b>	<b>Mean Pressure Gradient (mmHg)</b>	<b>EOA (cm<sup>2</sup>)</b>	<b>EOA (Cutoff Value) (cm<sup>2</sup>)</b>
14	23- SJ ST	Stenosis 35°-10°	2.2	61	0.72	3.26	1.91	20	0.97	1.58
15	25- SJ ST	Stenosis 56°-56°	1.9	47	0.77	4.3	1.25	42	0.52	1.73
16	27-SJ HP	Stenosis 35°-35°	2.3	100	1.15	3.29	1.96	17	1.56	2.34
17	27-CM TH	Stenosis 22°-32°	2.1	94	1.18	4.08	1.82	41	1.14	2.15

HP, Hemodynamic Plus; ST, Standard

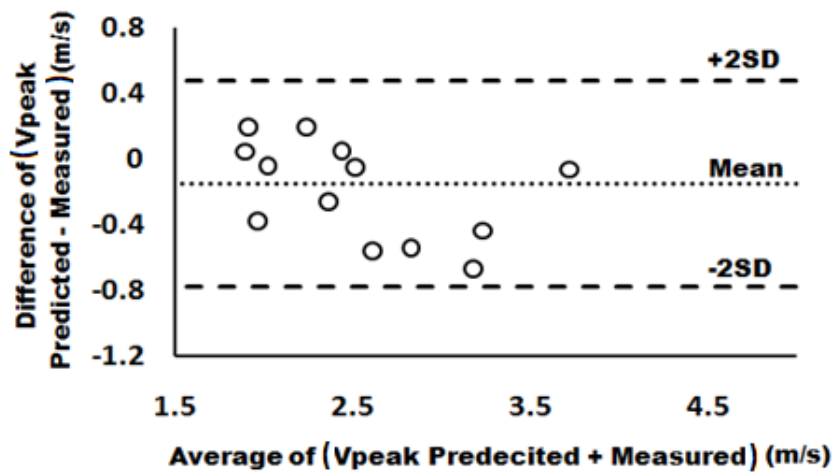
Table 5.5 Doppler-derived data for obstructed aortic bileaflet valves (Aoyagi et al., 2000)

<b>Prosthetic Valve</b>	<b>Diagnosis</b>	<b>Peak Velocity (m/s)</b>	<b>Peak Velocity Cut-off Value (m/s)</b>	<b>EOA (cm<sup>2</sup>)</b>	<b>EOA Cut-off Value (cm<sup>2</sup>)</b>	<b>(DVI)</b>
21-mm SJ ST	Stenosis 18° -18°	3.39	2.50	1.16	1.15	0.33
21-mm SJ ST	Stenosis 25°-25°	3.5	2.34	0.99	1.15	0.30
21-mm SJ ST	Stenosis 22°-22°	3.7	2.23	0.80	1.15	0.27
21-mm SJ ST	Stenosis 25°-25°	4.12	2.31	0.72	1.15	0.25
21-mm SJ ST	Stenosis 20°-20°	3.38	2.50	0.99	1.15	0.33

ST, Standard



(a)



(b)

Figure 5.11 (a) *In vivo* correlation between predicted and measured peak Doppler velocity. (b) Differences between predicted and measured peak Doppler velocity are presented on a Bland-Altman plot.

It is worth mentioning that accurate LVOT measurements (velocity and diameter) and information about the size and type of the implanted BMHV (actual GOA) are essential for precise predictions.

#### **5.4.2 Effective Orifice Area**

Equation 5.10 is the original definition of EOA. However, reaching to this fundamental definition based on the suggested formulas for the predicted velocity supports the method and the assumptions that led to the current theoretically derived parameters.

Based on *in vivo* data shown in tables 5.2 and 5.3, EOA cut-off values showed better accuracy in differentiating between normal and dysfunctional valves compared to other suggested parameters. Moreover, flow independency makes EOA more favourable than other Doppler derived parameters in this study. However, precise LVOT measurements (LVOT Diameter and  $VTI_{LVOT}$ ) are essential for getting accurate EOA.

#### **5.4.3 Mild to Moderate Severity of Valve Dysfunction (50% Dysfunction)**

Compared to normal cases, introducing 50% dysfunction to on leaflet did not significantly elevate the peak velocity, the  $TPG_{mean}$ , or the EOA. The values, as percentage increase, were  $17\% \pm 10.7\%$ ,  $40\% \pm 23.3\%$ , and  $17.9\% \pm 6.1\%$ , respectively (figures 5.3, 5.7, and 5.9). Consequently, accurate diagnosis for cases with 50% valve dysfunction can be difficult, especially with the presence of technical measurement errors in echocardiography measurements such as misalignment between the ultrasound beam and the velocity jet, or inaccurate measurement of the LVOT diameter (Chenzbraun, 2010).

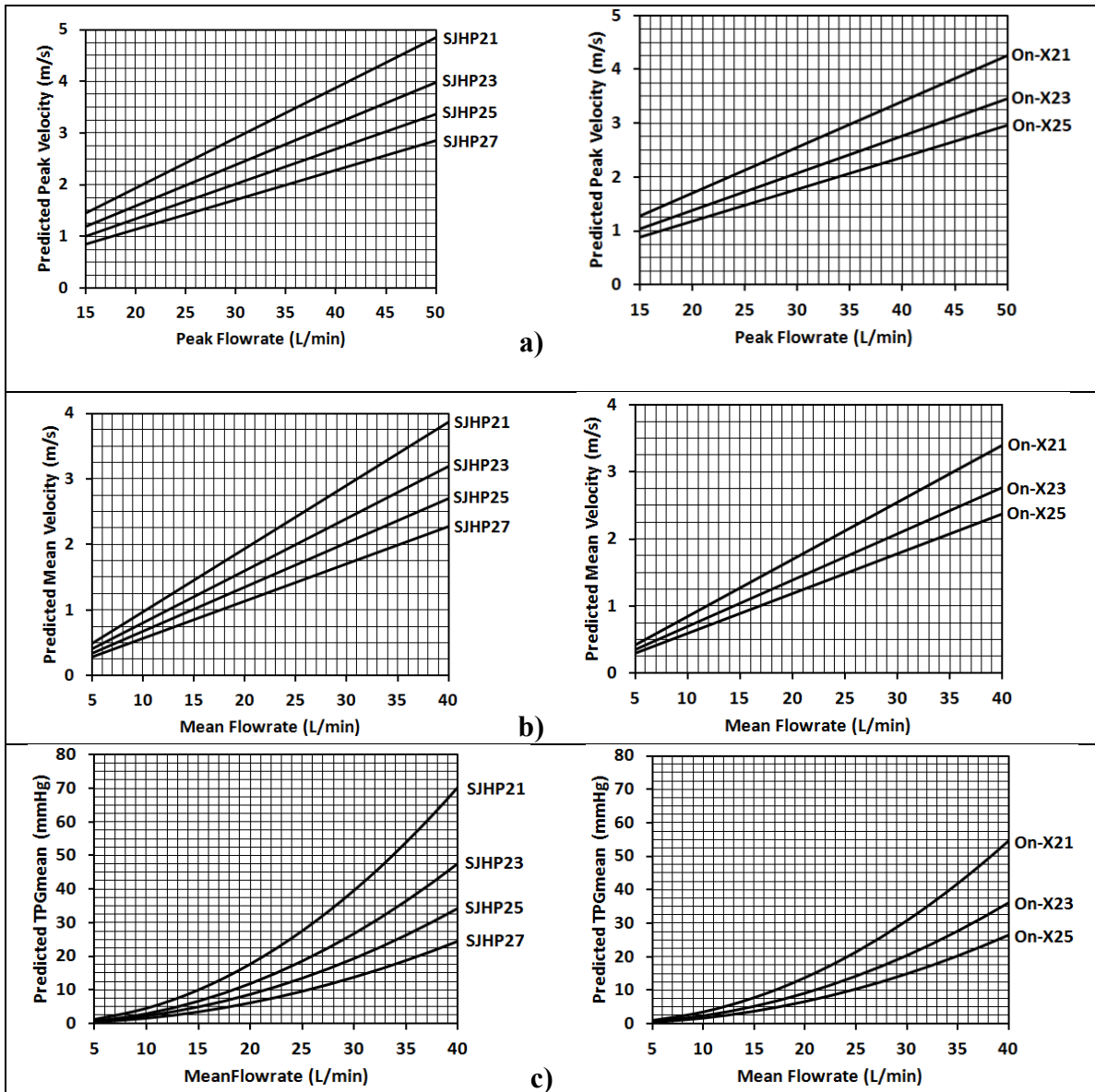


Figure 5.12 Plotted charts show relationships between peak/mean flowrate and predicted Doppler-derived parameters; a) Peak flowrate vs. Peak velocity; b) Mean flowrate vs. mean velocity; c) Mean flowrate vs. TPG<sub>mean</sub>.

#### **5.4.4 Charts**

Plotted charts for cut-off values of Doppler derived parameters as a function of flowrate and valves size/type could be a practical solution for quick and easy access to the information without any further calculations (Fig. 5.12).

### **5.5 Conclusion**

A reliable and practical mathematical model was proposed for predicting the normal reference values of Doppler-derived parameters for BMHVs. The proposed model was validated against *in vivo* and *in vitro* data in the current study. Moreover, good agreement was found between predicted and measured Doppler-derived parameters for normally functioning BMHVs. The theoretical model overcomes the shortcomings of the parameters suggested by the ASE guidelines as it accounts for flow conditions (LVOT measurements), valve size and valve type. Diagnostic accuracy significantly improved using the new theoretical parameters compared to ASE suggested parameters. Moreover, the new method improves the evaluation of the performance of BMHVs, not only after implantation, but early at the stage of design and manufacturing.

## Conclusions and Future work

### Conclusions

In the present study, blood flow dynamics through a dysfunctional bileaflet mechanical heart valve and the impact of valve dysfunction on clinical complications and clinical practices were investigated. Two dimensional, pulsatile and two-phase flow  $k-w$  turbulent models as well as 3-D, pulsatile, and FSI  $k-w$  turbulence models were used for numerical simulation. Numerically, (25 St. Jude hemodynamic Plus) BMHV was tested under normal flowrate conditions and for three different levels of dysfunction. A custom-made cardiac simulator was built and two different types of BMHVs with 7 different sizes were tested at wide range of flowrates and for three different levels of valve dysfunction. Moreover, *in vivo* data, from both echocardiography and cinefluoroscopy tests were analyzed for patients who have implanted aortic BMHV.

Numerical simulation for 2-D  $k-w$  turbulence models adapting the two-phase flow assumption showed that the flow through and downstream of a dysfunctional mechanical heart valve was highly influenced by dysfunction severity and this resulted in discrepancies between the Doppler echocardiographic and numerically derived transvalvular pressure gradients. Moreover, the flow downstream of the dysfunctional valve was characterized by abnormally elevated shear stresses and large-scale vortices. These characteristics can predispose to blood components damage. Finally, from a clinical point of view, clinicians should try, when possible, to check the maximal velocity

position not only at the central orifice, but also through the lateral orifices. Finding the maximal velocity in the lateral orifice could be an indication of valve dysfunction.

Three-dimensional FSI numerical simulations using  $k-w$  turbulence model was conducted using approximately 2.5 million elements. Three different levels of dysfunction at normal flowrate conditions were simulated. This study showed that the flow nature is strongly three dimensional and time dependent, especially in the existence of valve dysfunction. Therefore, in the presence of valve dysfunction, the pulsatile 3-D simulation should be used when the evolution of the vortical structure downstream of the BMHV is the objective of the study. Finally, it appears that 2-D pulsatile simulation was able to depict the main flow characteristics that are related to clinical diagnosis (pressure gradient and peak velocity).

*In vitro* and *in vivo* evaluations for the performance of Doppler-echocardiographic parameters for the detection of aortic mechanical prosthetic valve dysfunction were performed. Low sensitivity for the detection of valve dysfunction was found in all listed Doppler-echocardiographic parameters under the ASE guidelines. This was mainly due to considering fixed cut-off values regardless of flow conditions, valve size or valve type. Therefore, valve type, valve size and flowrate conditions have to be considered, especially when using peak Doppler velocity and mean transvalvular pressure gradient for evaluating mechanical heart valve performance. Doppler velocity index results should be interpreted with caution since they also depend on LVOT area. The reference

effective orifice area minus one standard deviation is a more stable and robust parameter for evaluating mechanical heart valve dysfunction.

A reliable and practical mathematical model was proposed for predicting the normal reference values of Doppler-derived parameters for BMHVs. The proposed model was validated against *in vivo* and *in vitro* data in the current study. Moreover, good agreement was found between predicted and measured Doppler-derived parameters for normally functioning valves. The theoretical model overcomes the shortcomings of the ASE suggested parameters by taking in to account flow conditions (LVOT measurements), valve size and valve type. Diagnostic accuracy significantly improved using the new theoretical parameters compared to ASE suggested parameters. Moreover, the new method improves the evaluation of the performance of BMHVs, not only after implantation, but also early at the stage of design and manufacturing.

## **Future Work**

### **Strongly Coupled 3-D FSI Realistic Model**

CFD is a major tool for investigating blood flow through mechanical heart valves. Although, up to date, there is no numerical method capable of accurately simulating the blood flow through mechanical heart valves under physiological conditions, CFD is widely used in this field. Therefore, it will be useful to consider a Direct Numerical Simulation (DNS) for blood flow through aortic BMHVs with strongly coupled 3-D FSI and using a very dense mesh (>10 million elements) capable of resolving the smallest turbulent scale (Kolmogorov scale). This will allow the study of the opening and closing

phases of dysfunctional BMHVs and also getting more precise information about the interaction between blood elements and flow field (platelet activation and hemolysis).

In the current study, a dysfunctional BMHV was studied in the aortic position and the same problematic mechanical heart valve was studied in the mitral position as this will affect the left ventricle's diastolic function.

### **Validation of 3-D FSI Numerical and Echo Doppler Results Using Particle Image Velocimetry**

As flow downstream of the MHV is inherently three dimensional and the systolic part of the cardiac cycle (most of our investigations are related to this part) is complete within 0.3 s, time resolved PIV measurements is needed to capture the flow characteristics downstream of the valve. The time resolved PIV measurements will be used as a gold standard to validate the numerical simulations and to extract the flow turbulent characteristics with the presence of valve dysfunction.

The same cardiac simulator that was used for the echo Doppler measurements will be used for the PIV measurements and under the same conditions. This will allow the validation of echo Doppler fluid mechanics assumptions (i.e., flat velocity profile, inviscid flow) and also the reliability of Doppler-derived parameters.

## References

- Alemu, Y., Bluestein, D., 2007. Flow-induced platelet activation and damage accumulation in a mechanical heart valve: Numerical studies. *Artificial Organs* 31(9), 677-688.
- Aoyagi, S., Nishimi, E., Kawano, M., Tayama, H., Fukunaga, S., Hayashida, N., Akashi, H., 2000. Obstruction of St. Jude Medical Valves in the Aortic Position: Significance of a combination of cineradiography and echocardiography. *J Thorac Cardiovasc Surg* 10(4), 339-344.
- Aslam A.K., Aslam A.F., Vasavada B.C., Khan I.A., 2007. Prosthetic heart valves: types and echocardiographic evaluation. *Int J Cardiol.* 122(2), 99-110.
- Bach, D.S., 2010. Echo Doppler evaluation of hemodynamics after aortic valve replacement. *J Am Coll Cardiol Img.* 3, 296-304.
- Balducci, A., Grigioni, M., Querzoli, G., Romano, G.P., Daniele, C., D'Avenio, G., Barbaro V., 2004. Investigation of the flow field downstream of an artificial heart valve by means of PIV and PTV. *Experiments in Fluids* 36,204-213
- Baumgartner, H., Khan, S., DeRobertis M., Czer L., Maurer G., 1990. Discrepancies between Doppler and catheter gradients in aortic prosthetic valves in vitro: A manifestation of localized gradients and pressure recovery. *Circulation* 82(4), 1467-75.
- Baumgartner H., Khan S., DeRobertis, M., Czer L., Maurer G., 1992. Doppler assessment of prosthetic valve orifice area: An in vitro study. *Circulation* 85(6), 2275-83.
- Baumgartner, H., Schima, H., and Kuhn, P., 1993. Effect of prosthetic valve dysfunction on the Doppler-catheter gradient relation for bileaflet aortic valve prostheses. *Circulation* 87, 1320-1327.
- Bech-Hanssen, O., Caidahl, K., Wallentin, I., Ask, P., Wranne, B., 2001. Assessment of effective orifice area of prosthetic aortic valves with Doppler echocardiography: an in vivo and in vitro study. *J Thorac Cardiovasc Surg.* 122(2), 287-95.
- Bluestein, D., Rambod, E., Gharib, M., 2000. Vortex shedding as a mechanism for free emboli formation in mechanical heart valves. *J. Biomech. Eng.* 122, 125-134.
- Bluestein, D., Li, Y.M., Krukenkamp, I.B., 2002. Free emboli formation in the wake of bi-leaflet mechanical heart valves and the effect of implantation techniques. *J. Biomech.* (35), 1533-1540.

Bluestein, D., Chandran, K. B., Manning, K. B., 2010. Towards non-thrombogenic performance of blood recirculating devices. *Ann. Biomed. Eng.* 38(3), 1236-1256.

Bonow, R.O., Carabello, B.A., Kanu, C., de Leon, A.C. Jr, Faxon, D.P., Freed, M.D., Gaasch, W.H., Lytle, B.W., Nishimura, R.A., O'Gara, P.T., O'Rourke, R.A., Otto, C.M., Shah, P.M., Shanewise, J.S., Smith, S.C. Jr, Jacobs, A.K., Adams, C.D., Anderson, J.L., Antman, E.M., Faxon, D.P., Fuster, V., Halperin, J.L., Hiratzka, L.F., Hunt, S.A., Lytle, B.W., Nishimura, R., Page, R.L., Riegel, B, 2006. ACC/AHA 2006 Guidelines for the management of patients with valvular heart disease a report of the american college of cardiology/american heart association task force on practice guidelines (writing committee to revise the 1998 guidelines for the management of patients with valvular heart disease). *Circulation.* 114(5), 84-231.

Botnar R., Nagel E., Scheidegger M.B., Pedersen E.M., Hess O., Boesiger P., 2000. Assessment of prosthetic aortic valve performance by magnetic resonance velocity imaging. *MAGMA* 10(1), 18-26.

Bottio T., Caprili L., Casarotto D., Gerosa G., 2004. Small aortic annulus: the hydrodynamic performances of 5 commercially available bileaflet mechanical valves. *J Thorac Cardiovasc Surg.* 128(3), 457-62.

Browne, P., Ramuzat, A., Saxena, R., and Yoganathan, A.P., 2000. Experimental investigation of the steady flow downstream of the St.Jude bileaflet heart valve: A comparison between laser doppler velocimetry and particle image velocimetry techniques. *Ann. Biomed. Eng.* (28), 39–47.

Brucker, Ch., 1997. Dual-camera DPIV for flow studies past artificial heart valves. *Experiments in Fluids* 22, 496-506.

Brucker, Ch., Steinseifer, U., Schroder, W., Reul, H., 2002. Unsteady flow through a new mechanical heart valve prosthesis analysed by digital particle image velocimetry. *Meas. Sci. Technol.* 13, 1043–1049.

Burda, G., Trittenwein, H., Carole, H., Trittenwein, G., 2004 . Testing of extracorporeal membrane oxygenation circuit related hemolysis using long-term stored packed red cells and fresh frozen plasma. *Artificial Organs* 28(5), 496-499.

Chafizadeh, E.R., Zoghbi, W.A., 1991. Doppler echocardiographic assessment of the St. Jude Medical prosthetic valve in the aortic position using the continuity equation. *Circulation* 83(1), 213-23.

Chambers, J.B., Oo, L., Narracott A., Lawford, P.M., Blauth, C.I., 2003. Nominal size in six bileaflet mechanical aortic valves: a comparison of orifice size and biologic equivalence. *J Thorac Cardiovasc Surg.* 125(6), 1388-93.

Chenzbraun, A., 2010. Pitfalls and challenges in the Echocardiographic diagnosis of aortic stenosis. *European Cardiology* 6(1), 10-13.

L, Chi-Pei., L, Chi-Wen., L, Po-Chien, 2010. Estimation of viscous dissipative stresses induced by a mechanical heart valve Using PIV data. *Annals of Biomedical Engineering* 38(3), 903–916.

Cianciulli, T.E., Lax, J.A., Beck, M.A., Cerruti, F.E., Gigena, G.E., Saccheri, M.C., Fernández, E., Dorelle, A.N., Leguizamón, J.H., Prezioso, H.A., 2005. Cinefluoroscopic assessment of mechanical disc prostheses: its value as a complementary method to echocardiography. *J Heart Valve Dis.* 14(5), 664-73.

Celik, I.B., Ghia U., Roache, P.J., Freitas, C.J., 2008. Procedure for estimation and reporting of uncertainty due to discretization in CFD applications. *Journal of fluids Engineering-Transactions of the ASME*, 130(7), 078001.

Dasi, L.P., Ge, L., Simon, H.A., Sotiropoulos, F., Yoganathan, A.P., 2007. Vorticity dynamics of a bileaflet mechanical heart valve in an axisymmetric aorta. *Physics of Fluids* 19(6), 067105-17.

DeGroff, C.G., Shandas, R., Valdes-Cruz, L., 1998. Analysis of the effect of flowrate on the Doppler continuity equation for stenotic orifice area calculations: A numerical study. *Circulation* (97), 1597-1605.

De Tullio, M.D., Cristallo, A., Balaras, E., Verzicco, 2009. Direct numerical simulation of the pulsatile flow through an aortic bileaflet mechanical heart valve. *J. Fluid Mech.* 622, 259–290

Dumesnil, J.G., Pibarot, P., Akins, C., 2008. New approaches to quantifying aortic stenosis severity. *Curr Cardiol Rep.* 10(2), 91-97.

Dumont, K., Astijen, J.M., Van De Vosse, F.N., and Verdonck, P.R., 2004. Validation of a fluid-structure interaction model of a heart valve using the dynamic mesh method in fluent”, *Computer Methods in Biomech. And Biomed. Eng.* 7(3), 139-146.

Dumont, K., Vierendeels, J., Kaminsky, R., van Nooten, G., Verdonck, P., Bluestein, D., 2007. Comparison of the hemodynamic and thrombogenic performance of two bileaflet mechanical heart valves using a CFD/FSI model. *J. Biomech. Eng.* 129(4), 558-565.

Fukumoto, Y., Tsutsui, H., Tsuchihashi M., Masumoto, A., Takeshita, A., 2003. The incidence and risk factors of cholesterol embolization syndrome, a complication of cardiac catheterization: Aprospective study. *J. Am. Coll. Cardiol.* 42(2), 211-217.

Garcia, D., Dumesnil, J.G, Durand, L., Kadem, L., and Pibarot, P., 2003. Discrepancies between catheter and Doppler estimates of valve effective orifice area can be predicted

from the pressure recovery phenomenon practical implications with regard to quantification of aortic stenosis severity. *J. Am. Coll. Cardiol.* 41(3), 435-442.

Garcia, D., Pibarot, P., Dumesnil, J.G., Sakr, F., Durand, L.G., 2000. Assessment of aortic valve stenosis severity: A new index based on the energy loss concept. *Circulation* 101, 765-771.

Garcia, D., Pibarot, P., Landry, C., Allard, A., Chayer, B., Dumesnil, J.G., Durand, L.G., 2004. Estimation of aortic valve effective orifice area by Doppler echocardiography: effects of valve inflow shape and flow rate. *J Am Soc Echocardiogr.* 17, 756-765.

Ge, L., Jones, S.C., Sotiropoulos, F., Healy, T.M., Yoganathan, A.P., 2003. Numerical simulation of flow in mechanical heart valves: grid resolution and the assumption of flow symmetry. *Journal of Biomechanical Engineering* 125, 709-719.

Ge, L., Jones, S.C., Sotiropoulos, F., Healy, T.M., Yoganathan, A.P., 2005. Flow in a mechanical bileaflet heart valve at laminar and near-peak systole flowrates: CFD simulations and experiments. *J. Biomech. Eng.* 127, 782-797.

Ge, L., Dasi, L., Sotiropoulos, F., Yoganathan, A., 2008. Characterization of hemodynamic forces induced by mechanical heart valves: Reynolds vs. viscous stresses. *Ann. Biomed. Eng.* 36(23), 276-297.

Girard, S.E., Miller, F.A., Orszulak, T.A., et al., 2001. Reoperation for prosthetic aortic valve obstruction in the era of echocardiography: trends in diagnostic testing and comparison with surgical findings. *J Am Coll Cardiol.* 37(2), 579-84.

Gosman, A. D., Ioannides, E., 1981. Aspects of computer simulation. of liquid-fueled combustors. *American Institute of Aeronautics and Astronautics* 7(6), 482-490.

Grigioni, M., Daniele, C., D'Avenio, G., Barbaro, V., 2001. The Influence of the leaflets' curvature on the flow field in two bileaflet prosthetic heart valves. *J. Biomech.* 34(5), 613-621.

Grigioni, M., Daniele, C., Gaudio, C.D., Morbiducci, U., D'Avenio, G., Barbaro, V., 2005. Three-Dimensional numerical simulation of flow through an aortic bileaflet valve in a realistic model of aortic root. *Am Soc Art Int Org.* 51(3), 176-183.

Gott, V.L., Alejo, D.E., Cameron, D.E., 2003. Mechanical Heart Valves: 50 Years of Evolution. *Ann Thorac Surg.* (76), 2230 -2239.

Guivier, C., Deplano, V., Pibarot, P., 2007. New insights into the assessment of the prosthetic valve performance in the presence of subaortic stenosis through a fluid-structure interaction model. *J. Biomech.* 40(10), 2283-2291.

Guivier-Curien, C., Deplano, V., Bertrand, E., 2009. Validation of a numerical 3-D fluid-structure interaction model for a prosthetic valve based on experimental PIV measurements. *Med Eng Phys. ysics* 31(8), 986-993.

Hage, F.G., Nanda, N.C., 2009. Real-time three-dimensional echocardiography: a current view of what echocardiography can provide? *Indian Heart J.* 61(2), 146-55.

Hasenkam, J.M., Ringgaard S, Houliind, K., Botnar, R.M., Stødkilde-Jørgensen, H., Boesiger, P., Pedersen, E.M., 1999. Prosthetic heart valve evaluation by magnetic resonance imaging. *Eur J Cardiothorac Surg.* 16(3), 300-5.

Hatle L., Anglesen, B., 1985. *Doppler Ultrasound in Cardiology*, 2<sup>nd</sup> Edition, Lea and Febiger.

Hellums, J., Peterson, D., Stathopoulos, N., Moake, J., Giorgio, T., 1987. Studies on the mechanisms of shear-induced platelet activation. Springer and Verlag, New York.

Izzat, M.B., Birdi, I., Wilde, P., Bryan, A.J., Angelini, G.D., 1996. Comparison of hemodynamic performances of St. Jude Medical and CarboMedics 21 mm aortic prostheses by means of dobutamine stress echocardiography. *J Thorac Cardiovasc Surg.* 111(2), 408-15.

Jesty, J., Yin, W., Perrotta, P., Bluestein, D., 2003. Platelet activation in a circulating flow loop: combined effects of shear stress and exposure time. *Platelets* 14(3), 143-149.

Kadir I., Wan I.Y., Walsh C., Wilde P., Bryan A.J., Angelini GD., 2001. Hemodynamic performance of the 21-mm Sorin Bicarbon mechanical aortic prostheses using dobutamine Doppler echocardiography. *Ann Thorac Surg.* 72(1), 49-53.

Kaminsky, R., Kallweit, S., Weber, H.J., Claessens, T., Jozwik, J., Verdonck, P., 2007. Flow visualization through two types of aortic prosthetic heart valves using stereoscopic high-speed particle image velocimetry. *Artificial Organs* 31(12), 869–879.

Khandheria, B.K., Seward, J.B., Oh, J.K., et al., 1991. Value and limitations of transesophageal echocardiography in assessment of mitral valve prostheses. *Circulation* 83(6), 1956-68.

King, M.J., David, T., Fisher, J., 1997. Three dimensional study of the effect of two leaflet opening angles on the time dependant flow through a bileaflet mechanical heart valve. *Med Eng Phys.* 19(3), 35-241.

Kvitting J.P., Dyverfeldt P., Sigfridsson A., et al., 2010. *In vitro* assessment of flow patterns and turbulence intensity in prosthetic heart valves using generalized phase-contrast MRI. *J Magn Reson Imaging* 31(5), 1075-80.

LaBounty, T.M., Agarwal, P.P., Chughtai, A., Bach, D.S., Wizauer, E., Kazerooni, E.A., 2009. Evaluation of mechanical heart valve size and function with ECG-gated 64-MDCT. *AJR Am J Roentgenol* 193(5), 389-96.

Liu, J.S., Lu, P.C., , Chu. S.H., 2000. Turbulence characteristics downstream of bileaflet aortic valve prostheses. *Transactions of ASME* 122, 118-124.

Lu, P.C., Lai, H.C., Liu, J.S., 2001. A re-evaluation and discussion on the threshold limit for hemolysis in a turbulent shear flow. *J Biomech.* 34, 1361-1364.

Maslow, A.D., Haering, J.M., Heindel, S., Mashikian, J., Levine, R., Douglas, P., 2000. An evaluation of prosthetic aortic valves using transesophageal echocardiography: the double-envelope technique. *Anesth Analg.* 91(3), 509-16.

Mohr-Kahaly, S., Kupferwasser, I., Erbel, R., et al., 1993. Value and limitations of transesophageal echocardiography in the evaluation of aortic prostheses. *J Am Soc Echocardiogr.* 6(1), 12-20.

Montorsi, P., Cavretto, D., Alimento, M., Muratori, M., Pepi, M., 2003. Prosthetic mitral valve thrombosis: can fluoroscopy predict the efficacy of thrombolytic treatment? *Circulation* 108, 79-84.

Nobili, M., Morbiducci, U., Ponzini, R., Del Gaudio, C., Balducci, A., Grigioni, M., Montevecchi, F.M., Redaelli, A., 2008. Numerical simulation of the dynamics of a bileaflet prosthetic heart valve using a fluid-structure interaction approach. *J Biomech.* 41(11), 2539-2550.

Peacock, J., Jones, T., Tock C., and Lutz R., 1998. The onset of turbulence in physiological pulsatile flow in a straight tube. *Experiments in Fluids* (24), 1-9.

Pedrizzetti, G., Domenichini, F., 2006. Flow-driven opening of a valvular leaflet. *Journal of Fluid Mech.* 569, 321–330.

Pibarot, P., Dumesnil, J.G., 2009. Prosthetic heart valves: selection of the optimal prosthesis and long-term management. *Circulation* 119, 1034-1048.

Pick, A., 2007. *The patient's guide to heart valve surgery*. Heart Valve Interactive Corp.

Rahimtoola, SH., 2010. Choice of prosthetic heart valve in adults: an update. *J Am Coll Cardiol.* 55(22), 2413-26.

Redaelli, A., Bothorel, H., Votta, E., Soncini, M., Morbiducci, U., Del Gaudio, C., Balducci, A., Grigioni, M., 2004. 3-D simulation of the St. Jude medical bileaflet valve opening process: fluid-structure interaction study and experimental validation. *The Journal of Heart Valve Disease* 13(5), 804-813.

Reul, H., Vahlbruck, A., Giersiepen, M., Schmitz-Rode, T.H., Hirtz, V., Effert, S., 1990. The geometry of the aortic root in health, at Valve Disease and after Valve Replacement. *J Biomech.* 23(2), 181-191.

Rizzoli, G., Guglielmi, C., Toscano, G., Pistorio, V., Vendramin, I., Bottio, T., Thiene, G., Casarotto, D., 1999. Reoperations for acute prosthetic thrombosis and pannus: an assessment of rates, relationship and risk. *Eur J Cardiothorac Surg.* 16(1), 74-80.

Rosenhek, R., Binder, T., Maurer, G., Baumgartner, H., 2003. Normal values for Doppler echocardiographic assessment of heart valve prostheses. *J Am Soc Echocardiogr.* 16(11), 1116-27.

Roudaut, R., Roques, X., Lafitte, S., Choukroun, E., Laborde, N., Madona, F., Deville, C., Baudet, E., 2003. Surgery for prosthetic valve obstruction: A single center study of 136 patients. *Eur J Cardiothorac Surg.* 24(6), 868-72.

Roudaut R., Serri K., Lafitte S., 2007. Thrombosis of prosthetic heart valves: diagnosis and therapeutic considerations. *Heart* 93(1), 137-42.

Sakamoto, Y., Hashimoto, K., Okuyama, H., Ishii, S., Shingo, T., Kagawa, H., 2006. Prevalence of pannus formation after aortic valve replacement: clinical aspects and surgical management. *J Art Org.* 9(3), 199-202.

Sallam, A.M., Hwang, N.H., 1984. Human red blood cell hemolysis in a turbulent shear flow: contribution of Reynolds shear stresses. *Biorheology* 21(6), 783-97.

Shandas, R., Kwon, J., Valdes-Cruz, L., 2000. A method for determining the reference effective flow areas for mechanical heart valve prostheses: *in vitro* validation studies. *Circulation* 101(16), 1953-9.

Shi, Y., Zhao Y., Joon, T., Yeo, H., Hwang, N., 2003. Numerical simulation of opening process in a bileaflet mechanical heart valve under pulsatile flow condition. *The Journal of Heart Valve Disease* (12) 245-256.

Smadi, O., Fenech, M., Hassan, I., Kadem, L., 2009. Flow through a dysfunctional mechanical heart valve: a steady flow analysis. *Med Eng Phys.* 31 (3), 295-305.

Smadi, O., Hassan, I., Pibarot, P., Kadem, L., 2010. Numerical and experimental investigations of pulsatile blood flow pattern through a dysfunctional mechanical heart valve. *J Biomech.* 43(8), 1565-1572.

Vesey, J.M., Otto, C.M., 2004. Complications of prosthetic heart valves *Curr Cardiol Rep.* 6(2), 106-11.

Vongpatanasin, W., Hillis, L.D., Lange, R.A., 1996. Prosthetic heart valves. *N Engl J Med.* 335(6), 407-16.

Wang, Z, Grainger, N, Chambers, J., 1995. Doppler echocardiography in normally functioning replacement heart valves: a literature review. *J Heart Valve Dis.* 4(6), 591-614.

Wilcox, D.C., 1998. *Turbulence modeling for CFD*, 2nd edition, DCW Industries, La Canada, California.

Yin, W., Alemu, Y., Affeld, K., Jesty, J., Bluestein, D., 2004. Flow induced platelet activation in bileaflet and monoleaflet mechanical heart valves. *Ann of Biomed Eng.* 32(8), 1058-1066.

Yin, W., Gallocher, S., Pinchuk, L., Schoepfoerster, R.T., Jesty, J., and Bluestein, D., 2005. Flow-induced platelet activation in a St. Jude mechanical heart valve, a trileaflet polymeric heart valve, and a St. Jude tissue valve. *Artificial Organs* 29(10), 826-831.

Yoganathan, A. P., He Z., and Jones, S.C., 2004. Fluid mechanics of heart valves. *Annu. Rev. Biomed. Eng.* (6), 331-62.

Yoganathan, A. P., Chandran, K.B., Sotiropoulos, F., 2005. Flow in prosthetic heart valves: State-of-the-Art and future directions. *Ann of Biomed Eng.* 33(12), 1689-1694.

Zaret, B.L., Moser, M., Cohen, L.S., Morrow, W., 1992. *Heart Book*, 1<sup>st</sup> Edition, Yale University, School of Medicine.

Zoghbi, W.A., Chambers, J.B., Dumesnil, J.G., Foster, E., Gottdiener, J.S., Grayburn, P.A., Khandheria, B.K., Levine, R.A., Mar, G.R., Miller, F.A. Jr, Nakatani, S., Quiñones, M.A., Rakowski, H., Rodriguez, L.L., Swaminathan, M., Waggoner, A.D., Weissman, N.J., Zabalgoitia, M., 2009. Recommendations for evaluation of prosthetic valves with echocardiography and doppler ultrasound: a report From the American Society of Echocardiography's Guidelines and Standards Committee and the Task Force on Prosthetic Valves, developed in conjunction with American College of Cardiology Cardiovascular Imaging Committee; Cardiac Imaging Committee of the American Heart Association; European Association of Echocardiography; European Society of Cardiology; Japanese Society of Echocardiography; Canadian Society of Echocardiography; American College of Cardiology Foundation; American Heart Association; European Association of Echocardiography; European Society of Cardiology; Japanese Society of Echocardiography; Canadian Society of Echocardiography. *J Am Soc Echocardiogr.* 22(9), 975-1014.